TESLA Report 1997-22

Resistive Wall Wake Fields

Diplomarbeit
zur Erlangung des Grades
eines Diplomphysikers

vorgelegt dem Fachbereich Physik
der Universität Hamburg
von Holger Schlarb

Hamburg
August 1997

Gutachter der Diplomarbeit:	Prof. Dr. P. Schmüser Dr. R. Brinkmann
Datum der Diplomarbeit:	28.08.1997
Vorsitzender des Prüfungsausschusses:	Prof. Dr. G. Zimmerer

Contents

List of Figures

List of Tables

Introduction

Over the past 30 years synchrotron radiation has been turned into a most powerful research tool applied in many different fields of science: in physics, chemistry and biology, in material sciences, geophysics and in medical diagnostic.

The recent advances in the development of linear accelerators by the performance of low emittance electron guns and very precise undulators open the possibility to build a Free Electron Laser (FEL) as synchrotron radiation sources of the 4rd generation.

The FEL proposed at DESY will be driven by the superconducting TESLA Test Facility (TTF) linear accelerator upgraded to 1 GeV supplement by a low emittance injector and longitudinal bunch compressors. The goal is a unique light source which emits radiation up to photon energies of about 200 eV. [1]

The TTF-FEL is based on the principle of Self Amplified Spontaneous Emission (SASE). The electron bunch with an extremely high power density moves through a long undulator which consists of alternating dipole magnets (planar undulator type). Initially, by synchrotron radiation an intense photon beam is created at a wavelength λ_0 determined by the electron energy, the magnetic field, and the period of the undulator. The radiated electromagnetic field interacts with the electron bunch. This interaction leads to a longitudinal density modulation of the bunch with a periodicity equal to the wavelength λ_0, which in turn enhances the power and the coherency of the radiation field emitted by the bunch. The so-called "Self Amplification" starts near the beginning of the undulator and reaches saturation at close to its end.

This enables the TTF-FEL to produce radiation in the spectral range of the VUV without using a seed laser or mirrors. For high beam energies, as planned for an X-ray FEL foreseen in the project of a future e^+e^- collider TESLA, the spectral range can be extended into the soft or even hard X-rays. The average and the peak spectral brilliance of such FEL's are by several orders of magnitude higher than the values reached by the new 3rd generation of synchrotron radiation sources [1].

In order to reach saturation within a not too long undulator, very high peak currents are required with a small transverse emittance $\epsilon_\perp$ and a small longitudinal emittance ϵ_z. The small transverse emittance provides a small beam diameter and small beam divergence, and the small longitudinal emittance achieves high instantaneous beam currents with a small energy width. Especially, the very high peak currents cause various problems for the high beam qualities required.

For example, the design values of TTF-FEL drive beam are $\epsilon_\perp = 2\pi$ mm mrad for the transverse emittance and $\epsilon_z = 50$ keV mm for the longitudinal emittance with a peak current of 2.5 kA. This extremely high peak current can only be produced by compressing the initial 2 mm long bunch at the electron gun in three stages along the TTF linac down to a final bunch length of 50 μm at the entrance of the undulator.

High charged ultra-short electron bunches cause unavoidably a strong interaction with their self-generated electromagnetic fields, the wake fields. The wake fields lead longitudinally to a correlated energy spread and transversally to a deformation of the bunch. Both effects could reduce the beam quality and cause beam instabilities.

Therefore, it has to be proven that the stringent requirements on the high beam quality for the drive beam of the FEL are preserved along the linac, including the injector, the superconducting acceleration modules and the bunch compressors.

In particular, the vacuum chamber of the undulator has a very small inner diameter to achieve sufficiently high peak magnetic fields. It has to be carefully designed in order to keep the amplitudes of the wake fields below an acceptable limit. The largest contribution among the different sources of wake fields inside an undulator vacuum chamber is expected to be from the resistivity of metal. The contribution of the so-called resistive wall wake fields has been estimated in this diploma thesis.

In the first chapter the basic concept of wake fields is introduced. The analytical treatment and the numerical results of the resistive wall wake fields is presented in the second chapter. In the third chapter the results for the TTF-Undulator for different metals and designs are given.

The influence on an electron beam has been analyzed in a more general context including beam pipe radii relevant for transport systems as planned for the X-ray FEL project [2].

Chapter 1

Basic Concepts of Wake Fields

A beam of charged particles, as in traveling wave tubes, klystrons and accelerators, interacts with its immediate surroundings by means of co-propagating electromagnetic fields. The performance of modern high-current particle accelerators, which have tightly bunched beams with peak currents of several kA and bunch lengths much smaller than 1 mm, are seriously affected by this interaction. As the beam intensity is increased the electromagnetic fields self-generated by the beam will perturb the external prescribed fields. For sufficiently strong perturbation the beam quality is degraded. Particularly for the FEL the stringent requirements on the beam parameters do not allow stronger perturbations.

The electromagnetic field generated by the beam are known as the wake fields. The net effect on the beam due to wake fields in a beam pipe is described by the wake potential. The most important aspects of the wake potentials are summarized in this chapter, which is organized as follows: In the first section a brief introduction to electromagnetic fields for relativistic charges is given, together with a discussion on some typical structures in which wake fields are excited. In the second section the concepts of wake function and wake potential are introduced as the time domain descriptions of the interaction. The third section deals with the corresponding frequency descriptions known as the coupling impedances. The remaining three sections are treatments of some particular aspects of the wake fields, namely the properties of the wake potential of round structures, an integration method for cylindrical pipes and the distance of beam-wake field interaction.

1.1 Introduction to Electromagnetic Theory of Wake Fields

Consider a point charge q moving in free space at a constant velocity $\mathbf{v}^*$ close to the speed of light. An observer at a perpendicular distance b from the trajectory of the particle measures a Lorentz contracted electromagnetic field concentrated in a thin disk perpendicular to the particle direction of motion. For the longitudinal and transverse components of an electromagnetic field, carried by a relativistic point charge one finds [3]:

*Variables that are written with bold letters indicate vectors.

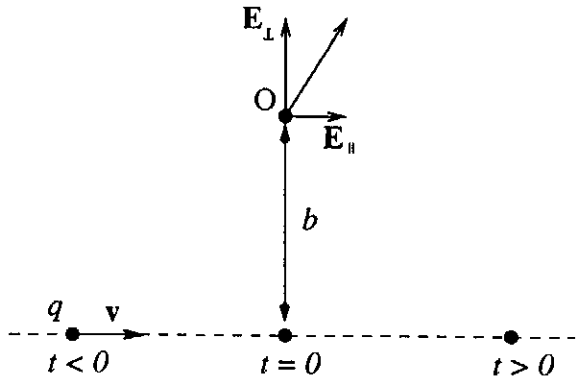

Figure 1.1: Particle of a charge q moving at constant velocity $\mathbf{v}$ passes an observation point O at the impact parameter b.

$$\begin{aligned}
\mathbf{E}_{\parallel}(b,t) &= -\frac{q}{4\pi\epsilon_0}\frac{\gamma v t}{[b^2+(\gamma v t)^2]^{3/2}}\mathbf{e}_{\parallel}\,, \\
\mathbf{E}_{\perp}(b,t) &= \frac{q}{4\pi\epsilon_0}\frac{\gamma b}{[b^2+(\gamma v t)^2]^{3/2}}\mathbf{e}_{\perp} \\
\mathbf{B}_{\perp}(b,t) &= \frac{1}{c^2}\,\mathbf{v}\times\mathbf{E}_{\perp}(b,t)\,,
\end{aligned} \tag{1.1}$$

where the relativistic factor is defined by

$$\gamma = \frac{1}{\sqrt{1-\beta^2}} \qquad \text{with} \quad \beta = \frac{v}{c}\,. \tag{1.2}$$

Here, $\mathbf{e}_{\parallel}$ is the unit vector parallel to $\mathbf{v}$ of charge, $\mathbf{e}_{\perp}$ the unit vector perpendicular to $\mathbf{v}$ in the direction towards the observer, and ϵ_0 is the permittivity of free space.

The magnetic field is a purely azimuthal field and has no field components in the longitudinal or the radial direction. The amplitude of the transverse electric field, as seen by the observer, is an even function of time. The peak value is reached at $t = 0$ when the particle passes the point at minimum distance to the observer. The time interval in which the amplitude of the transverse electric field rises to half the peak value is approximately given by:

$$\triangle t \approx \sqrt{2}\frac{b}{\gamma v} \tag{1.3}$$

with the peak value

$$\mathbf{E}_{\perp}(b,0) = \frac{q}{4\pi\epsilon_0}\frac{\gamma}{b^2}\,\mathbf{e}_{\perp}\,. \tag{1.4}$$

In contrast to this, the longitudinal electric field is an odd function of time and the peak values at $\pm\triangle t/2$ are independent of the relativistic factor. Consequently for $\gamma \gg 1$ the electric field is concentrated into a small disk with opening angle in the order of $1/\gamma$.

It can be seen from Eq. (1.1) that with increasing γ the longitudinal electric field

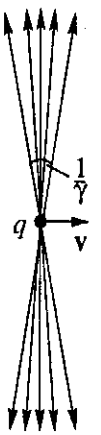

Figure 1.2: Electric field carried by a relativistic point charge in free space.

$\mathbf{E}_{\|}$ decreases (proportional to $1/\gamma$), while the radial electric field $E_r\mathbf{e}_r = \mathbf{E}_\perp$ and the azimuthal magnetic field $B_\phi\mathbf{e}_\phi = \mathbf{B}_\perp$ increase (proportional to γ).

In the ultra-relativistic limit $\gamma \to \infty$ (or $v \to c$), the disk containing the fields shrinks into a δ-distribution where the non-vanishing field components are:

$$E_r(r,z,t) \;=\; \frac{q}{2\pi\epsilon_0 r}\delta(z-ct) \qquad\qquad B_\phi \;=\; \frac{1}{c}E_r\,. \tag{1.5}$$

The normalization of the fields can be obtained either by applying Gauss's law or simply by integrating the transverse electric fields over time. The electromagnetic field distribution described in Eq. (1.5) is sometimes called the "pan-cake" term. Since the electric field $\mathbf{E}$ is perpendicular to the trajectory, the field components in front and behind the point charge vanish. Consequently a test charge moving synchronous and parallel within an arbitrarily small longitudinal distance to the source charge suffers no forces. Therefore, the particles in a beam can be considered to be "frozen" at their longitudinal positions in the ultra-relativistic limit.

In the following, a beam is considered as a bunched beam, where the individual charges are collected in beam bunches. The single beam bunches can be assumed to be longitudinally of Gaussian shape with a rms-length σ_z.

The situation for bunch in free space is different from that in a vacuum chamber, in which the electromagnetic field interacts with the walls of the chamber. Along the beam trajectory various structures modify the cross section of the beam pipe. Additional fields occur due to the discontinuities and the gradients along the pipe, and the finite conductivity of the pipe wall material.

Some scenarios are shown in Fig. 1.3 where the pan-cake term of a bunched beam can be disturbed. For instance, the fields of the bunch can excite resonance modes in a single cavity acting back on the bunch. For sufficiently large quality factors of the resonance modes, additional interaction with the following bunches can take place. At higher frequencies, discontinuities generate diffraction patterns travelling in the cavity and filling the volume of the beam pipe. These diffracted fields are mainly responsible for the short-range behaviour of the interaction. The energy loss suffered by an ultra-short

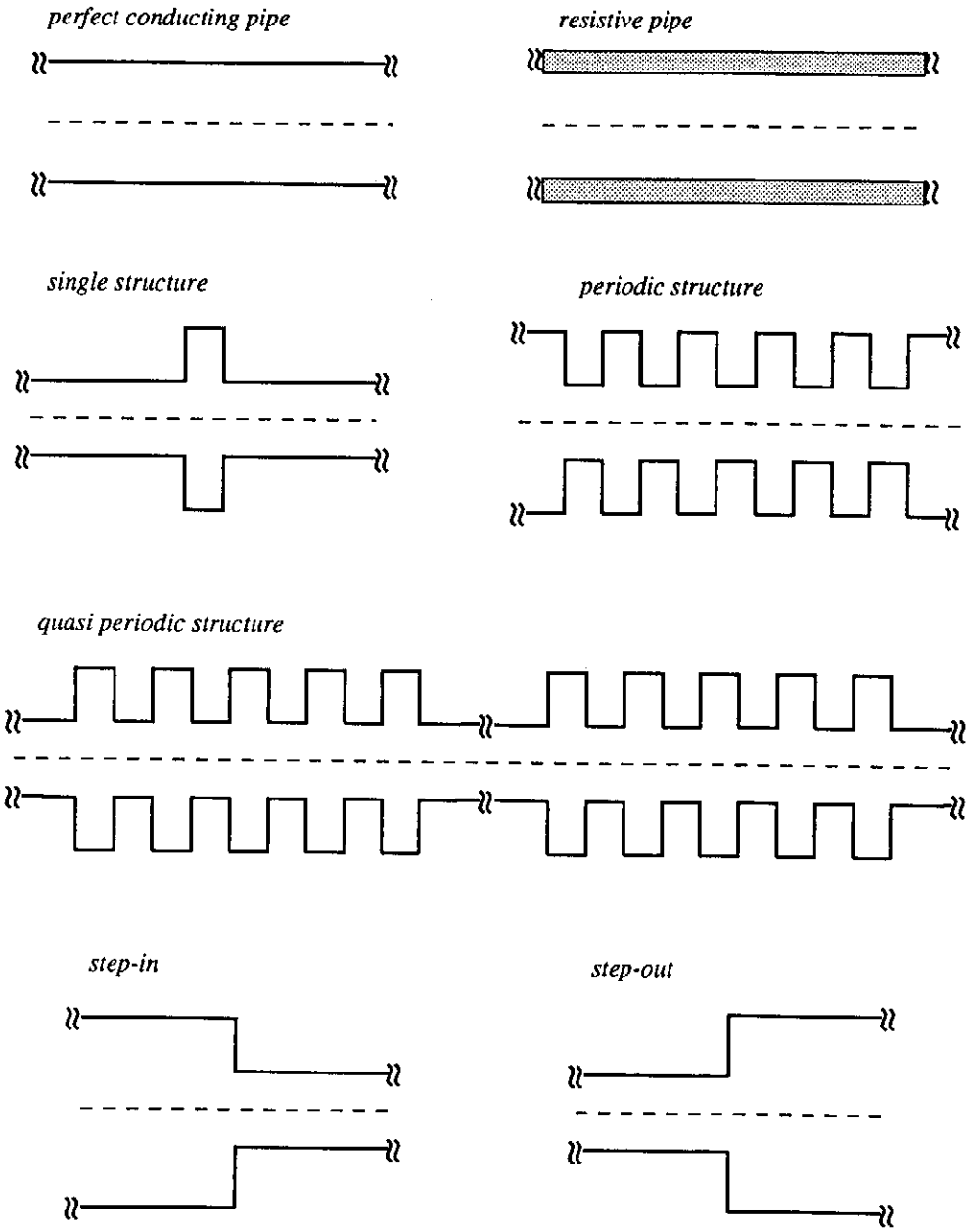

Figure 1.3: Various cylindrically symmetric structures relevant for beam instabilities. The beam enters from the left and moves to the right.

bunch is caused by these fields.

The effect of the different structures and beam parameters have been analyzed by many authors and several computer codes are available for calculating the electromagnetic fields [4]. It is interesting to note that the fields generated by a single cavity differ significantly from those of a periodic cavity. For example, the energy loss of a bunch for a periodic array of cells becomes for sufficiently short bunches independent on the bunch length σ_z while for a single cavity the energy loss of a bunch to the environment scales like $\propto \sigma_z^{-1/2}$ [5].

A transition for the behaviour of the wake fields for a given bunch length from a single cell structure to a periodic structure takes place for increasing cell numbers. A periodic solution is approximately obtained for cell number $M > b^2/(2d\sigma_z)$, where b is the beam pipe radius and d the periodicity of cells [6].

Obviously, the situation becomes more involved in case of cavities consisting of a certain number M of equivalent cells that are interrupted by smooth pipes (quasi-periodic structure) as for TESLA. This has been studied in [7] for different cell numbers of the TESLA cavities and for a chain of TESLA cavities both analytically (using an optical resonator model) and numerically.

Another important issue for accelerator physics are the electromagnetic fields radiated by a beam moving from a larger beam pipe radius to a smaller (step-in) and the opposite case from a smaller radius to a larger (step-out). It is interesting to note, that for a step-in transition a bunch can be accelerated while passing through the discontinuity [8].

1.2 Time Domain Description

1.2.1 Wake Function and Wake Potential

In Fig. 1.3 some examples of vacuum chamber structures where the beam interacts with its self-generated electromagnetic fields are shown. Consider now charges travelling with velocity $v = \beta c$ on trajectories parallel to the axis of a vacuum chamber. A small test charge q follows the source charge q_s at a distance ζ. Let z_s denote the longitudinal and $\mathbf{r}_{s\perp}$ the transverse vector position of the source charge and z, $\mathbf{r}_\perp$ those of the test charge (see Fig. 1.4).

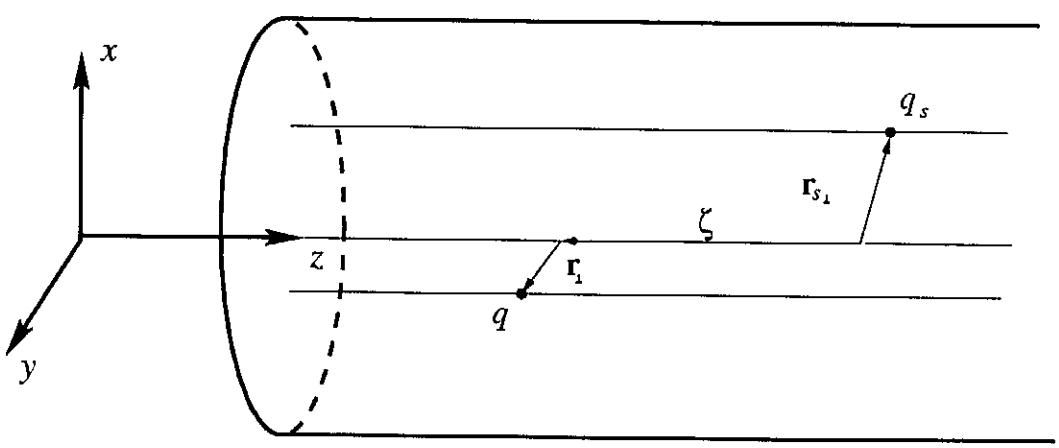

Figure 1.4: Coordinates of the source and the test particles. The test particle follows the source for $\zeta > 0$ and vice versa for $\zeta < 0$.

The electromagnetic fields $\mathbf{E}$ and $\mathbf{B}$ produced by the source charge q_s in a given structure can be derived by solving the Maxwell equations with proper boundary conditions.

In order to suppress the scattering with rest gas atoms and molecules the vacuum chamber is always kept at low pressure and the beam can be assumed to be travelling in vacuum. The Maxwell equations in vacuum read:

$$\nabla \times \mathbf{B} = \mu_0 \mathbf{j} + \frac{1}{c^2} \partial_t \mathbf{E} \tag{1.6}$$

$$\nabla \cdot \mathbf{E} = \frac{1}{\epsilon_0} \rho \tag{1.7}$$

$$\nabla \times \mathbf{E} = -\partial_t \mathbf{B} \tag{1.8}$$

$$\nabla \cdot \mathbf{B} = 0 . \tag{1.9}$$

For a point-like particle the charge and the current density are written as

$$\rho(\mathbf{r},t) = q_s \, \delta^2(\mathbf{r}_\perp - \mathbf{r}_{s\perp}) \, \delta(z - vt) , \qquad \mathbf{j}(\mathbf{r},t) = \mathbf{v} \, \rho(\mathbf{r},t) , \tag{1.10}$$

where δ^2 denotes the delta function in two dimensions. The Lorentz force acting on the test charge q at a position $(\mathbf{r}_\perp, z)$ is

$$\mathbf{F}(\mathbf{r}_\perp, z, t) = q \left\{ \mathbf{E}(\mathbf{r}_\perp, z, t) + \mathbf{v} \times \mathbf{B}(\mathbf{r}_\perp, z, t) \right\} . \tag{1.11}$$

After passing through the structure the energy and the transverse momentum of both charges are modified. The source charge is affected by its own interaction with the environment and a small test charge is predominantly affected by the fields generated by the source. Consider now the case of particles at high energies. Then the change of the trajectories while passing through the chamber can by treated as a perturbation. The treatment of wake fields in this work is restricted to the case where the variation of the electromagnetic field due to the perturbation of the trajectories is negligible. In this case, the integrated forces along the length L of the structure can be used to describe the beam dynamics caused by wake fields*.

The wake force acting on a small test charge is given by:

$$\mathbf{F}(\mathbf{r}_\perp, \mathbf{r}_{s\perp}, \zeta, t) = q \left\{ \mathbf{E}(\mathbf{r}_\perp, \mathbf{r}_{s\perp}, z = vt - \zeta, t) + v \, \mathbf{e}_z \times \mathbf{B}(\mathbf{r}_\perp, \mathbf{r}_{s\perp}, z = vt - \zeta, t) \right\} . \tag{1.12}$$

Note, that $\mathbf{F}$ depends in addition on the transverse vector position $\mathbf{r}_{s\perp}$ of the field-generating source charge. The momentum change due to the interaction with the beam environment is obtained be integrating the wake forces:

$$\Delta \mathbf{p}(\mathbf{r}_\perp, \mathbf{r}_{s\perp}, \zeta) = \int_L dt \, \mathbf{F}(\mathbf{r}_\perp, \mathbf{r}_{s\perp}, \zeta, t) . \tag{1.13}$$

Since the variables ζ, z, and t are related, the above integration with respect to time can be replaced by an integration with respect to the longitudinal position z of the source charge. This leads to the definition of the so-called wake function† [9]‡:

$$\mathbf{W}^\delta(\mathbf{r}_\perp, \mathbf{r}_{s\perp}, \zeta) = \frac{1}{q_s} \int_{-\infty}^{\infty} dz \, \left\{ \mathbf{E}(\mathbf{r}_\perp, \mathbf{r}_{s\perp}, z, t) + v \, \mathbf{e}_z \times \mathbf{B}(\mathbf{r}_\perp, \mathbf{r}_{s\perp}, z, t) \right\}_{t=(z+\zeta)/v} . \tag{1.14}$$

*To describe the more complicated wake fields, where the perturbation of the trajectory is large, the equations of the dynamics in combination with Maxwell equations have to be taken into account.

†In literature the wake function is also called delta wake potential.

‡An opposite sign for the wake function has been chosen.

The superscript δ refers to the δ-function like charge distribution of the source. The wake function describes the shock response of a structure due to the field of a point-like particle.

At a given distance ζ the longitudinal component of the wake function $W_{\parallel}^{\delta}$ describes the energy gain or loss of a test charge, depending on the sign of the wake function. If the test and the source charge have the same sign then a positive (negative) wake function means an accelerating (decelerating) force on the test charge.

The energy loss of the source charge itself as the work done by the longitudinal electromagnetic force along the structure is related to the wake function at $\zeta = 0$ by

$$\triangle E \;=\; q_s^2 k_{\parallel}^{\delta} \quad \text{with} \quad k_{\parallel}^{\delta} \equiv -W_{\parallel}^{\delta}(0)\,, \tag{1.15}$$

where the quantity $k_{\parallel}^{\delta}$ is called the loss factor.

The component perpendicular to the direction of motion is called the transverse wake function and leads to a kick of the trailing particle. It describes the net momentum change perpendicular to $\mathbf{e}_z$.

Consider now a line charge density λ moving with constant velocity $\mathbf{v}$ on a trajectory parallel to the z-axis. The wake potential at a distance ζ with respect to a reference particle inside the bunch ($\mathbf{r}_{\perp} = \mathbf{r}_{s\perp}$) is obtained by convolving the charge density with the wake function [10]:

$$\mathbf{W}^{\lambda}(\mathbf{r}_{\perp} = \mathbf{r}_{s\perp}, \zeta) \;=\; \int_{-\infty}^{\infty} d\zeta' \lambda(\zeta')\, \mathbf{W}^{\delta}(\mathbf{r}_{\perp} = \mathbf{r}_{s\perp}, \zeta - \zeta')\,, \tag{1.16}$$

where the charge distribution is normalized to unity

$$\int_{-\infty}^{\infty} dz\, \lambda(z) \;=\; 1\,. \tag{1.17}$$

Therefore the wake function as the solution for a point-like source is the Green's function* for the wake potential of a line charge distribution.
The wake potential of a bunch with three-dimensional extension is calculated by superimposing the wake functions for different values of $\mathbf{r}_{s\perp}$, weighted by the transverse charge distribution $\lambda(\mathbf{r}_{s\perp})$.

In the above definitions the integration extends over an infinite length, while in a real machine all structures are of finite length. Some of the fields excited by a bunch may be confined to a limited region, for example resonant fields in a cavity whose frequency is below the cut-off frequency of the beam pipe, others propagate into the vacuum chamber.

A smooth pipe with regular cross section is interrupted by various devices like RF cavities, Higher Order Mode couplers, beam monitors, etc. The contribution of the wake fields to the wake potential for a single device in a beam-line can be calculated separately if the wake fields are dominantly confined to the considered device. In this case, the integration over the finite length L of the device can be extended to infinity and the above definition for the wake potential can be used.

*Two assumptions have been made : (1) the trajectory of the line charge distribution is unperturbed by its own wake fields, (2) the reaction of the environment due to the beam grows linear with the charge density (i.e non-linear reaction of the matter must be excluded).

In general, the integral along an infinite path has to be replaced by a finite integral:

$$\mathbf{W}^{\delta}(\mathbf{r}_{\perp},\mathbf{r}_{s\perp},\zeta) \;=\; \frac{1}{q_s}\int\limits_{-L/2}^{L/2} dz\,\left\{\mathbf{E}(\mathbf{r}_{\perp},\mathbf{r}_{s\perp},z,t) + v\,\mathbf{e}_z\times\mathbf{B}(\mathbf{r}_{\perp},\mathbf{r}_{s\perp},z,t)\right\}_{t=(z+\zeta)/v}\,. \quad (1.18)$$

The solution of the electromagnetic field in Eq. (1.18) depends on the boundary conditions and in addition on the electromagnetic field leaving the openings of the device. Thus, it is also depending on the devices that are already passed by the particles.

Wake forces generated by geometrical distortions or discontinuities of the surrounding are complicated functions of the coordinates z and t. The integration becomes simple for uniform pipes of infinite length. Then the fields propagate with the bunch as functions of the variable $(z-vt)$. The wake forces are constant along the beam-pipe and the wake potential grows linearly with the length L:

$$\mathbf{W}^{\delta}(\mathbf{r}_{\perp},\mathbf{r}_{s\perp},\zeta) \;=\; \frac{L}{q\,q_s}\,\mathbf{F}(\mathbf{r}_{\perp},\mathbf{r}_{s\perp},\zeta)\,. \quad (1.19)$$

In this cases, it is useful to introduce a wake function per unit length:

$$\frac{d\mathbf{W}^{\delta}(\mathbf{r}_{\perp},r_{s\perp},\zeta)}{dz} \;=\; \frac{1}{qq_s}\,\mathbf{F}(\mathbf{r}_{\perp},\mathbf{r}_{s\perp},\zeta)\,. \quad (1.20)$$

Using a wake function per unit length is justified if the transient effects (rise of the field before reaching a stationary field) and the diffraction effects (at the entrance of the beam pipe) can be neglected.

1.2.2 Panofsky-Wenzel Theorem

Using Faraday's law of induction

$$\mathbf{e}_z\times\partial_t\mathbf{B}_{\perp} \;=\; \partial_z\mathbf{E}_{\perp} - \nabla_{\perp}E_z$$

a relation between the transverse and the longitudinal wake potential can be derived in the following way*†:

$$\begin{aligned}
\partial_{\zeta}\,\mathbf{W}_{\perp}(\mathbf{r}_{\perp},\zeta) \;&=\; \frac{1}{q_s}\int\limits_{-L/2}^{L/2} dz\,\left\{\partial_{\zeta}\mathbf{E}_{\perp}(\mathbf{r}_{\perp},z,\frac{\zeta+z}{v}) + v\,\mathbf{e}_z\times\partial_{\zeta}\mathbf{B}_{\perp}(\mathbf{r}_{\perp},z,\frac{\zeta+z}{v})\right\}\\
&=\; \frac{1}{q_s}\int\limits_{-L/2}^{L/2} dz\,\left\{\frac{1}{v}\partial_t\mathbf{E}_{\perp}(\mathbf{r}_{\perp},z,\frac{\zeta+z}{v}) + \mathbf{e}_z\times\partial_t\mathbf{B}_{\perp}(\mathbf{r}_{\perp},z,\frac{\zeta+z}{v})\right\}\\
&=\; \frac{1}{q_s}\int\limits_{-L/2}^{L/2} dz\,\left\{\left(\partial_z+\frac{1}{v}\partial_t\right)\mathbf{E}_{\perp}(\mathbf{r}_{\perp},z,\frac{\zeta+z}{v}) - \nabla_{\perp}E_z(\mathbf{r}_{\perp},z,\frac{\zeta+z}{v})\right\}\\
&=\; \frac{1}{q_s}\int\limits_{-L/2}^{L/2} dz\,\left\{\frac{d}{dz}\mathbf{E}_{\perp}(\mathbf{r}_{\perp},z,\frac{\zeta+z}{v}) - \nabla_{\perp}E_z(\mathbf{r}_{\perp},z,\frac{\zeta+z}{v})\right\}\\
&=\; -\nabla_{\perp}W_{\parallel}(\mathbf{r}_{\perp},\zeta) + \frac{1}{q_s}\,\mathbf{E}_{\perp}(\mathbf{r}_{\perp},z,\frac{\zeta+z}{v})\Big|_{-L/2}^{L/2}\,. \qquad (1.21)
\end{aligned}$$

*The wake potential is assumed to be a differentiable function of the variables $\mathbf{r}_{\perp}$ and ζ.

†The dependence on the position of the source charge $\mathbf{r}_{s\perp}$ is not always written in the formulas.

If the transverse electric fields for a given ζ are equal at the beginning and the end of the structure the last term on the right hand side of Eq. (1.21) vanishes. The relation is then written

$$\partial_\zeta \mathbf{W}_\perp(\mathbf{r}_\perp, \zeta) \;=\; -\nabla_\perp W_\parallel(\mathbf{r}_\perp, \zeta) \tag{1.22}$$

and referred to as the Panofsky-Wenzel theorem [11]. The derivation only makes use of Faraday's law of induction. Consequently the theorem is also valid for non-relativistic particles. Integration of Eq. (1.22) with respect to ζ gives

$$\mathbf{W}_\perp(\mathbf{r}_\perp, \zeta) \;=\; -\nabla_\perp \int_{-\infty}^{\zeta} d\zeta' \, W_\parallel(\mathbf{r}_\perp, \zeta') \,, \tag{1.23}$$

one obtains the transverse wake potential from the longitudinal wake potential.

1.2.3 The Longitudinal Wake Potential as a Harmonic Function

In the previous section a general relation between the longitudinal and the transverse wake potential has been derived. Another important property of the longitudinal wake potential can be seen as follow. From the Maxwell equations and the vector identity

$$\nabla \times (\nabla \times \mathbf{E}) \;=\; \nabla(\nabla \cdot \mathbf{E}) - \triangle \mathbf{E}$$

one obtains for the electric field the equation:

$$\triangle \mathbf{E} - \partial_{ct}^2 \mathbf{E} \;=\; \frac{1}{\epsilon_0}\left(\nabla \rho + \frac{1}{c}\partial_{ct}\mathbf{j}\right) \quad \text{with} \quad \partial_{ct} \equiv \frac{1}{c}\frac{\partial}{\partial t} \,. \tag{1.24}$$

Since the charge distribution ρ is a function of the variable $(z - vt)$, the current is given by $\mathbf{j} = v\rho\,\mathbf{e}_z$. Using this, the time derivative of the current can be expressed by

$$\frac{1}{c}\partial_{ct}\mathbf{j}_z \;=\; -\frac{v^2}{c^2}\partial_z \rho \,. \tag{1.25}$$

The equation for the longitudinal electric fields can be written as:

$$\triangle_\perp E_z \;=\; -\left[\partial_z^2 - \partial_{ct}^2\right] E_z + \frac{1}{\epsilon_0 \gamma^2}\partial_z \rho \,, \tag{1.26}$$

where $\triangle_\perp$ denotes the 2-dimensional Laplacian acting on the transverse coordinates. If the quantities are now Fourier-transformed to the frequency and longitudinal wave number domain by:

$$f(\mathbf{r}_\perp, z, t) \;=\; \frac{1}{2\pi}\int_{-\infty}^{\infty} d\omega \int_{-\infty}^{\infty} dk \, \hat{f}(\mathbf{r}_\perp, k, \omega)\, e^{-i(kz - \omega t)} \tag{1.27}$$

the inhomogeneous wave equation reads:

$$\triangle_\perp \hat{E}_z \;=\; \left[k^2 - \left(\frac{\omega}{c}\right)^2\right] \hat{E}_z - \frac{ik}{\epsilon_0 \gamma^2}\hat{\rho} \,. \tag{1.28}$$

Integrating with respect to z yields:

$$\begin{aligned}\triangle_\perp W_\parallel(\mathbf{r}_\perp,\zeta) &= \frac{1}{q_s}\int_{-L/2}^{L/2} dz\, \triangle_\perp E_z(\mathbf{r}_\perp, z, \frac{z+\zeta}{v}) \qquad (1.29)\\ &= \frac{1}{2\pi q_s}\int_{-L/2}^{L/2} dz \int_{-\infty}^{\infty} d\omega \int_{-\infty}^{\infty} dk \left\{\left[k^2 - \left(\frac{\omega}{c}\right)^2\right]\hat{E}_z - \frac{ik}{\epsilon_0\gamma^2}\hat{\rho}\right\} e^{-i(k-\omega/v)z}\, e^{i(\omega/v)\zeta}\\ &= \frac{1}{2\pi q_s}\int_{-\infty}^{\infty} d\omega \int_{-\infty}^{\infty} dk \left\{\left[k^2 - \left(\frac{\omega}{c}\right)^2\right]\hat{E}_z - \frac{ik}{\epsilon_0\gamma^2}\hat{\rho}\right\} \left(\frac{\sin\left[(k-\omega/v)L/2\right]}{(k-\omega/v)/2}\right) e^{i(\omega/v)\zeta}.\end{aligned}$$

The ratio in the parentheses restricts the integral in the (k,ω)-plane to a small band along $k=\omega/v$ whose width is approximately given by $|k-\omega/v| \leq 2\pi/L$. Thus for a finite integration length L the contributions of electromagnetic fields to the wake potential consist also of waves which are not exactly co-propagating with the bunch (see Fig. 1.5).

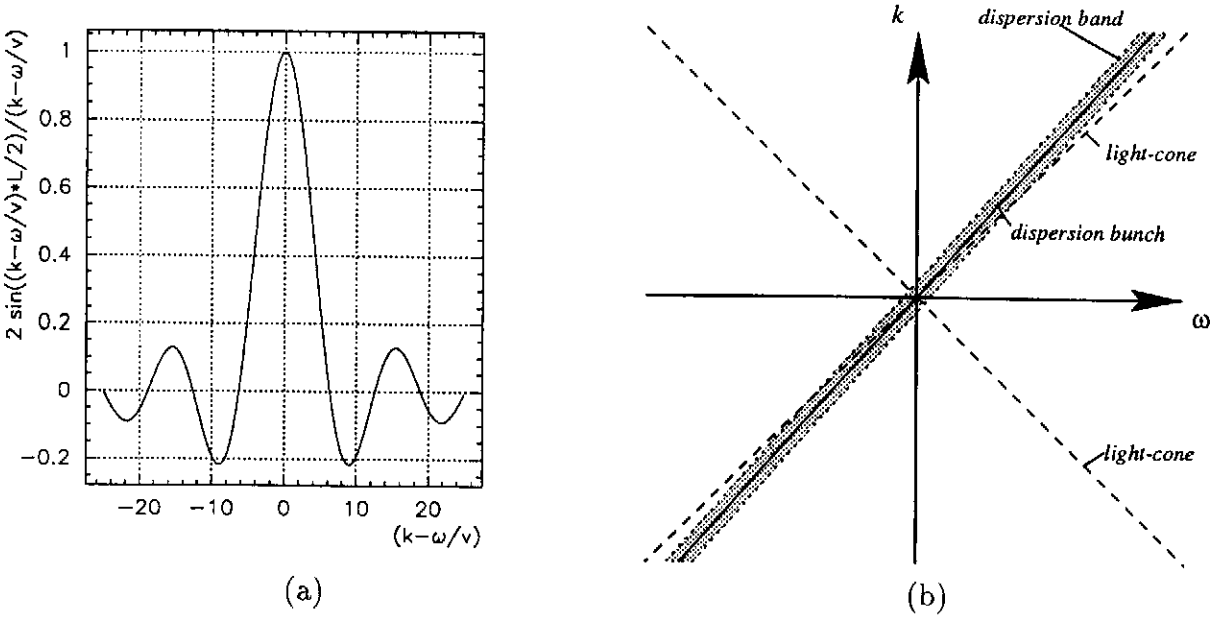

Figure 1.5: (a) Behaviour of the filter function in the parenthesis of Eq. (1.29) for $L = 1\text{m}$. (b) Scheme of the contributing integration area for a structure of finite length

Expanding the integral in Eq. (1.29) into an integral including the source ($\propto \hat{\rho}$) and an integral including the longitudinal electric field ($\propto \hat{E}_z$):

$$\triangle_\perp W_\parallel = \triangle_\perp W_\parallel^{(1)} + \triangle_\perp W_\parallel^{(2)}. \qquad (1.30)$$

Since the source ρ is a function of the combination $(z-vt)$ in the (z,t) domain the corresponding expression in the (k,ω) domain yields:

$$\begin{aligned}\hat{\rho}(k,\omega) &= \frac{1}{2\pi}\int_{-\infty}^{\infty} dz \int_{-\infty}^{\infty} dt\, \rho(z-vt)\, e^{i(kz-\omega t)} \\ &= \frac{1}{2\pi}\int_{-\infty}^{\infty} dz\, e^{i(k-\omega/v)z} \int_{-\infty}^{\infty} dt'\, \rho(-vt')\, e^{-i\omega t'} \\ &= \delta(k-\omega/v)\,\tilde{\rho}(\omega)\,, \end{aligned} \tag{1.31}$$

where $\tilde{\rho}$ is given by

$$\tilde{\rho}(\omega) = \int_{-\infty}^{\infty} dt\, \rho(-vt)\, e^{-i\omega t}\,. \tag{1.32}$$

Obviously, the relation between the wave number k and the frequency ω of the charge distribution is given by $\omega = vk$ with equal phase and group velocity v. Performing the integration with respect to the wave number k and the frequency ω in the integral representation for $\triangle_\perp W_\parallel^{(1)}$ one finds:

$$\begin{aligned}\triangle_\perp W_\parallel^{(1)}(\mathbf{r}_\perp,\zeta) &= -\frac{1}{2\pi q_s}\int_{-\infty}^{\infty} d\omega \frac{i\omega}{\epsilon_0 v\gamma^2}\tilde{\rho}(\omega)\, L\, e^{i(\omega/v)\zeta} \\ &= -\frac{L}{2\pi q_s \epsilon_0 \gamma^2}\int_{-\infty}^{\infty} d\omega\, i(\omega/v)\,\tilde{\rho}(\omega)\; e^{i(\omega/v)\zeta} \\ &= -\frac{L}{q_s\epsilon_0\gamma^2}\,\partial_\zeta \rho(r_{s\perp},\zeta) = \mathcal{O}\left(\gamma^{-2}\right)\,. \end{aligned} \tag{1.33}$$

Thus the contribution vanishes for $\gamma \to \infty$.
For finite but large pipe length ($L \gg 1$) one can write

$$\left(\frac{\sin\left[(k-\omega/v)L/2\right]}{(k-\omega/v)/2}\right) \approx 2\pi\,\delta(k-\omega/v) \quad (L \gg 1) \tag{1.34}$$

and therefore the 2-dimensional integral representation for $\triangle_\perp W_\parallel^{(2)}$ reduces to the integration along the dispersion relation of the bunch:

$$\begin{aligned}\triangle_\perp W_\parallel^{(2)}(\mathbf{r}_\perp,\zeta) &= \frac{1}{q_s}\int_{-\infty}^{\infty} d\omega \int_{-\infty}^{\infty} dk \left[k^2 - \left(\frac{\omega}{c}\right)^2\right] \hat{E}_z\,\delta(k-\omega/v)\, e^{i(\omega/v)\zeta} \\ &= \frac{1}{q_s}\int_{-\infty}^{\infty} d\omega \left(\frac{\omega}{v\gamma}\right)^2 \hat{E}_z(k=\omega/v,\omega)\, e^{i(\omega/v)\zeta}\,. \end{aligned}$$

For $\gamma \gg 1$ the dispersion line approaches the light cone and the integral is proportional to $1/\gamma^2$. Therefore one can write

$$\triangle_\perp W_\parallel^{(2)}(\mathbf{r}_\perp,\zeta) = 0 + \mathcal{O}(\gamma^{-2})\,, \tag{1.35}$$

which implies that in the ultra-relativistic limit the longitudinal wake potential $W_\parallel(\mathbf{r}_\perp,\zeta)$ is a harmonic function of the transverse coordinates:

$$\triangle_\perp W_\parallel(\mathbf{r}_\perp,\zeta) = 0 \qquad (\gamma \to \infty)\,. \tag{1.36}$$

1.2.4 Properties of the Wake Function in the Ultra-Relativistic Limit

The Panofsky-Wenzel theorem applies also to a delta-like excitation assuming that the integral on the right hand side of Eq. (1.23) exists. In the following an ultra-relativistic particle ($\gamma \to \infty$) and infinite beam pipes with equal cross sections for $z \to \pm\infty$ are considered.

Causality requires that a test charge moving in front of the source cannot experience a wake force. This implies that the wake function has to vanish for $\zeta < 0$. Directly behind the bunch the forces are repulsive [12]. With the definition for the wake function used here, the amplitude at very short distances is negative, implying an energy loss for the test charge:

$$W_{\parallel}(\zeta < 0) = 0\,, \qquad W_{\parallel}(0^+) \leq 0\,, \tag{1.37}$$

with $0^+ \equiv \lim_{\epsilon \to 0}\{0+\epsilon\}$. For point-like particles, the wake function at $\zeta = 0$ describes the energy transfer of the source charge to its environment. In the ultra-relativistic limit the wake function is not necessarily a continuous function at $\zeta = 0$.

Consider a continuous charge distribution with a finite length σ_z. The wake potential is obtained by convolving the charge distribution with the wake function

$$W^{\lambda}(\zeta, \sigma_z) = \int_{-\infty}^{\infty} d\zeta'\, \lambda(\zeta', \sigma_z)\, W^{\delta}(\zeta - \zeta') \qquad \text{with} \qquad \lim_{\sigma_z \to 0} \lambda(\zeta, \sigma_z) = \delta(\zeta)\,. \tag{1.38}$$

The energy loss of the bunch is obtained by integrating the wake potential weighted by the charge density:

$$\begin{aligned} k_{\parallel}(\sigma_z) &\equiv -\int_{-\infty}^{\infty} d\zeta\, \lambda(\zeta, \sigma_z)\, W^{\lambda}(\zeta) \\ &= -\int_{-\infty}^{\infty} d\zeta\, \lambda(\zeta, \sigma_z) \int_{-\infty}^{\infty} d\zeta'\, \lambda(\zeta', \sigma_z)\, W^{\delta}(\zeta - \zeta')\,. \end{aligned} \tag{1.39}$$

The loss factor of a charge distribution λ is a measure of the average energy loss per particle in the bunch. For sufficiently short bunches the wake function*can be approximated by $W(0^+)$. For the loss factor one finds [12]:

$$\begin{aligned} k_{\parallel}(\sigma_z) &\approx -W_{\parallel}^{\delta}(0^+) \int_{-\infty}^{\infty} dz\, \lambda(z, \sigma_z) \int_{-\infty}^{z} d\zeta\, \lambda(\zeta, \sigma_z) \\ &= -W_{\parallel}^{\delta}(0^+) \int_{-\infty}^{\infty} dz\, \frac{1}{2}\frac{d}{dz} \left(\int_{-\infty}^{z} d\zeta\, \lambda(\zeta, \sigma_z) \right)^2 \\ &= -W_{\parallel}^{\delta}(0^+)\, \frac{1}{2} \left(\int_{-\infty}^{z} d\zeta\, \lambda(\zeta, \sigma_z) \right)^2 \Bigg|_{-\infty}^{\infty} \\ &= -\frac{W_{\parallel}^{\delta}(0^+)}{2}\,. \end{aligned} \tag{1.40}$$

*Here is assume that at least the wake function is of bounded variation ($W_{\parallel} \in \mathrm{BV}$) on a finite closed interval including $\zeta = 0$.

With the above assumptions, the right side of the last equation becomes independent of the bunch length. Consequently the loss factor for sufficiently short bunches is just half the wake potential at $\zeta = 0^+$. Multiplied with the bunch charge this yields the energy transfer of the particle to the environment. This relation is also called the fundamental theorem of beam loading:

$$k_{\parallel}(0) \;=\; -\frac{W_{\parallel}^{\delta}(0^+)}{2}\,. \tag{1.41}$$

Consider now a test particle at a distance ζ with a charge q. If no energy is supplied from an external source into the structure the two-particle system never could gain energy. The energy loss of the source particle is $\triangle E_s = -q_s^2 W_{\parallel}^{\delta}(0)$ and the energy loss of the trailing particle is $\triangle E = -q^2 W_{\parallel}^{\delta}(0) - q_s q W_{\parallel}^{\delta}(\zeta)$ where the second term is caused by the leading particle. Therefore, in the case of $q = \pm q_s$ the energy budget reads:

$$\triangle E_s \;=\; -q_s^2\, W_{\parallel}^{\delta}(0) \qquad\qquad \triangle E \;=\; -q_s^2\,(W_{\parallel}^{\delta}(0) \pm W_{\parallel}^{\delta}(\zeta)) \tag{1.42}$$

and

$$\triangle E_s + \triangle E \;\leq\; 0$$

hence

$$|W_{\parallel}^{\delta}(\zeta)| \;\leq\; |W_{\parallel}^{\delta}(0^+)|\,. \tag{1.43}$$

The maximum and minimum amplitude of the wake function is bounded by the amplitude of the wake immediately behind the source charge. Hence, by the results Eq. (1.43) and Eq. (1.41) one can concluded that the wake function has to be discontinuous function at $\zeta = 0$ or it vanishes identically.

According to Eq. (1.16) the wake potential reduces for a uniform beam to the integral over the wake function. A small test charge inside the uniform beam cannot be accelerated. Otherwise the whole beam would gain energy all by itself. Therefore one can write

$$\int_0^{\infty} d\zeta\, W_{\parallel}^{\delta}(\zeta) \;\leq\; 0\,. \tag{1.44}$$

Due to the Panofsky-Wenzel theorem, the transverse wake function can be derived by integrating the transverse gradient of the longitudinal wake function. In contrast to the discontinuity of the longitudinal wake function at $\zeta = 0$ the transverse wake function is a continuous function of the distance and vanishes when the test charge approaches the source charge. This is caused by the requirement that the integrand vanishes for negative distances in order to preserve causality. It follows that a point charge does not experience any deflecting force due to self-generated fields. The amplitude for small $\zeta > 0$ increases monotonically. For ultra-short bunches the longitudinal forces are dominant, while the transverse forces become negligible small.

1.3 Impedance

1.3.1 Definition of the Impedances

The wake potential is expressed as a function of the distance ζ. For high energies the bunch can be assumed to be rigid and moves with a constant velocity $v = \beta c$, ($\beta \approx 1$)

through the vacuum chamber. Either time or distance can therefore be used to describe the wake potential.

Introducing a variable $\tau = \zeta/\beta c$ as the time difference between the source and the test charge. The Fourier transform of the longitudinal wake function with respect to τ defines the impedance or so-called coupling impedance:

$$Z_{\parallel}(\mathbf{r}_{\perp}, \mathbf{r}_{s\perp}, \omega) \equiv -\int_{-\infty}^{\infty} d\tau\, W_{\parallel}^{\delta}(\mathbf{r}_{\perp}, \mathbf{r}_{s\perp}, \zeta = \beta c\tau)\, e^{i\omega\tau}\,. \tag{1.45}$$

Changing the variables from τ to ζ one finds the definition for the impedance given by [10]:

$$Z_{\parallel}(\mathbf{r}_{\perp}, \mathbf{r}_{s\perp}, \omega) \equiv \frac{-1}{\beta c}\int_{-\infty}^{\infty} d\zeta\, W_{\parallel}^{\delta}(\mathbf{r}_{\perp}, \mathbf{r}_{s\perp}, \zeta)\, e^{i(\omega/\beta c)\zeta}\,. \tag{1.46}$$

The wake function in the time domain or the impedance in the frequency domain describes the interaction of the beam with its environment.

It is often useful to examine the impulsive excitation of the various elements in the frequency domain. For cavities the spectra usually contain a number of sharp peaks in the lower frequency range, corresponding to the resonance frequencies of the cavity (see Fig. 1.6). At higher frequencies the impedance shows a smooth continuous spectrum of the beam pipe modes, which determines the behaviour of the short-range wake fields acting on the bunch itself.

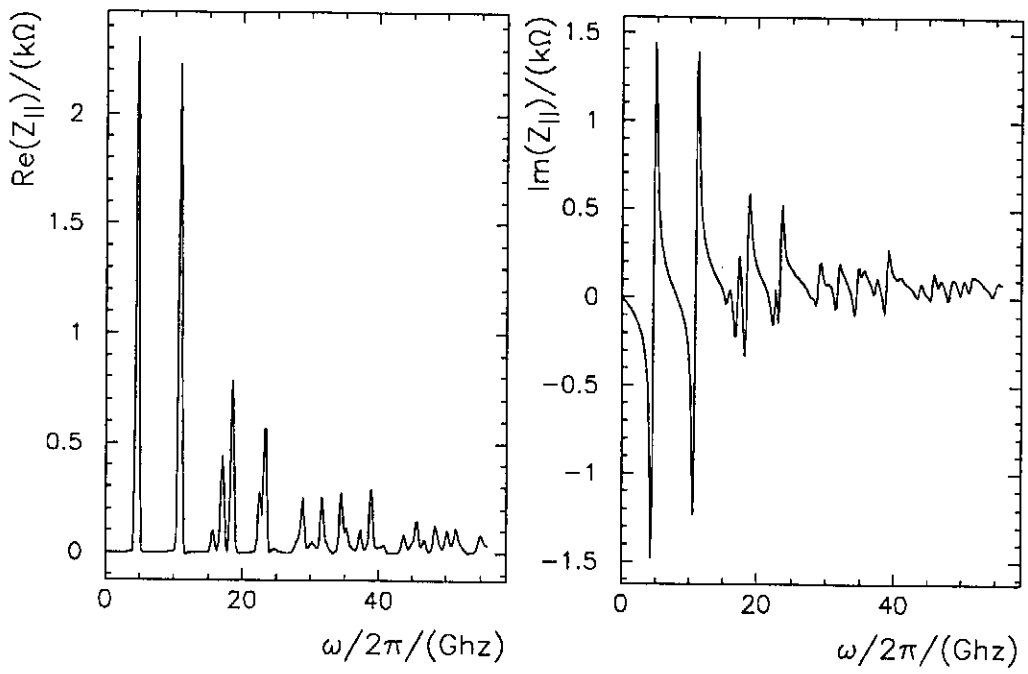

Figure 1.6: Real and imaginary part of the impedance of a cavity.

The transverse impedance is defined by:

$$\mathbf{Z}_{\perp}(\mathbf{r}_{\perp}, \mathbf{r}_{s\perp}, \omega) \equiv \frac{-i}{\beta c}\int_{-\infty}^{\infty} d\zeta\, \mathbf{W}_{\perp}(\mathbf{r}_{\perp}, \mathbf{r}_{s\perp}, \zeta)\, e^{i(\omega/\beta c)\zeta}\,. \tag{1.47}$$

The additional factor $(-i)$ is introduced for convenience to obtain equivalent formulas for the longitudinal and the transverse beam instabilities [9]. If the impedance is known over the whole frequency range the wake function is obtained by the inverse Fourier transform. According to the definition in Eq. (1.46) and Eq. (1.47) one can write

$$W_{\parallel}^{\delta}(\mathbf{r}_{\perp},\mathbf{r}_{s\perp},\zeta) \;=\; -\frac{1}{2\pi}\int_{-\infty}^{\infty} d\omega\, Z_{\parallel}(\mathbf{r}_{\perp},\mathbf{r}_{s\perp},\omega)\, e^{-i(\omega/\beta c)\zeta}\,, \tag{1.48}$$

for the longitudinal wake function and

$$\mathbf{W}_{\perp}^{\delta}(\mathbf{r}_{\perp},\mathbf{r}_{s\perp},\zeta) \;=\; \frac{i}{2\pi}\int_{-\infty}^{\infty} d\omega\, \mathbf{Z}_{\perp}(\mathbf{r}_{\perp},\mathbf{r}_{s\perp},\omega)\, e^{-i(\omega/\beta c)\zeta}\,. \tag{1.49}$$

for the transverse wake function.

The Panofsky-Wenzel theorem written in the frequency domain yields:

$$\frac{\omega}{\beta c}\,\mathbf{Z}_{\perp}(\mathbf{r}_{\perp},\mathbf{r}_{s\perp},\omega) \;=\; \nabla_{\perp} Z_{\parallel}(\mathbf{r}_{\perp},\mathbf{r}_{s\perp},\omega)\,, \tag{1.50}$$

which can be obtained by substituting $\partial_{\zeta} \rightarrow -i\omega/\beta c$ in Eq. (1.22). Note that the transverse gradient acts at the position of the test charge and not at the location of the source.

For a line charge distribution λ the wake potential is obtained from the impedance by applying the convolution theorem (see Eq. (1.16))

$$W_{\parallel}^{\lambda}(\mathbf{r}_{\perp}=\mathbf{r}_{s\perp},\zeta) \;=\; -\frac{1}{2\pi}\int_{-\infty}^{\infty} d\omega\, \tilde{\lambda}(\omega)\, Z_{\parallel}(\mathbf{r}_{\perp}=\mathbf{r}_{s\perp},\omega)\, e^{-i(\omega/\beta c)\zeta}\,, \tag{1.51}$$

with $\tilde{\lambda}(\omega) = \int_{-\infty}^{\infty} d\zeta' \lambda(\zeta') \exp\left[-(\omega/\beta c)\zeta'\right]$ the Fourier transform of λ. In particular for a bunch with longitudinal Gaussian distribution of rms-length σ_z the above equation reads:

$$W_{\parallel}^{\lambda}(\mathbf{r}_{\perp}=\mathbf{r}_{s\perp},\zeta) \;=\; -\frac{1}{2\pi}\int_{-\infty}^{\infty} d\omega\, e^{-\omega^2\sigma_z^2/(2\beta^2c^2)}\, Z_{\parallel}(\mathbf{r}_{\perp}=\mathbf{r}_{s\perp},\omega)\, e^{-i(\omega/\beta c)\zeta}\,. \tag{1.52}$$

Obviously, the integrand is damped exponentially for frequencies above $\omega_b = \beta c/\sigma_z$, which is sometimes referred to as "cut-off" frequency of the bunch.

1.3.2 Properties of the Impedance

The wake potential is a real function of the distance ζ while the impedance is a complex function of ω, and hence can be written:

$$Z_{\parallel}(\omega) \;=\; Z_{\parallel,r}(\omega) \,+\, i\, Z_{\parallel,i}(\omega)\,. \tag{1.53}$$

It can be shown that the real part is an even function of frequency while the imaginary part has to be odd. For that, the exponential function Eq. (1.48) is expanded into its

real and imaginary part and the different terms are grouped together. One finds:

$$\begin{aligned} W_{\parallel}^{\delta}(\zeta) &= -\frac{1}{2\pi}\int_{-\infty}^{\infty} d\omega\, Z_{\parallel}(\omega)\, e^{i(\omega/\beta c)\zeta} \\ &= -\frac{1}{2\pi}\int_{-\infty}^{\infty} d\omega \left[Z_{\parallel,r}(\omega)\, \cos\left(\frac{\omega}{\beta c}\zeta\right) - Z_{\parallel,i}(\omega)\, \sin\left(\frac{\omega}{\beta c}\zeta\right)\right] \\ &+ \frac{i}{2\pi}\int_{-\infty}^{\infty} d\omega \left[Z_{\parallel,r}(\omega)\, \sin\left(\frac{\omega}{\beta c}\zeta\right) + Z_{\parallel,i}(\omega)\, \cos\left(\frac{\omega}{\beta c}\zeta\right)\right] \end{aligned} \tag{1.54}$$

that imaginary part vanishes for all ζ if and only if the following conditions hold:

$$\begin{aligned} Z_{\parallel,r}(\omega) &= Z_{\parallel,r}(-\omega) \\ Z_{\parallel,i}(\omega) &= -Z_{\parallel,i}(-\omega)\,. \end{aligned} \tag{1.55}$$

Using Eq. (1.55) one can introduce an even and an odd wake function which are related to the real and the imaginary part of the impedance as:

$$W_{\parallel}^{e}(\zeta) = -\frac{1}{2\pi}\int_{-\infty}^{\infty} d\omega\, Z_{\parallel,r}(\omega)\, \cos\left(\frac{\omega}{\beta c}\zeta\right) \tag{1.56}$$

$$W_{\parallel}^{o}(\zeta) = \frac{1}{2\pi}\int_{-\infty}^{\infty} d\omega\, Z_{\parallel,i}(\omega)\, \sin\left(\frac{\omega}{\beta c}\zeta\right)\,. \tag{1.57}$$

Obviously the integral over ζ vanishes for a purely imaginary impedance. The forces exerted on a bunch are then of conservative nature. An example is the impedance caused by the longitudinal space-charge effect in a perfectly conducting beam pipe (see section 2.1.2).

Relation to the loss factor

For $\zeta = 0$, the odd wake function $W_{\parallel}^{o}$ vanishes. Thus according to the definition of the loss factor $k_{\parallel}^{\delta}$, only the even part of the impedance contributes to the energy loss of a particle:

$$k_{\parallel}^{\delta} = -W_{\parallel}^{\delta}(0) = \frac{1}{\pi}\int_{0}^{\infty} d\omega\, Z_{\parallel,r}(\omega)\,. \tag{1.58}$$

Therefore the real part of the impedance describes the frequency spectrum of energy loss for a unit point charge. It is also called the resistance while the imaginary part is sometimes referred to as reactance [13]. The complex impedance can be thought of as the complex power spectrum related to the energy loss [9].

According to Eqs. (1.39, 1.51) the loss factor of a bunch is written as:

$$k_{\parallel}(\sigma_z) = \frac{1}{\pi}\int_{0}^{\infty} d\omega\, |\tilde{\lambda}(\omega)|^2\, Z_{\parallel,r}(\omega)\,. \tag{1.59}$$

For a longitudinal Gaussian distribution with rms-length σ_z this becomes:

$$k_{\|}(\sigma_z) \;=\; \frac{1}{\pi}\int_0^\infty d\omega\; e^{-\omega^2\sigma_z^2/(\beta^2c^2)}\; Z_{\|,r}(\omega)\;. \tag{1.60}$$

Ultra-relativistic limit

Furthermore, in the particular case of $\beta = 1$, the wake function must vanish for negative distances ($\zeta < 0$) to guarantee causality. This is only possible if the even and the odd part of the wake function cancel each other ($W^e_{\|}(\zeta < 0) = -W^o_{\|}(\zeta < 0)$) for a test charge moving in front of the source charge. In terms of impedance, the relation becomes:

$$\int_{-\infty}^{\infty} d\omega\; Z_{\|,r}(\omega)\,\cos\left(\frac{\omega}{\beta c}\zeta\right) \;=\; \int_{-\infty}^{\infty} d\omega\; Z_{\|,i}(\omega)\,\sin\left(\frac{\omega}{\beta c}\zeta\right) \qquad (\zeta < 0,\; \beta = 1)\,. \tag{1.61}$$

1.3.3 Equivalent-Circuit Models

Equation (1.61) shows a general property of the impedance in the ultra-relativistic limit ($\beta = 1$). This relation is equivalent to a Hilbert transform relating the real and the imaginary parts of a network impedance [9], [12]. Therefore a network can be found which approximates the impedance of the vacuum chamber. The impulsive excitation of the chamber by a point-like current can then be interpreted as an impulsive excitation by a current source of an equivalent circuit. For example a single Higher Order Mode in an RF-cavity can be represented by a parallel resonance circuit (see Fig. 1.7).

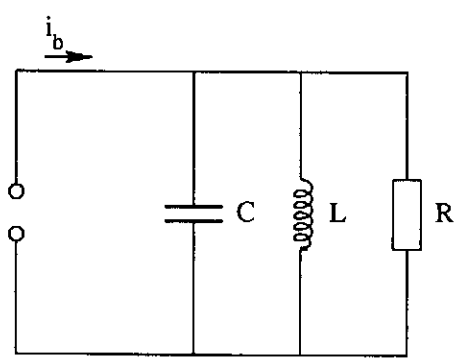

Figure 1.7: Parallel resonance circuit consisting of a capacitor, a coil, and a resistor.

The differential equation for the voltage $V(\tau)$ of a circuit reads ($\tau = \zeta/c$):

$$V''(\tau) + \frac{1}{RC}V'(\tau) + \frac{1}{LC}V(\tau) \;=\; 0\,, \tag{1.62}$$

and the impedance of this circuit is written:

$$Z(\omega) \;=\; \frac{R}{1 + iQ\left(\frac{\omega_r}{\omega} - \frac{\omega}{\omega_r}\right)}\,. \tag{1.63}$$

where ω_r denotes the resonance frequency and Q the quality factor of the circuit;

$$\omega_r = \frac{1}{\sqrt{C\,L}}, \qquad Q = \frac{\omega_r}{2\,\Gamma}, \qquad \Gamma = \frac{1}{2\,R\,C}. \tag{1.64}$$

The real (imaginary) part of this impedance is indeed an even (odd) function of the frequency.

In order to obtain the wake function one can use the impedance of a parallel resonance circuit as a model for the impedance of a single mode in a cavity. For that purpose the impedance has to be evaluated at the two singularities $\omega_{1/2} = -i\Gamma \pm \overline{\omega}_r$ with $\overline{\omega}_r = \sqrt{\omega_r^2 - \Gamma^2}$. Integrating the impedance with respect to τ (Eq. (1.48)) under consideration of the integration paths shown in Fig. 1.8 the wake function yields:

$$W_{\parallel}^{\delta}(\tau) = -\frac{e^{-\Gamma\tau}}{C}\left\{\cos\left(\overline{\omega}_r\tau\right) - \frac{\Gamma}{\overline{\omega}_r}\sin\left(\overline{\omega}_r\tau\right)\right\}\theta(\tau). \tag{1.65}$$

The function θ designates the Heaviside step function that vanishes for negative argu-

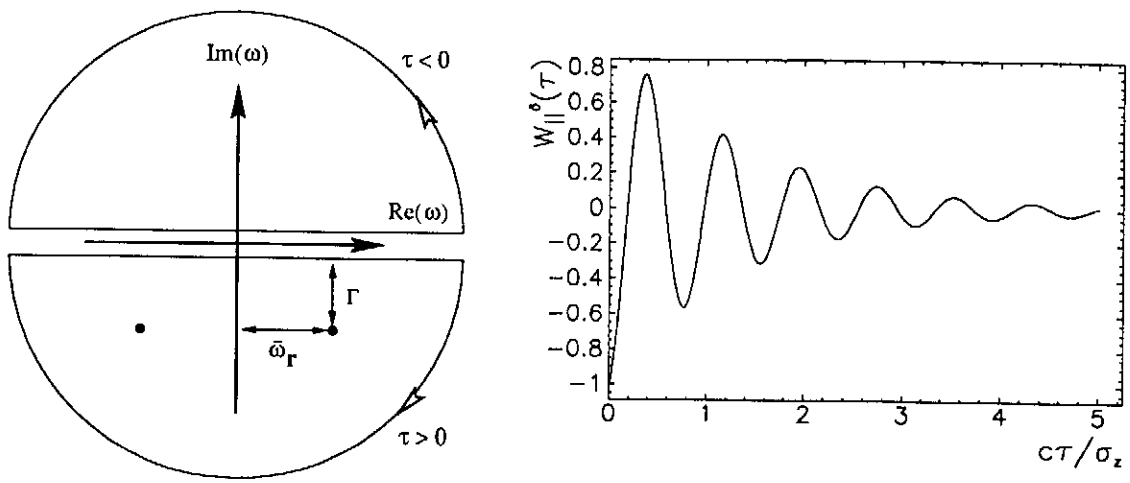

Figure 1.8: (a) Integration path of the inverse Fourier transformation for $\tau < 0$ and $\tau > 0$. The area in the upper half does not contain any singularities and the contribution for negative times vanishes. (b) Behaviour of the wake function for a single mode in a cavity.

ments and is equal to unity for positive values. The solution is a damped oscillation for $\tau > 0$ with a frequency $\overline{\omega}_r$ and a the damping factor Γ. These two quantities determine the behaviour of the solution and can be directly obtained form the real and imaginary part of the poles in the complex frequency plane, respectively.

If the poles are close to the real axis (small Γ) then the wake function undergoes many oscillations before the amplitude can be neglected. This corresponds to a mode in a cavity of high quality factor Q, where the electromagnetic energy stored in the cavity is slowly dissipated on the wall*. In case of poles which are far away from the real axis the mode is

*Usually Higher Order Mode couplers are used in order to suppress these oscillations. The quality factor of a single mode is then well approximated by an external Q_{ext}. For the acceleration mode of a super-conducting cavity the main coupler determines the quality factor of the mode.

heavily damped. Then the oscillation of the wake function vanishes rapidly and the corresponding Q value is small. For poles having a large distance to the imaginary axis the wake fields oscillate with a high frequency and form the short-range shape of the wake function.

Wake potential of a single mode

It is customary to characterize a wake potential as inductive, resistive or capacitive if the impedance of the equivalent circuit in the frequency range relevant for the bunch is dominated by L, R or C, respectively. It is useful to decompose the impedance into its real and imaginary part:

$$\mathrm{Re}(Z_{\|}(\omega)) = \frac{1}{C}\frac{2\Gamma\omega^2}{(\omega^2-\omega_r^2)^2+(2\Gamma\omega)^2}\,, \tag{1.66}$$

$$\mathrm{Im}(Z_{\|}(\omega)) = \frac{1}{C}\frac{(\omega^2-\omega_r^2)\,\omega}{(\omega^2-\omega_r^2)^2+(2\Gamma\omega)^2}\,. \tag{1.67}$$

The wake potential of a Gaussian-distributed bunch for a single mode can be written as (see Eq. (1.65)):

$$W_{\|}(\zeta) = -\frac{1}{\sqrt{2\pi}\,\sigma_z}\int_0^\infty d\zeta'\, e^{-(\zeta-\zeta')^2/(2\sigma_z^2)}\,\frac{e^{-\Gamma\zeta'/c}}{C}\left\{\cos(\overline{\omega}_r\zeta'/c)-\frac{\Gamma}{\overline{\omega}_r}\sin(\overline{\omega}_r\zeta'/c)\right\} \tag{1.68}$$

or, using Eq. (1.51) and Eq. (1.63), as:

$$W_{\|}(\zeta) = -\frac{1}{2\pi}\int_{-\infty}^{\infty} d\omega\, e^{-\omega^2\sigma^2/(2c^2)}\,\frac{1}{C}\,\frac{i\,\omega}{\omega^2-\omega_r^2+i\,2\Gamma\omega}\,e^{-i\omega\zeta/c}\,. \tag{1.69}$$

The two integral representations for the wake potential cannot be solved analytically. However, the integrals can be approximately solved in case of inductively, resistively or capacitively dominated wake potentials:

- **Inductive wake potential:** The resonance frequency ω_r is far above the "cut-off" frequency $\omega_b = c/\sigma_z$ of the bunch. The impedance is dominated by its negative imaginary part which grows proportional to ω in the frequency range of the bunch. The wake fields transfer energy from the head to the tail of the bunch. The overall energy loss is proportional to the real part of the impedance and can be neglected. The shape of the wake potential is approximately given by the gradient of the current:

$$\mathrm{Im}(Z_{\|}(\omega)) \propto -\omega \quad \Rightarrow \quad W_{\|} \propto -\lambda' \propto \sigma_z^{-2} \quad (\text{for} \quad \omega_r \gg \omega_b)\,. \tag{1.70}$$

- **Resistive wake potential:** The impedance is given by a broad band resonator at a frequency close to ω_b. The real part of the impedance dominates while the imaginary part switches sign for frequencies below ω_r and frequencies above ω_r which partly cancel each other. The shape of the wake potential for resistive impedance can be approximated by the shape of the charge distribution itself:

$$\mathrm{Re}(Z_{\|}(\omega)) \approx \text{const.} \quad \Rightarrow \quad W_{\|} \propto -\lambda \propto \sigma_z^{-1} \quad (\text{for} \quad \omega_r \simeq \omega_b)\,. \tag{1.71}$$

- **Capacitive wake potential:** The resonance frequency is much lower than ω_b and the impedance is dominated by the capacitor $\propto i/\omega$ while the real part due to the resistivity is proportional to $1/\omega^2$. The resulting shape of the wake potential is approximately proportional to the integration of the charge distribution:

$$\mathrm{Im}(Z_{\|}(\omega)) \propto \omega^{-1} \quad \Rightarrow \quad W_{\|} \propto -\int_z^{\infty} dz' \, \lambda \propto \sigma_z^0 \quad (\text{for} \quad \omega_r \ll \omega_b) \, . \tag{1.72}$$

The impedance, the wake function, and the resulting wake potential in the above cases are shown in Fig. 1.9. Note that the amplitudes of the wake functions are equal for $\zeta = 0^+$. The resonance frequencies and the quality factors for the single modes of a cavity can be determined experimentally. The amplitude of the wake function Eq. (1.65) at $\zeta = 0^+$ is inversely proportional to the capacitance C, which is not given by Q and Γ. It describes the coupling of the beam to the cavity mode and is given by the geometry of the cavity. The fundamental theorem of beam-loading theorem states that the capacitance is uniquely related to the loss factor by:

$$\frac{1}{C} \;=\; 2\, k_{\|}^{\delta} \, . \tag{1.73}$$

The complex voltage V induced by a charge in the cavity can by calculated by:

$$V(\mathbf{r}_{s\perp}) \;=\; \int dz \, E_{\|}(\mathbf{r}_{s\perp}, z)\, e^{-i\omega_r z/c} \, , \tag{1.74}$$

where the electric field is integrated along the trajectory of the charge. Together with the energy U stored in this mode,

$$U \;=\; \frac{\epsilon_0}{2} \int_V d^3r \, |\mathbf{E}(\mathbf{r})|^2 \tag{1.75}$$

one can obtained the loss factor $k_{\|}^{\delta}$ by [14]:

$$k_{\|}^{\delta} \;=\; \frac{|V|^2}{4\,U} \, . \tag{1.76}$$

Now all parameters of the electric circuit L, R and C can be determined from the loss factor $k_{\|}^{\delta}$, the resonance frequency ω_r and the quality factor Q of the considered mode.

Often, a mode of a cavity is characterize by its shunt impedance R_{sh} instead of the loss factor:

$$\omega_r \frac{R_{sh}}{Q} \;=\; 2\, k_{\|}^{\delta} \tag{1.77}$$

while the important value for beam dynamics is given by R_{sh}/Q.

Wake potential for a large number of modes

A cavity can be excited by a large number of modes. Each mode can be represented by a pair of singularities in the complex plane with opposite sign for the real parts. The impedance for $v = c$ is an analytic function of the frequency in the upper half plane in

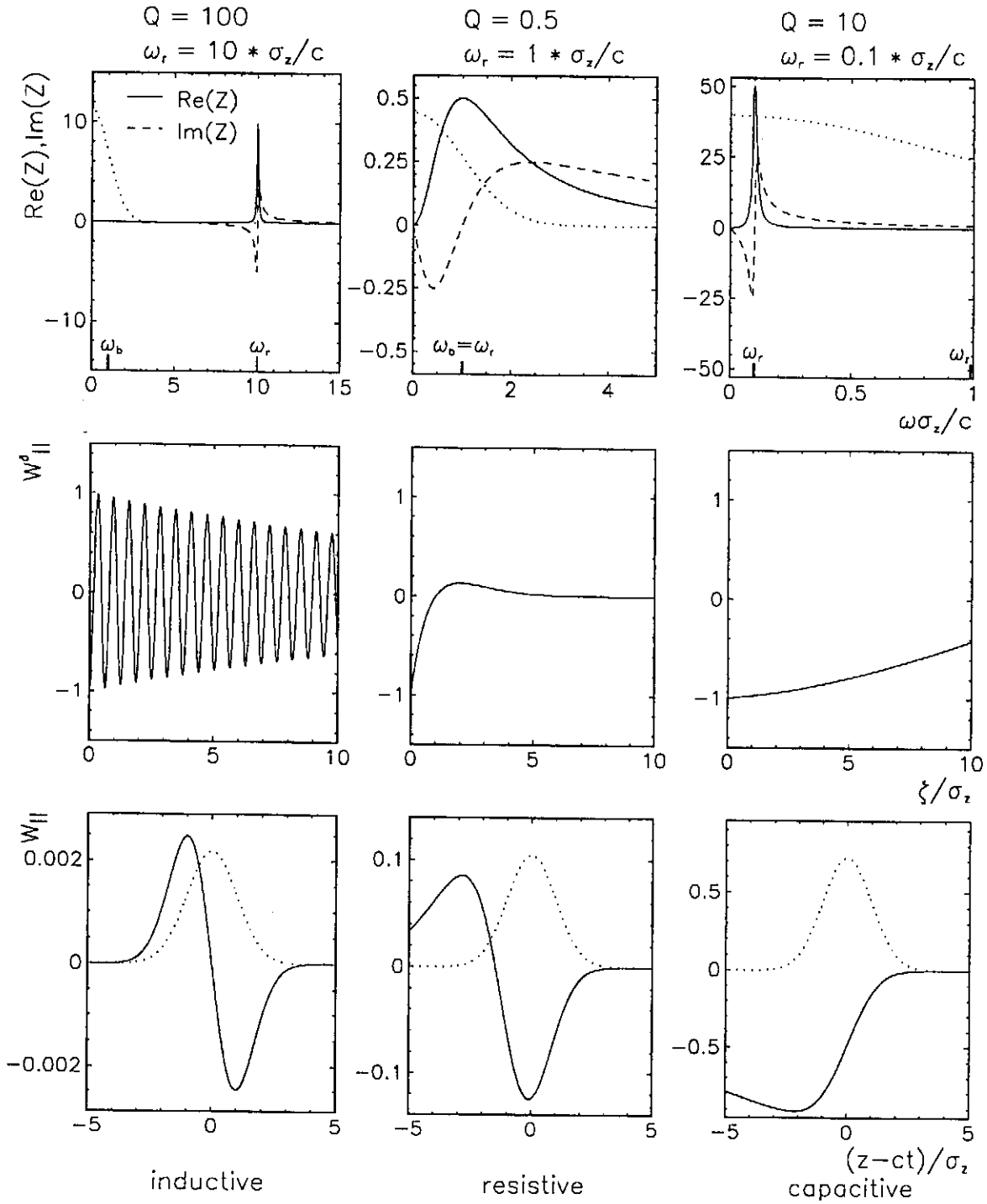

Figure 1.9: Impedance, wake function and wake potential for single modes acting mainly inductively, resistively or capacitively on the bunch. The dotted curves indicate the bunch distribution in frequency domain (first row of plots) and in time domain (last row of plots).

order to guarantee causality, and has simple poles in the lower half plane. A mode n can be described by either (L_n, R_n, C_n) or $(k_{n,||}, Q_n, \omega_n)$ which determines the impedance $Z_{n,||}$

and the wake function $W^{\delta}_{n,\|}$, respectively.

The wake potential $W_{\|}$ of a line-charge distribution is obtained by the sum of the wake potentials $W_{n,\|}$ for the single modes. Hence, one can write:

$$W_{\|}(\zeta) = \sum_{n=0}^{N} W_{n,\|}(\zeta) = \sum_{n=0}^{N} \int_{-\infty}^{\infty} d\zeta\, \lambda(\zeta - \zeta')\, W^{\delta}_{n,\|}(\zeta') \tag{1.78}$$

with

$$W^{\delta}_{n,\|}(\zeta) = -2\, k_{n,\|}\, e^{-\Gamma_n \zeta/c} \left\{ \cos\left(\overline{\omega}_{r,n}\zeta/c\right) - \frac{\Gamma_n}{\overline{\omega}_{r,n}} \sin\left(\overline{\omega}_{r,n}\zeta/c\right) \right\} . \tag{1.79}$$

The number of modes N to be considered grows with decreasing bunch length and for very short bunches the numerical calculations become difficult.

The transverse wake potential is obtained from the wake potential by applying the Panofsky-Wenzel theorem. Thus only these wake potentials $W_{n,\|}$ contribute to the transverse wake potential that are dependent on $\mathbf{r}$.

Not all structure can be treated by using an equivalent circuit model. For instance the resistive wall wake fields of a round pipe has a different approach, and the behaviour of the impedance varies from that of a parallel resonance circuit. Nevertheless, as will be derived in the next chapter, the main contribution can also be described by a high-frequency broad-band resonator.

1.4 Structures with Cylindrical Symmetry

1.4.1 Multipole Expansion

In the previous section the boundary conditions have not been specified. Consider now an axisymmetric structure and point-like source and test charges moving on trajectories parallel to the symmetry axis. A cylindrical coordinate system (r, ϕ, z) is used with the symmetry axis of the structure at $r = 0$. Let $(r_s, \phi_s, z_s = \beta ct)$ be the coordinates of the leading charge and $(r, \phi, z = \beta ct - \zeta)$ those of the trailing one. The azimuthal angle for the leading charge can be assumed to be zero ($\phi_s = 0$).

The charge density ρ_s written in cylindrical coordinates reads:

$$\rho_s(r, \phi, z, t) = \frac{q_s}{r}\, \delta(r - r_s)\, \delta(\phi)\, \delta(z - z_s) . \tag{1.80}$$

Exploiting the azimuthal periodicity one can expend $\delta(\phi)$ as

$$\delta(\phi) = \frac{1}{2\pi} \sum_{m=-\infty}^{\infty} e^{im\phi} = \frac{1}{2\pi} \sum_{n=0}^{\infty} (2 - \delta_{n,0}) \cos(n\phi) . \tag{1.81}$$

This yields the multipole expansion of the charge density:

$$\rho_s(r, \phi, z, t) = \sum_{n=0}^{\infty} \rho_n(r, \phi, z, t) \tag{1.82}$$

with

$$\rho_n = q_s \frac{(2 - \delta_{n,0})}{2\pi r}\, \delta(r - r_s)\, \delta(z - z_s) \cos(n\phi) . \tag{1.83}$$

According to the above expression a charge that moves down a pipe with an offset r_s with respect to the symmetry axis can be thought of as a superposition of charged rings with an angular dependence $\cos(n\phi)$. The rings are infinitesimally extended in the radial $[r_s, r_s + \delta r]$ and in the longitudinal direction $[z_s, z_s + \delta z]$. The monopole term $n = 0$ describes a charged ring with uniform density while the dipole term is proportional to $\cos(\phi)$ and consists of a positive charged half ring for $\phi \in (-\pi/2, +\pi/2)$ as well as a negative charged half ring for $\phi \in (\pi/2, 3\pi/2)$.
Consider now as a source a ring with multipole moment n traveling through a cylindrical pipe. Due to the symmetry, the charges induced by the beam at the wall of the vacuum chamber must have the same angular dependence proportional to $\cos(n\phi)$.

One can show that this also applies to the longitudinal wake function. Consequently the wake function can be decomposed with respect to the azimuthal moments [9]:

$$\begin{aligned} W^{\delta}_{\parallel}(\mathbf{r}_\perp, \mathbf{r}_{s\perp}, \zeta) &= \sum_{n=0}^{\infty} W^{\delta}_{n,\parallel}(\mathbf{r}_\perp, \mathbf{r}_{s\perp}, \zeta) \\ W^{\delta}_{n,\parallel}(\mathbf{r}_\perp, \mathbf{r}_{s\perp}, \zeta) &= \overline{W}^{\delta}_{n,\parallel}(r, r_s, \zeta)\, \cos(n\phi) \end{aligned} \tag{1.84}$$

The longitudinal wake function $\overline{W}_{n,\parallel}$ is a Green's function for a ring-like charge distribution with a well defined even angular dependence. Each of the wake functions $\overline{W}^{\delta}_{n,\parallel}$ for the various multipoles n depends only on the radius of the source ring r_s, the radial position of the test charge r, and the longitudinal distance ζ between them.

Consider next a source with transverse expansion given by a charge distribution $\rho_\perp$,

$$\rho_s(r, \phi, z, t) = q_s\, \rho_\perp(r, \phi)\, \delta(z - z_s) \tag{1.85}$$

which is normalized to unity,

$$\int_0^{\infty} r\, dr \int_0^{2\pi} d\phi\, \rho_\perp(r, \phi) = 1\,. \tag{1.86}$$

The charge distribution can be rewritten as:

$$\rho_\perp(r, \phi) = \sum_{n=0}^{\infty} \frac{2 - \delta_{n,0}}{2\pi} \left\{ R^o_n(r)\, \sin(n\phi) + R^e_n(r)\, \cos(n\phi) \right\}\,. \tag{1.87}$$

where R^o_n (R^e_n) describes the n^{th} odd (even) multipole moment of the transverse charge density. If the wake functions $\overline{W}^{\delta}_{n,\parallel}$ are known for all multipoles n, then by superposition the wake function for an impulsive excitation with transverse extension $\rho_\perp$ can be calculated by:

$$W_{\parallel}(r, \phi, \zeta) = \sum_{n=0}^{\infty} \int_0^{\infty} dr_s\, r_s \left\{ R^o_n(r_s)\, \sin(n\phi) + R^e_n(r_s)\, \cos(n\phi) \right\} \overline{W}_{n,\parallel}(r, r_s, \zeta)\,. \tag{1.88}$$

The wake potential for a bunch with a longitudinal extension is found according to Eq. (1.16), by convolving the longitudinal charge distribution with the solution obtained for the transverse charge density. In this case the functions $R^{o,e}_n$ depend also on ζ ($R^{o,e}_n(r, \zeta)$).

1.4.2 Ultra-Relativistic Limit

The electromagnetic field of a source charge is the solution of the Maxwell equations including the boundary conditions. In order to fulfill the boundary conditions an additional electromagnetic field is superimposed to the field generated by a charge in free space. The additional fields are solution of the homogeneous Maxwell equations. Using the results in section 1.2.3 for $\hat{\rho} = 0$ and $k = \omega/v$ the Fourier component of the longitudinal electric field moving synchronously with the charge obeys the Lorentz contracted equation:

$$\nabla_\perp^2 \tilde{E}_z - \left(\frac{\omega}{\beta c \gamma}\right)^2 \tilde{E}_z = 0 . \tag{1.89}$$

In case of ultra-relativistic particles ($\gamma \to \infty$) the equation reduces to a two dimensional potential problem for the longitudinal electric field:

$$\nabla_\perp^2 \tilde{E}_z = 0 . \tag{1.90}$$

The solution of the above equation in cylindrical coordinates leads to the following radial dependence of the wake function [14] :

$$\overline{W}_{n,\parallel}(r, r_s, \zeta) = r^n r_s^n \overline{\overline{W}}_{n,\parallel}(\zeta) . \tag{1.91}$$

The strength of the monopole term $n = 0$ is independent on the radial position of the source charge as well as on the witness charge. This simplifies the calculation of the longitudinal monopole wake function.

1.4.3 Transverse Wake Function

The transverse wake expanded in a series of multipoles reads [9]:

$$\mathbf{W}_\perp(\mathbf{r}_\perp, \mathbf{r}_{s\perp}, \zeta) = \sum_{n=1}^{\infty} \mathbf{W}_{\perp,n}(\mathbf{r}_\perp, \mathbf{r}_{s\perp}, \zeta) . \tag{1.92}$$

For $\gamma \to \infty$ and according to the Panofsky-Wenzel theorem, see Eq. (1.23), Eq. (1.84) and Eq. (1.91) the contribution to the n^{th} multipole order is given by

$$\mathbf{W}_{\perp,n}(\mathbf{r}_\perp, \mathbf{r}_{s\perp}, \zeta) = -n\, r^{n-1} r_s^n \left(\cos(n\phi)\hat{\mathbf{e}}_r - \sin(n\phi)\hat{\mathbf{e}}_\phi\right) \int_{-\infty}^{\zeta} d\zeta' \overline{\overline{W}}_{\parallel,n}(\zeta') , \tag{1.93}$$

where $\hat{\mathbf{e}}_r$ and $\hat{\mathbf{e}}_\phi$ denote the unit vectors in radial and azimuthal direction. As mentioned before the monopole wake function is independent of the transverse coordinates and the first non-vanishing term is the dipole term. Here one finds the important result that for cylindrically symmetric boundary conditions the dipole forces are independent of the transverse offset of the test charge:

$$\mathbf{W}_{\perp,1}(\mathbf{r}_{s\perp}, \zeta) = \mathbf{r}_{s\perp} \int_{-\infty}^{\zeta} d\zeta' \overline{\overline{W}}_{\parallel,1}(\zeta') . \tag{1.94}$$

1.4.4 Transverse Coupling Impedance

For completeness, define $\overline{Z}$, $\overline{\overline{Z}}$ as the Fourier transforms of $\overline{W}$, $\overline{\overline{W}}$, respectively. Finally, according to Eq. (1.50) and Eq. (1.94) one finds for the transverse coupling impedance of a dipole:

$$\mathbf{Z}_{\perp,1}(\mathbf{r}_{s\perp},\omega) \;=\; \frac{c}{\omega}\overline{\overline{Z}}_{\parallel,1}(\omega)\mathbf{r}_{s\perp}\,. \tag{1.95}$$

For small beam offsets the transverse dynamics of the beam are dominated by the transverse dipole impedance.

1.5 Integration Path

In the previous section the longitudinal wake potential was introduced as the integral of the synchronous fields along the particle trajectory. The trajectory of the beam and the integration path for calculating the wake potential are identical. It is an advantage for analytical and numerical calculations of the wake potentials if the integration path can be chosen such that the geometry of the environment can be taken into account.

For instance, in an analytical calculation of the electromagnetic field usually very large and complicated expressions occur which can be simplified and restricted to the relevant parts if the integration path can be deformed in a proper way.

In particular for numerical computation working in the time domain, the problem occurs, that essentially the integration is restricted to a finite length. The high-frequency contributions of the wake fields that are diffracted in a small opening angle, i.e at a discontinuity of the pipe wall, reach the bunch at the center of the pipe far away from the considered structure (see section 1.6). Thus by using the direct method* of integration the pipe length has to be extended to values far above the original length of the structure. Therefore, an indirect integration method is used in order to obtain the wake potential of a structure for short bunches.

In the following cylindrically symmetric structures are considered. In the ultra-relativistic limit the wake potential of the n^{th} multipole depends on the radial position of the test charge proportional to r^n. If the wake potential of the n^{th} multipole for a line charge distribution at r_s is integrated on a path at an offset r_{path}, then by multiplying the obtained quantity with $(r_s/r_{path})^n$ the origin wake potential is recovered.

For perfectly conducting walls, the integral along the beam tube vanishes for the tangential (longitudinal and azimuthal) components of the electric field. The cavity gap at the integration path $\mathcal{L}_r$ yields the only contribution to the longitudinal wake potential (see Fig. 1.10).

This integration path can only be used if the beam tubes have equal radii ($r_{in} = r_{out}$) in front and behind the cavity and when no part of the cavity is of smaller radius. For structures like single tapers and steps, collimators, or cavities with smaller aperture irises, a integration along a straight line at the allowable radius is the only alternative.

A generalized method to compute wake potentials created by axisymmetric structures for ultra-relativistic beams in case of perfectly conducting walls has been found in [15]. The method allows to calculate the wake fields along any arbitrary contour spanning the structure longitudinally.

*Direct method means an integration path at the trajectory of the bunch.

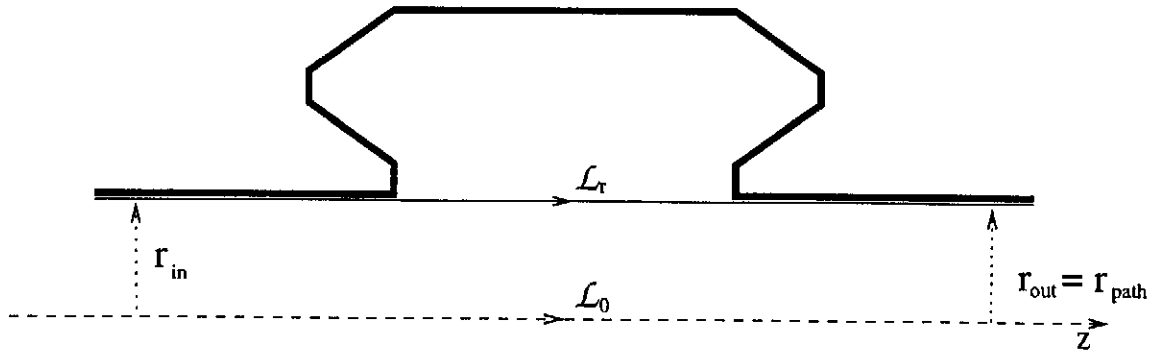

Figure 1.10: Integration across the cavity gap.

The derivation of the method can be summarized in three steps:

1. The electromagnetic field is decomposed into the fields generated by the source in free space $(\mathbf{E}^{(0)}, \mathbf{B}^{(0)})$ (the solutions of the inhomogeneous Maxwell equations) and the "radiated fields" $(\mathbf{E}^{(r)}, \mathbf{B}^{(r)})$, which are the solutions of the homogeneous Maxwell equations:

$$\begin{aligned} \mathbf{E} &= \mathbf{E}^{(0)} + \mathbf{E}^{(r)}, \\ \mathbf{B} &= \mathbf{B}^{(0)} + \mathbf{B}^{(r)}, \end{aligned} \tag{1.96}$$

such that the boundary conditions for $(\mathbf{E}, \mathbf{B})$ are fulfill. Next, the fields are separated into even and odd parity according to their angular dependence $(\mathbf{r}_{s\perp} \equiv (r_s, \phi_s = 0))$:

$$\begin{aligned} (E_r, B_\phi, E_z) &= \sum_{n=0}^{\infty} (e_{n,r}, b_{n,\phi}, e_{n,z}) \cos(n\phi), \\ (B_r, E_\phi, B_z) &= \sum_{n=0}^{\infty} (b_{n,r}, e_{n,\phi}, b_{n,z}) \sin(n\phi). \end{aligned} \tag{1.97}$$

In order to calculate the wake fields as electromagnetic fields moving synchronously with the bunch the following definition is introduced:

$$\overline{\varphi}(r, z, \zeta) = \varphi(r, z, t = (z + \zeta)/c). \tag{1.98}$$

2. From the Maxwell equations one can show that the two-dimensional vectors $\mathbf{S}_n$ and $\mathbf{D}_n$ in the (r, z)-plane defined by (see [15])

$$\mathbf{S}_n = r^n \cdot \begin{Bmatrix} \left(\overline{e}_{n,r}^{(r)} + c\,\overline{b}_{n,\phi}^{(r)} - \overline{e}_{n,\phi}^{(r)} + c\,\overline{b}_r^{(r)}\right) \\ \left(\overline{e}_{n,z}^{(r)} + c\,\overline{b}_{n,z}^{(r)}\right) \end{Bmatrix} \tag{1.99}$$

and

$$\mathbf{D}_n = r^{-n} \cdot \begin{Bmatrix} \left(\overline{e}_{n,r}^{(r)} + c\,\overline{b}_{n,\phi}^{(r)} + \overline{e}_{n,\phi}^{(r)} - c\overline{b}_r^{(r)}\right) \\ \left(\overline{e}_{n,z}^{(r)} - c\,\overline{b}_{n,z}^{(r)}\right) \end{Bmatrix} \tag{1.100}$$

satisfy the equations

$$\begin{aligned} \partial_r S_{n,z}(r,z,\zeta) - \partial_z S_{n,r}(r,z,\zeta) &= 0\,, \\ \partial_r D_{n,z}(r,z,\zeta) - \partial_z D_{n,r}(r,z,\zeta) &= 0\,. \end{aligned} \tag{1.101}$$

The vanishing rotation of these vectors implies that the integral along any closed contour vanishes. This property allows to deform the wake-field integration along a straight line $\mathcal{L}_r$ to any of the contours $\mathcal{C}'$ shown in Fig 1.11.

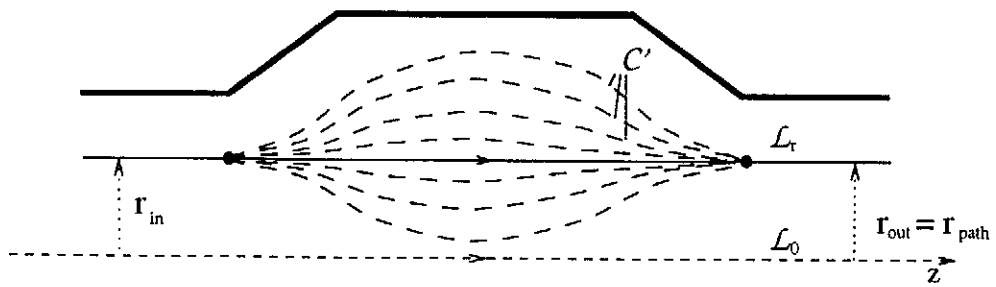

Figure 1.11: Deformation of the integration contour.

3. The next step is slightly different for the monopole mode ($n = 0$) and the higher modes ($n > 0$). Since the treatment of the monopole mode is easier the following calculation will be restricted to this case.

   The non-zero field components of a charge moving in free space are given by:

$$\begin{aligned} E^{(0)}_{0,r}(r,z,t) &= q_s/(2\pi\epsilon_0 r)\cdot\lambda(ct-z)\,, \\ c\,B^{(0)}_{0,\phi}(r,z,t) &= E^{(0)}_{0,r}(r,z,t)\,. \end{aligned} \tag{1.102}$$

   The same fields are obtained for a perfectly conducting beam tube. It therefore coincides with the asymptotic form of the total fields $(\mathbf{E},\mathbf{B})$ at both ends of the structure, for $z \to \pm\infty$ but ζ finite. As a consequence one finds that the radiative fields

$$(\overline{E}_{0,r}, \overline{B}_{0,\phi}, \overline{E}_{0,z})(r,z,\zeta) \;\to\; 0 \qquad \text{for} \qquad z \to \pm\infty \tag{1.103}$$

   while the other components $(\overline{B}_{0,r}, \overline{E}_{0,\phi}, \overline{B}_{0,z})$ are zero. This enables to deform the integration path from a straight line $\mathcal{L}_r$ to a contour $\mathcal{C}$ with $r_{in} \neq r_{out}$ (see Fig. 1.12), in such a way that

$$\int_{\mathcal{L}_r} \mathbf{S}_0(r,z,\zeta)\cdot d\mathbf{l} \;=\; \int_{\mathcal{C}} \mathbf{S}_0(r,z,\zeta)\cdot d\mathbf{l} \tag{1.104}$$

   since, the Eq.(1.103) ensures that the integral along the radial segments connecting $\mathcal{L}_r$ and $\mathcal{C}$ at $z = -\infty$ and $z = \infty$, vanish.

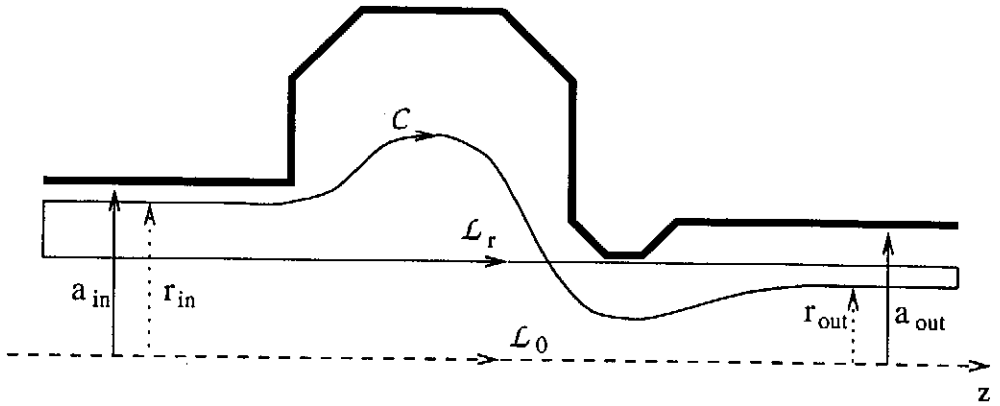

Figure 1.12: Integration path for a contour of unequal radii at both ends.

Finally, the above steps are repeated for the longitudinal wake potential and one finds:

$$
\begin{aligned}
W_{0,\parallel}(\zeta) &= \frac{1}{q_s}\int_{-\infty}^{\infty} dz\, \overline{e}_{0,z}^{(r)}(r,z,\zeta) \\
&= \frac{1}{q_s}\int_{-\infty}^{\infty} \mathbf{S}_0(r,z,\zeta)\cdot d\mathbf{l} \\
&= \frac{1}{q_s}\int_{\mathcal{L}_r} \mathbf{S}_0(r,z,\zeta)\cdot d\mathbf{l} \\
&= \frac{1}{q_s}\int_{C} \mathbf{S}_0(r,z,\zeta)\cdot d\mathbf{l} \\
&= \frac{1}{q_s}\int_{C} \left[\overline{e}_{0,z}^{(r)}(r,z,\zeta)\,dz + \left\{\overline{e}_{0,r}^{(r)} + c\,\overline{b}_{0,\phi}^{(r)}\right\}(r,z,\zeta)\,dr\right] \\
&= \frac{1}{q_s}\int_{C} \left[E_{0,z}\,dz + (E_{0,r} + c\,B_{0,\phi})\,dr\right](r,z,t)\Big|_{t=(z+\zeta)/c} \\
&\qquad + \frac{1}{\pi\epsilon_0}\ln\left(\frac{r_{out}}{r_{in}}\right)\lambda(\zeta)
\end{aligned}
\tag{1.105}
$$

with r_{in} and r_{out} the end radii of the contour C. For the last step Eq. (1.96) has been used and the radiative fields are substituted by the whole fields. The logarithmic term in the final result of Eq. (1.105) has to be added if the contour ends at different radii.

For a contour chosen along the cavity surface only the azimuthal magnetic field $B_{0,\phi}$ contributes to the integral. Therefore in order to evaluate the solution for a step-in (see Fig. 1.13) only the azimuthal component of the magnetic field $B_{0,\phi}$ at the discontinuity has to be known [16].

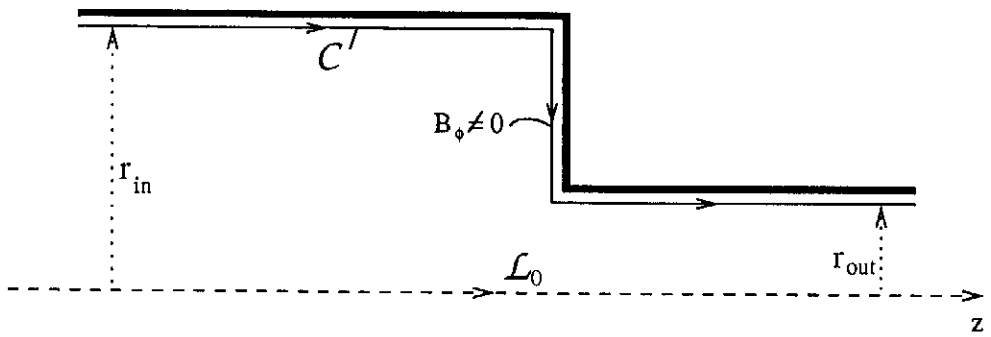

Figure 1.13: Integration contour in case of a step-in where only the azimuthal magnetic field contributes.

1.6 Distance of Beam-Wake Field Interaction

The integration method introduced in section 1.5 enables to calculate the wake potential without knowledge of the position where the interaction between the wake fields and the bunch takes place. In some cases such as an energy dependent trajectory, i.e. in a bending system of a bunch compressor the time structure of the interaction has to be taken into account.

As an example, the wake fields, which are generated at the wall by diffraction at a small enlargement $z = 0$ of the pipe with transverse distance b to the particle are considered. The width of the electromagnetic field distribution of the charge at the wall can be neglected if the considered distance ζ between the test and the exciting charge is large compare to b/γ. Using rays for the wake fields one can estimate the distance D for catching up a test charge downstream the pipe.

As sketched in Fig. 1.14 the diffracted ray reaches the test charge at a distance D such that

$$\frac{D+\zeta}{v} = \frac{\sqrt{b^2 + D^2}}{c}. \tag{1.106}$$

Expressing v by γ and resolve Eq. (1.106) to D one finds:

$$D(\gamma, \zeta, b) = \gamma^2 \left(\beta \sqrt{\zeta^2 + \frac{b^2}{\gamma^2}} - \zeta \right) \tag{1.107}$$

The distance $D(\gamma, \zeta, b)$ as a function of the distance ζ for two energies $E_0 = 1\,\mathrm{GeV}$ and $E_0 = 30\,\mathrm{GeV}$ for different pipe radii b is plotted in Fig. 1.15.

For the TTF-FEL drive beam ($E_0 = 1\,\mathrm{GeV}$, $\sigma_z = 50\,\mu\mathrm{m}$, $b = 0.5\,\mathrm{cm}$) the typical distance D is 25 cm if one chose the bunch length σ_z as the distance $\zeta = \sigma_z$ between source and test charge.

However, if one considers a bunch of $\sigma_z = 2\,\mu\mathrm{m}$ and an energy $E_0 = 30\,\mathrm{GeV}$ in a beam pipe of $b = 5\,\mathrm{cm}$ the catch-up distance is 600 m and even in an undulator of a gap of 2 cm one finds $D = 24\,\mathrm{m}$.

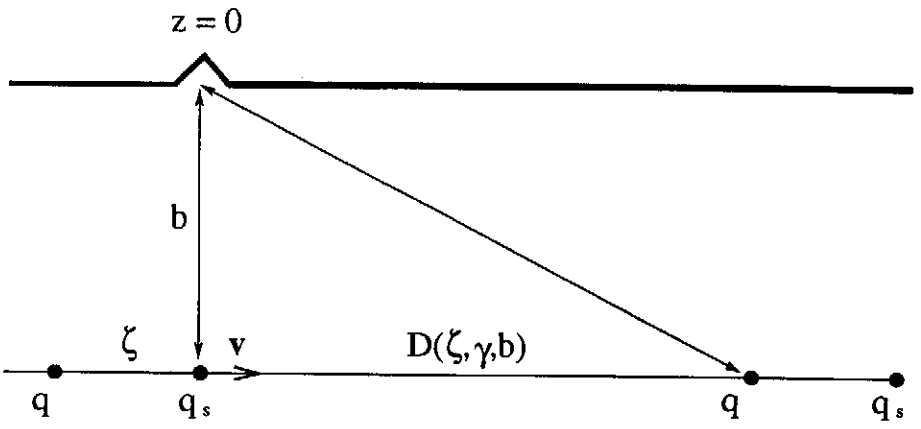

Figure 1.14: Diffracted ray emitted at an enlargement $z = 0$.

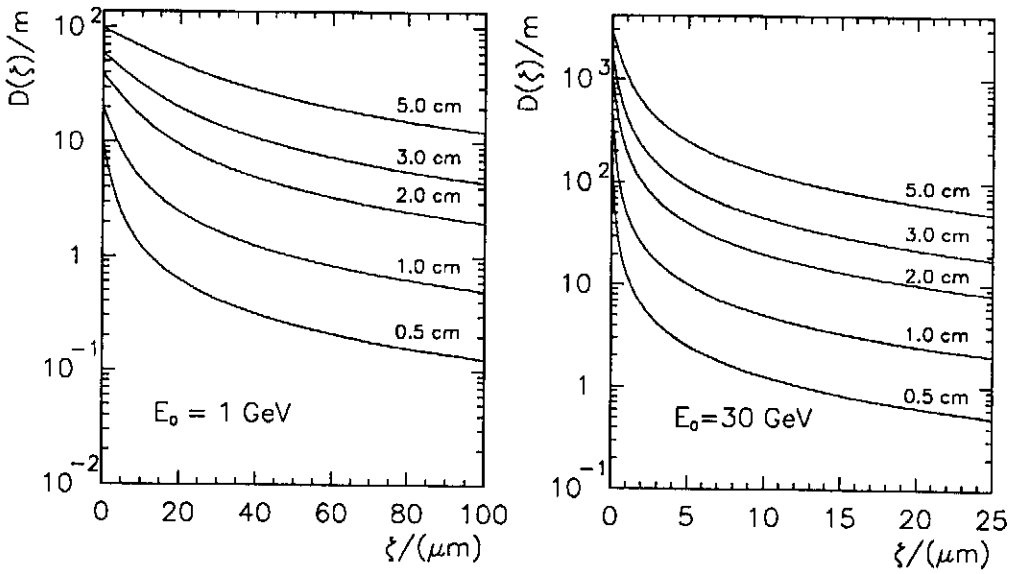

Figure 1.15: Distance D as a function of ζ for different pipe radii b for a test charge to be subjected to wake forces generated by the wall at the location $z = 0$.

Therefore, for sufficiently high energies and sufficiently short bunches, the photon beam generated by a FEL-drive beam may reaches saturation before an interaction between the electron bunch and the wake fields can take place.

Chapter 2

Resistive Wall Wake Fields of a Round Pipe

In this chapter the short and the long-range resistive wall wake fields for a cylindrical tube are presented. The properties of the impedances and the wake potentials for cross sections different from a round pipe can be described by additional form factors. Calculations show that for a given gap the effect of resistive wall wake fields on a bunch is mainly determined by the conductivity of the wall material and the bunch length while the form factors depend only weakly on the geometry of the cross sections (see [17]). Therefore, in this chapter an explicit analytical treatment of the wake fields for a round pipe is given.

2.1 General Description of the Method

The usual way to calculate wake fields is to solve Maxwell's equations as a system of coupled partial differential equations for charged particles in the ultra-relativistic limit. In order to eliminate the azimuthal derivatives the charge distribution is expanded into multipole moments of infinite small charged rings. The systems of equations obtained for the different multipoles m are decoupled. The translation invariance of a longitudinally uniform pipe can be used by inserting the variable $\zeta = (vt - z)$. A transformation into the frequency domain reduces the system of partial differential equations to a system of ordinary differential equations, which can be solved by standard methods. This is done both in vacuum and in the metal region. By taking the boundary conditions into account the solutions for both regions are matched and can thus be determined uniquely.

In this chapter a cylindrically symmetric coordinate system (r, ϕ, z) is considered. The transverse offset of a point-like source charge is given by the radial displacement r_s with respect to the symmetry axis of the tube and the azimuthal angle ϕ_s with respect to a reference axis $\mathbf{e}_x$. As derived in section 1.4.1 the multipole moments ρ_m for a point-like charge distribution can be written as:

$$\rho_m(r, \phi, z, t) = \frac{q_s}{2\pi r_s}\delta(r - r_s)e^{im(\phi-\phi_s)}\delta(z - vt) \qquad m \in \mathbb{Z}\,. \tag{2.1}$$

Therefore, an infinite number of multipoles contribute to the complete solution of a wake function for a source charge with an offset.

The electromagnetic field excited by a source charge in a realistic beam pipe can by decomposed into three parts,

$$\begin{aligned} \mathbf{E} &= \mathbf{E}^{(sp)} + \mathbf{E}^{(ind)} + \mathbf{E}^{(res)} , \\ \mathbf{B} &= \mathbf{B}^{(sp)} + \mathbf{B}^{(ind)} + \mathbf{B}^{(res)} , \end{aligned} \tag{2.2}$$

where $(\mathbf{E}^{(sp)}, \mathbf{B}^{(sp)})$ are the fields in free space and $(\mathbf{E}^{(ind)}, \mathbf{B}^{(ind)})$ are the fields excited by the induced charges and currents at the surface of perfectly conducting walls. Finally, $(\mathbf{E}^{(res)}, \mathbf{B}^{(res)})$ denotes the electromagnetic field due to the resistivity of the wall, which is treated as a perturbation.

2.1.1 Electromagnetic Field in a Perfectly Conducting Tube

Following [18], one can use the scalar potential Φ and the vector potential $\mathbf{A}$ instead of the electromagnetic field as an alternative way to solve the Maxwell equations. In fact this only means that the eight Maxwell equations of first order for the field components are replaced by four equations of second order and an additional gauge condition,

$$\frac{1}{c^2}\partial_t \Phi + \nabla \cdot \mathbf{A} = 0 . \tag{2.3}$$

The electromagnetic field in free space and the one due to the perfectly conducting walls (see Eq. (2.3)) can be derived by introducing the potentials $(\Phi^{(sp)}, \mathbf{A}^{(sp)})$ and $(\Phi^{(ind)}, \mathbf{A}^{(ind)})$, respectively. The electromagnetic fields are recovered from the vector potentials by:

$$\mathbf{E} = -\nabla\Phi - \partial_t \mathbf{A} , \tag{2.4}$$

$$\mathbf{B} = \nabla \times \mathbf{A} . \tag{2.5}$$

In the case of an infinite beam pipe radius or perfectly conducting walls the components of the vector potential perpendicular to $\mathbf{v}$ vanish: $\mathbf{A}_\perp \equiv 0$. Obviously the electromagnetic field is purely electrostatic in the particle rest frame. Thus it can described by a scalar potential Φ alone. Electromagnetic fields and potentials are transformed from one frame to another by the Lorentz transformation (see [3]). Therefore, in the case of a uniform movement along $\mathbf{e}_z$ the components of the vector potential perpendicular to $\mathbf{e}_z$ are invariant. Consequently, the potentials reduce to (Φ, A_z) in the laboratory frame. They fulfill the relations,

$$A_z^{(sp)} = \frac{v}{c^2}\Phi^{(sp)} , \tag{2.6}$$

$$A_z^{(ind)} = \frac{v}{c^2}\Phi^{(ind)} , \tag{2.7}$$

and thus satisfy the Lorentz gauge condition Eq. (2.3). Therefore, the electromagnetic fields are known if the corresponding scalar potentials are known.
The scalar potential $\Phi^{(sp)}$ $(\Phi^{(ind)})$ is a solution of the inhomogeneous (homogeneous) wave equation. If the transverse derivatives are separated from the longitudinal ones the equation reads:

$$\left[\left(\frac{1}{c^2}\partial_t^2 - \partial_z^2\right) - \Delta_\perp\right] \Phi(\mathbf{r}_\perp, z, t) = \frac{1}{\epsilon_0}\rho(\mathbf{r}_\perp, z, t) . \tag{2.8}$$

The inhomogeneity is given by an impulsive source which is a function of the variable $\zeta = (vt - z)$. Therefore the stationary solution of the scalar potential has the same dependence $\Phi(\mathbf{r}_\perp, z, t) = \Phi(\mathbf{r}_\perp, vt - z)$. The parenthesis on the left hand side of the above equation becomes $-1/\gamma^2 \cdot \partial_\zeta^2$ and one can write:

$$\left[\frac{1}{\gamma^2}\partial_\zeta^2 + \triangle_\perp\right] \Phi(\mathbf{r}_\perp, \zeta) \;=\; -\frac{q_s}{\epsilon_0}\,\delta^{(2)}(\mathbf{r}_\perp - \mathbf{r}_{s\perp})\,\delta(\zeta)\,. \tag{2.9}$$

In order to calculate the scalar potential Φ conveniently, a set of orthonormal eigen-functions of the Lorentz contracted operator in the square brackets is introduced:

$$\Psi_{(m,q,k)}(r, \phi, \zeta) \;=\; \frac{1}{2\pi} e^{im\phi}\, J_m(qr)\, e^{-ik\zeta} \qquad (m \in \mathbb{Z})\,. \tag{2.10}$$

Here J_m is the Bessel function of first kind and of the m^{th} order. The eigen-functions $\Phi_{(m,q,k)}$ are associated with eigen-values given by:

$$\lambda_{(m,q,k)} \;=\; -\left(\frac{k^2}{\gamma^2} + q^2\right)\,. \tag{2.11}$$

Equation (2.11) can be proved by expanding the 2-dimensional Laplace operator $\triangle_\perp$ in polar coordinates:

$$\triangle_\perp \;=\; \frac{1}{r}\partial_r\, r\partial_r + \frac{1}{r^2}\partial_\phi^2 \;=\; \partial_r^2 + \frac{1}{r}\partial_r + \frac{1}{r^2}\partial_\phi^2\,, \tag{2.12}$$

and by the definition of the Bessel function J_m as a solution of the Bessel differential equation:

$$\left(x^2\partial_x^2 + x\partial_x\right) J_m(x) + \left(x^2 - m^2\right) J_m(x) \;=\; 0 \qquad (x = qr)\,. \tag{2.13}$$

The function system $\Psi_{(m,q,k)}$ fulfills the following completeness relation:

$$\sum_{m=-\infty}^{\infty} \int_0^\infty q\,dq \int_{-\infty}^{\infty} dk\, \Psi_{(m,q,k)}(r, \phi, \zeta)\, \Psi_{(m,q,k)}(r_s, \phi_s, 0) \;=\; \frac{\delta(r - r_s)}{r}\,\delta(\phi - \phi_s)\,\delta(\zeta)\,. \tag{2.14}$$

Hence, the scalar potential can be written in terms of the orthonormal set $\Psi_{(m,q,k)}$ as

$$\Phi^{(sp)}(r, \phi, \zeta) \;=\; \sum_{m=-\infty}^{\infty} \int_0^\infty q\,dq \int_{-\infty}^{\infty} dk\, \tilde{\Phi}(m, q, k)\, \Psi_{(m,q,k)}(r, \phi, \zeta)\,, \tag{2.15}$$

where the Fourier coefficients are denoted by $\tilde{\Phi}(m, q, k)$. In order to calculate $\tilde{\Phi}$ the completeness relation Eq. (2.14) is applied in combination with the eigen-values of the orthonormal system Eq. (2.11) for the differential operator Eq. (2.9). One finds for the coefficients:

$$\tilde{\Phi}(m, q, k) \;=\; \frac{q_s}{2\pi\epsilon_0} \frac{1}{\left(\frac{k^2}{\gamma^2} + q^2\right)} e^{-im\phi_s}\, J_m(qr_s)\,. \tag{2.16}$$

Finally, the scalar potential for the multipole ρ_m is given by*:

$$\Phi_m^{(sp)}(r,\phi,\zeta) = \frac{1}{(2\pi)^2}\frac{q_s}{\epsilon_0}\int_0^\infty q\,dq\int_{-\infty}^\infty dk\,\frac{1}{\left(\frac{k^2}{\gamma^2}+q^2\right)}e^{im(\phi-\phi_s)}\,J_m(qr)\,J_m(qr_s)\,e^{-ik\zeta}\,. \quad (2.17)$$

The derived formula for $\Phi_m^{(sp)}$ is the integral representation for the scalar potential of the m^{th} multipole moment expressed in cylindrical coordinates. For the case where the source charge (or test charge) moves on axis, only the monopole term $\Phi_0^{(sp)}$ contributes to the scalar potential Φ ($J_m(0) = 0$ for $m \neq 0$). Note, that the potentials are symmetric relative to the exchange of the variables r and r_s.

The integrand of Eq. (2.17) has two poles at $k = \pm i\gamma q$ placed on the imaginary axis in the complex k-plane. As derived in section 1.3.3, poles in the upper half of the complex plane lead to a force for negative distances ζ. Therefore a test charge suffers an energy variation even if it is traveling in front of the source charge. The poles move to infinity for $\gamma \to \infty$. Thus the corresponding distances $\zeta \sim 1/k$ where an interaction between the test and the source charges can take place vanish.

If the integrals for q and k are interchanged, the Fourier transforms of the potentials are given as even functions of the wave number k. According to Eq. (2.4) the longitudinal electrical field is obtained from the scalar potential by:

$$E_z(\mathbf{r}_\perp,\mathbf{r}_{s\perp},\zeta) = \frac{1}{\gamma^2}\partial_\zeta\Phi(\mathbf{r}_\perp,\mathbf{r}_{s\perp},\zeta)\,. \quad (2.18)$$

The equation written in the k-domain ($\partial_\zeta \to -ik$) leads to an odd function of k for the Fourier transform of E_z, which is purely imaginary. Hence, the longitudinal forces are conservative and the acceleration (deceleration) of the leading charge equals the deceleration (acceleration) of the trailing charge.

Instead of solving the exceedingly complicated integral in Eq. (2.17), the calculations are continued for ultra-relativistic particles ($\gamma \to \infty$). The double integral then reduces to:

$$\Phi_m^{(sp)}(r,\phi,\zeta) = \frac{1}{2\pi}\frac{q_s}{\epsilon_0}\,\delta(\zeta)\,e^{im(\phi-\phi_s)}\int_0^\infty dq\,\frac{1}{q}\,J_m(qr)\,J_m(qr_s)\,. \quad (2.19)$$

The solutions of the integrals are found in App A.1. The result for $m \neq 0$ is written:

$$\Phi_m^{(sp)}(r,\phi,\zeta) = \frac{q_s}{2\pi\epsilon_0}\,\delta(\zeta)\,e^{im(\phi-\phi_s)}\,\frac{1}{2|m|}\left(\frac{r_<}{r_>}\right)^{|m|} \quad (2.20)$$

and for the monopole ($m = 0$):

$$\Phi_0^{(sp)}(r,\phi,\zeta) = \frac{q_s}{2\pi\epsilon_0}\,\delta(\zeta)\left[A + \ln\left(\frac{r_s}{r}\right)\theta(r-r_s)\right] \quad (2.21)$$

with $r_> = \sup(r,r_s)$, $r_< = \inf(r,r_s)$. Without boundary conditions the integral for the monopole potential diverges. Therefore a constant $A(\epsilon)$ is introduced with the cut-off parameter ϵ.

*The integral with respect to the variable q is known as the inverse Hankel transform.

The boundary conditions of a beam pipe with perfectly conducting walls require a vanishing scalar potential at the surface of the environment. Then the induced charges cancel the tangential components of the electric field and the induced currents the normal component of the magnetic field at the pipe walls. Therefore, the scalar potential $\Phi_m^{(ind)}$ satisfies the following relations:

$$\begin{aligned} \Phi_m^{(ind)}(b,\phi,\zeta) &= -\Phi_m^{(sp)}(b,\phi,\zeta) \\ \Rightarrow \quad \Phi_m^{(ind)}(r,\phi,\zeta) &= -\Phi_m^{(sp)}(b,\phi,\zeta)\, f_m(r) \quad \text{with} \quad \lim_{r\to b} f_m(r) = 1\,, \end{aligned} \tag{2.22}$$

where b denotes the radius of the tube. The dependence of the function f_m on the radius can be directly obtained from the above solutions $\Phi_m^{(sp)}$ for $r < r_s$. One finds for the scalar potentials due to the image charges the following equations:

$$\Phi_m^{(ind)}(r,\phi,\zeta) = -\frac{q_s}{2\pi\epsilon_0}\,\delta(\zeta)\,e^{im(\phi-\phi_s)}\,\frac{1}{2|m|}\left(\frac{rr_s}{b^2}\right)^{|m|} \tag{2.23}$$

for $m \neq 0$ and for the monopole:

$$\Phi_0^{(ind)}(r,\phi,\zeta) = -\frac{q_s}{2\pi\epsilon_0}\,\delta(\zeta)\left[A + \ln\left(\frac{r_s}{b}\right)\right]. \tag{2.24}$$

Combine the solutions Eq. (2.20) and Eq. (2.21) for the direct space charge scalar potential with the solutions Eq. (2.23) and Eq. (2.24) yielding:

$$\Phi^{(per)}(r,\phi,z,t) = \frac{q_s}{2\pi\epsilon_0}\,\delta(z-vt)\left\{\ln\left(\frac{b}{r_>}\right) + \sum_{n=1}^{\infty}\frac{\cos(n\phi)}{n}\left[\left(\frac{r_<}{r_>}\right)^n - \left(\frac{rr_s}{b^2}\right)^n\right]\right\}. \tag{2.25}$$

The superscript (per) denotes electromagnetic potentials or fields for a pipe that is perfectly conducting. In the above formula the azimuthal offset angle ϕ_s has been chosen to be zero ($\phi_s = 0$) and the terms for m and $(-m)$ are collected.

The electric field components perpendicular to v are derived from the scalar potential according to Eq. (2.4) and Eq. (2.5):

$$\begin{aligned} E_r^{(per)} &= -\partial_r\Phi^{(per)} \\ &= \frac{q_s}{2\pi\epsilon_0}\,\delta(z-vt) \\ &\quad \times\left(\frac{1}{r}\right)\cdot\left\{\theta(r-r_s) - \sum_{n=1}^{\infty}\cos(n\phi)\left[\left(\frac{r_<}{r_>}\right)^n\cdot\{1-2\,\theta(r-r_s)\} - \left(\frac{rr_s}{b^2}\right)^n\right]\right\} \end{aligned} \tag{2.26}$$

$$\begin{aligned} E_\phi^{(per)} &= -\frac{1}{r}\partial_\phi\Phi^{(per)} \\ &= \frac{q_s}{2\pi\epsilon_0}\,\delta(z-vt)\left(\frac{1}{r}\right)\cdot\sum_{n=1}^{\infty}\sin(n\phi)\left[\left(\frac{r_<}{r_>}\right)^n - \left(\frac{rr_s}{b^2}\right)^n\right] \end{aligned} \tag{2.27}$$

in agreement with the solution calculated in [12]. The function θ denotes the Heaviside step function defined by*

$$\theta(x) = \begin{cases} 1 & x > 0 \\ \frac{1}{2} & x = 0 \\ 0 & x < 0 \end{cases}. \tag{2.28}$$

*The amplitude of the function θ at $x = 0$ is chosen to be equal to $\theta(0) = \lim_{\epsilon\to 0}[\theta(x+\epsilon) - \theta(x-\epsilon)]$ according to the theorem for inverse Fourier transform of discontinuous functions.

Finally, using Eq. (2.5), the magnetic field components are related to the components of the electric field as follow:

$$B_r^{(per)} = \frac{1}{r}\partial_\phi A_z^{(per)} = -\frac{v}{c^2}E_\phi^{(per)}, \tag{2.29}$$

$$B_\phi^{(per)} = -\partial_r A_z^{(per)} = \frac{v}{c^2}E_r^{(per)}. \tag{2.30}$$

2.1.2 Wake Fields for a Perfectly Conducting Pipe

The ultra-relativistic limit ($\gamma \to \infty$) has been used in order to estimate the integral in Eq. (2.17). This is justified in case of a beam pipe radius b that is much smaller than $\gamma\sigma_z$. In this case the effective length b/γ produced by a point-like charge at the pipe wall can be neglected. The longitudinal distribution of the induced charges on the wall is dominantly given by the charge distribution of the bunched beam*.

According to Eq. (2.18) the longitudinal electric field for a perfectly conducting tube yields:

$$E_z^{(per)}(r,\phi,\zeta;r_s) = -\frac{q_s}{2\pi\epsilon_0\gamma^2}\partial_\zeta\delta(\zeta)\cdot\left\{\ln\left(\frac{b}{r_>}\right)+\sum_{n=1}^{\infty}\frac{\cos(n\phi)}{n}\left[\left(\frac{r_<}{r_>}\right)^n-\left(\frac{rr_s}{b^2}\right)^n\right]\right\}. \tag{2.31}$$

The derivative of the delta-function with respect to ζ indicates a non-vanishing longitudinal electric field E_z proportional to the gradient of the beam current. The convolution theorem predicts longitudinal forces proportional to $\lambda'(z-\beta ct)/\gamma^2$ where the prime denotes the derivative with respect to z. In particular for a charge distribution of Gaussian shape one finds:

$$\lambda'(z-\beta ct) = -\frac{1}{\sqrt{2\pi}\sigma_z^2}f(u) \qquad f(u) \equiv u\,e^{-u^2/2}, \tag{2.32}$$

where $u = (z-\beta ct)/\sigma_z$ defines the longitudinal position in the bunch. Therefore particles that move in front of the bunch center ($u > 0$) gain energy due to the wake fields, while particles behind the bunch center ($u < 0$) lose energy. The minimum and the maximum amplitude of the longitudinal space charge wake forces are reached at $u = \pm\sigma_z$ (see Fig. 2.1).

The above formula Eq. (2.31) for the longitudinal electric field component diverges in the case of a line charge ($r = r_s, \phi = 0$) by means of the direct space charge effect. This divergence is removed by extending the beam transversely. For the following calculations one considers a beam that travels on axis. Therefore the higher multipoles of the electromagnetic field vanish. The treatment is hereby simplified.

Uniform disk

For a bunch with uniform transverse distribution up to a radius a,

$$\lambda_\perp(r_s,\phi) = \frac{1}{\pi a^2}\theta(a-r), \tag{2.33}$$

*Here it is assumed that $\lambda'/\lambda \ll 1$. If substructures in the bunched beam are present, i.e. micro bunches due to the SASE-FEL process, then additional space charge forces have to be take into account.

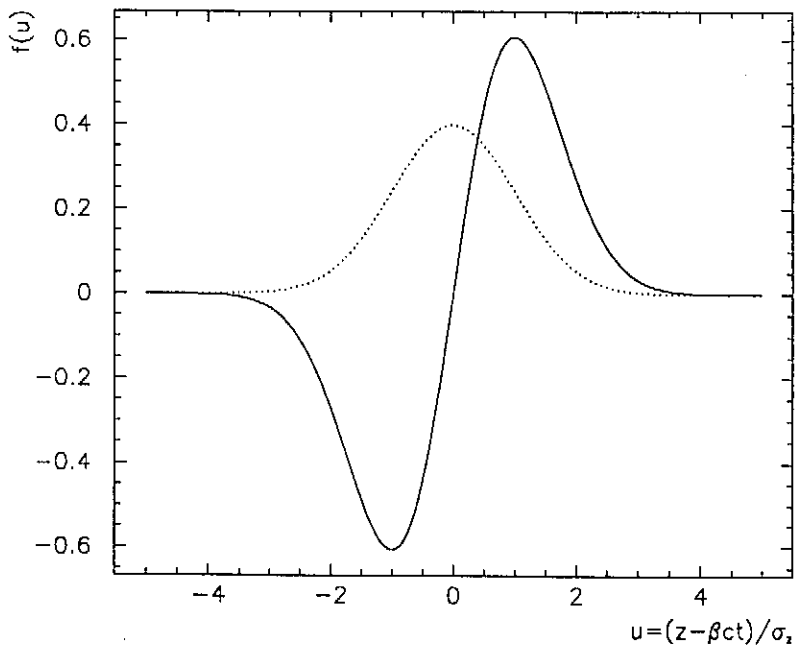

Figure 2.1: The function $f(u)$ of Eq. (2.32) for the longitudinal space charge wake effect (solid curve); the dotted curve shows a Gaussian distribution ($\sigma_z = 1$).

the longitudinal electric field is obtained by superposition

$$E_z^{\lambda} = \int_0^b \int_0^{2\pi} r_s dr_s \, d\phi \, \lambda_\perp(r_s) \cdot E_z^{(per)}(r, r_s, \zeta) \tag{2.34}$$

yielding:

$$E_z^{\lambda,uni}(r, u; a) = \frac{QZ_0c}{(2\pi)^{3/2}} \cdot \frac{f(u)}{(\gamma\sigma_z)^2} \cdot \left[\frac{1}{2}\left\{1 - \left(\frac{r}{a}\right)^2\right\} + \ln\left(\frac{b}{a}\right)\right] \qquad (r < a) \tag{2.35}$$

where the bunch charge is given by Q. The amplitude of the longitudinal electric field as a function of the radius reaches its maximum at $r = 0$.

Gaussian transverse distribution

For comparison, the corresponding electric field for a transverse Gaussian distribution with rms-value $\sigma_\perp$ reads :

$$E_z^{\lambda,gauss}(r, u; \sigma_\perp) = \frac{QZ_0c}{(2\pi)^{3/2}} \cdot \frac{f(u)}{(\gamma\sigma_z)^2} \cdot \left[\int_{r/\sigma_\perp}^{b/\sigma_\perp} d\tilde{r} \, \frac{1 - e^{-\tilde{r}^2/2}}{\tilde{r}}\right] \tag{2.36}$$

The functions of the radius r in the brackets of Eq. (2.36) and Eq. (2.35) are plotted for different values of a in Fig. 2.2.

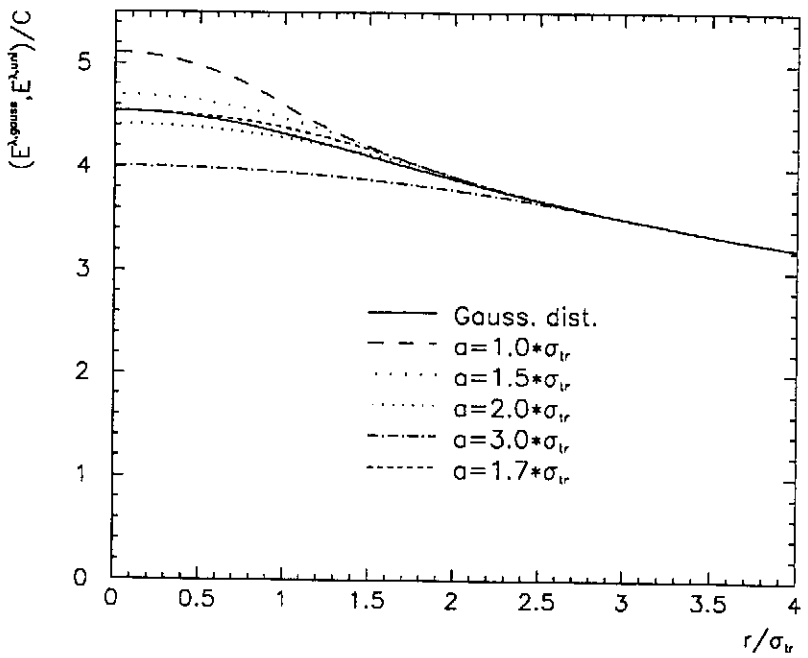

Figure 2.2: The longitudinal electric fields $E^{\lambda,gauss}$ (solid) and $E^{\lambda,uni}$ for different a as a function of the radius; $(b/\sigma_\perp = 100,\ C = QZ_0c/(2\pi)^{3/2} \cdot f(u)/(\gamma\sigma_z)^2)$.

The disk radius a leading to the same longitudinal forces on axis as for an Gaussian distribution with rms-value $\sigma_\perp$ can be calculated by

$$\frac{a(\sigma_\perp, b)}{\sigma_\perp} = \frac{b}{\sigma_\perp} \cdot \exp\left(- \int_0^{b/\sigma_\perp} d\tilde{r}\, \frac{1 - e^{-\tilde{r}^2/2}}{\tilde{r}} + \frac{1}{2} \right) \overset{\sigma_\perp \ll b}{\approx} 1.75\,. \tag{2.37}$$

For both a uniform disk and a Gaussian transverse charge distribution the forces are unbounded in the limit $b \to \infty$. By means of the approximation $b/\gamma \approx 0$ that has been used in the derivation of the above formulas, the calculation breaks down for radii much larger than $\gamma\sigma_z$. Here one has to consider the finite Lorentz factor in the calculation.

2.2 Wake Fields in a Resistive Tube

An electromagnetic field in a metal can be described by the Maxwell equations and a current density $\mathbf{j}$ that is proportional to the electric field $\mathbf{E}$ (Ohm's law). The proportionality constant σ_0 between the electric field at a point in the metal and the current density that it induces is called the conductivity of a metal. In this section a frequency-independent (or DC) conductivity is considered as well as an electromagnetic wave, in which the induced charge density ρ vanishes [19]:

$$\mathbf{j} \;=\; \sigma_0 \mathbf{E} \qquad \rho \;=\; 0\,. \tag{2.38}$$

The assumption is justified in case of time intervals $\triangle t$ that are large compared to the relaxation time τ ($\sim 1-10$fsec.) of the conduction electrons in the metal, hence for bunch length $\sigma_z \gg c\tau$.
The boundary conditions at the vacuum metal interface require continuity of the normal and the tangential components of $\mathbf{B}$, and of the tangential components of $\mathbf{E}$ [3]:

$$\lim_{\epsilon\to 0}\Big[\mathbf{n}\times(\mathbf{E}(\mathbf{r}-\epsilon\mathbf{n}) - \mathbf{E}(\mathbf{r}+\epsilon\mathbf{n}))\Big]_{\mathbf{r}\in S} \;=\; 0 \tag{2.39}$$

$$\lim_{\epsilon\to 0}\Big[\mathbf{B}(\mathbf{r}-\epsilon\mathbf{n}) - \mathbf{B}(\mathbf{r}+\epsilon\mathbf{n})\Big]_{\mathbf{r}\in S} \;=\; 0\,. \tag{2.40}$$

Here $\mathbf{n}$ is the unit normal vector at $\mathbf{r}\in\mathbf{S}$, a position on the surface of the chamber wall. The now given derivation is similar to that in [12]. The following definitions are used for the electromagnetic field components:

$$\begin{aligned} f_{m,com}(r,\zeta) &= \tfrac{1}{2\pi}\int_{-\infty}^{\infty} dk\, \hat{f}_{m,com}(r,k)\, e^{-ik\zeta} \\ f_{com}(r,\phi,\zeta) &= \sum_{m=-\infty}^{\infty} f_{m,com}(r,\zeta)\, e^{im\phi}\,. \end{aligned} \tag{2.41}$$

The Fourier transform with respect to the wave number k is described by $\hat{f}_{m,com}$ where the subscripts m and com denote the multipole ($m\in\mathbb{Z}$) and the component ($com = r,\phi,z$) of the electromagnetic field. The longitudinal impedance per unit length of the n^{th} multipole ($n\in\mathbb{N}$) is obtained from the longitudinal electric field $\hat{E}_z$ by (see section 1.4):

$$\begin{aligned} \overline{Z}_{n,\|}(k) &= -\frac{1}{q_s c(1+\delta_{0,n})}\int_{-\infty}^{\infty} d\zeta\, (E_{n,z}(\zeta) + E_{-n,z}(\zeta))\, e^{ik\zeta} \\ \Rightarrow\; \overline{Z}_{n,\|}(k) &= -\frac{1}{q_s c(1+\delta_{0,n})}\left(\hat{E}_{n,z}(k) + \hat{E}_{-n,z}(k)\right), \end{aligned} \tag{2.42}$$

where q_s is the charge of the source particle. Using Eq. (2.38) and the above definitions the Maxwell equations can be written*:

*The superscript (res) is suppressed in the following sections. The context will always make clear which electromagnetic field is referred to.

$$\frac{1}{r}\partial_r(r\hat{E}_{m,r}) + \frac{im}{r}\hat{E}_{m,\phi} + ik\hat{E}_{m,z} = 0 \tag{2.43}$$

$$\frac{im}{r}\hat{B}_{m,z} - ik\hat{B}_{m,\phi} + \frac{ik}{c}\hat{E}_{m,r} = \mu_0\sigma_0\hat{E}_{m,r}\theta(r-b) \tag{2.44}$$

$$ik\hat{B}_{m,r} - \partial_r\hat{B}_{m,z} + \frac{ik}{c}\hat{E}_{m,\phi} = \mu_0\sigma_0\hat{E}_{m,\phi}\theta(r-b) \tag{2.45}$$

$$\frac{1}{r}(\partial_r(r\hat{B}_{m,\phi}) - im\hat{B}_{m,r}) + \frac{ik}{c}\hat{E}_{m,z} = \mu_0\sigma_0\hat{E}_{m,z}\theta(r-b) \tag{2.46}$$

$$\frac{im}{r}\hat{E}_{m,z} - ik\hat{E}_{m,\phi} - ikc\hat{B}_{m,r} = 0 \tag{2.47}$$

$$ik\hat{E}_{m,r} - \partial_r\hat{E}_{m,z} - ikc\hat{B}_{m,\phi} = 0 \tag{2.48}$$

$$\frac{1}{r}(\partial_r(r\hat{E}_{m,\phi}) - im\hat{E}_{m,r}) - ikc\hat{B}_{m,z} = 0 \tag{2.49}$$

$$\frac{1}{r}\partial_r(r\hat{B}_{m,r}) + \frac{im}{r}\hat{B}_{m,\phi} + ik\hat{B}_{m,z} = 0\,. \tag{2.50}$$

The Heaviside step function θ guarantees that the system of equations is valid for $r < b$ inside the vacuum chamber and for $r > b$ in the metal wall of the tube where b denotes the radius of the beam pipe.

The charge and the current distribution of the beam can be taken into account by adding in the vacuum the solution of the inhomogeneous electromagnetic field $(\mathbf{E}^{(per)}, \mathbf{B}^{(per)})$ (see previous section) to the field $(\mathbf{E}^{(res)}, \mathbf{B}^{(res)})$. The only non-vanishing field component of $(\mathbf{E}^{(per)}, \mathbf{B}^{(per)})$ at the surface is the azimuthal magnetic field $\hat{B}_\phi^{(per)}$ which is therefore sometimes referred to as the driving term of the resistive wall wake fields. Consequently the boundary conditions of the above system of equations with the definition $b^\pm \equiv \lim_{\epsilon\to 0}(b \pm \epsilon)$ read:

$$\begin{aligned}
\hat{B}^{(per)}_{m,\phi}(b^-) + \hat{B}^{(r)}_{m,\phi}(b^-) &= \hat{B}^{(r)}_{m,\phi}(b^+) \\
\hat{B}^{(r)}_{m,r}(b^-) &= \hat{B}^{(r)}_{m,r}(b^+) \\
\hat{B}^{(r)}_{m,z}(b^-) &= \hat{B}^{(r)}_{m,z}(b^+) \\
\hat{E}^{(r)}_{m,\phi}(b^-) &= \hat{E}^{(r)}_{m,\phi}(b^+) \\
\hat{E}^{(r)}_{m,z}(b^-) &= \hat{E}^{(r)}_{m,z}(b^+)\,.
\end{aligned} \tag{2.51}$$

2.2.1 Monopole

Solution in vacuum

In the case $m = 0$ the system of Eqs. (2.43-2.50) can be sorted into two sets, fields components of even $(\hat{E}_{0,z}, \hat{E}_{0,r}, \hat{B}_{0,\phi})$ and of odd $(\hat{E}_{0,\phi}, \hat{B}_{r,0}, \hat{B}_{0,z})$ parity. Since the driving term, $\hat{B}_\phi^{(per)}$ couples to the fields with even parity, the odd components vanish identically $(\hat{E}_{0,\phi}, \hat{B}_{r,0}, \hat{B}_{0,z}) \equiv 0$.

Taking this result into account and combining Eqs. (2.44), (2.48), and (2.43) one finds:

$$\partial_r \hat{E}_{0,z} = 0 \quad \Rightarrow \quad \hat{E}_{0,z}(r,k) = A_0(k) \tag{2.52}$$

$$\hat{E}_{0,r} = c\hat{B}_{0,\phi} = -ik\, A_0(k)\, \frac{r}{2} \tag{2.53}$$

with a coefficient A_0 depending on the wave number (frequency $\omega = ck$). Note that the Fourier transform of the longitudinal electric field in the ultra-relativistic limit is constant over the cross-section of the pipe, a result which has been derived earlier. The dependence of the wake function on the distance between the leading and the trailing charge is obtained from the inverse Fourier transform of the coefficient A_0, and is related to the impedance $Z_{0,\parallel}$ by:

$$\overline{Z}_{0,\parallel}(k) = -\frac{1}{q_s c} A_0(k)\,. \tag{2.54}$$

Solution in the metal

Compared to the fields in vacuum the fields in metal are completely different in behaviour. The modification due to Ohm's law leads to a current that is in phase (neglecting the frequency-dependence of the conductivity) and proportional to the electric fields $\hat{E}_{0,z}$, $\hat{E}_{0,r}$. The electromagnetic field can penetrate into the wall and by dissipation the electromagnetic fields energy is transferred to heat. Thus a source charge that travels down a pipe with resistive walls suffers an energy loss.

For the monopole excitation the three non-redundant equations of the system Eqs. (2.43-2.50) can be rewritten as:

$$\hat{B}_{0,\phi} = \frac{1}{c}\left(1 - \frac{\mu_0\sigma_0 c}{ik}\right)\hat{E}_{0,r} \tag{2.55}$$

$$\hat{E}_{0,r} = \frac{1}{\mu_0\sigma_0 c}\,\partial_r \hat{E}_{0,z} \tag{2.56}$$

$$\frac{1}{r}\partial_r(r\partial_r \hat{E}_{0,z}) = -ik\mu_0\sigma_0 c\hat{E}_{0,z}\,. \tag{2.57}$$

Define a parameter λ by:

$$\lambda(k) = \sqrt{\frac{\mu_0\sigma_0 c|k|}{2}}\,[i + \mathrm{sign}(k)] \tag{2.58}$$

with $\lambda^2 = ik\mu_0\sigma_0 c$. The imaginary part $\mathrm{Im}(\lambda)$ has been chosen positive. The parameter λ^{-1} has the dimension of a length; it is related to the skin depth by:

$$\delta_{skin}(\omega) = \frac{1}{\mathrm{Im}(\lambda)} = \sqrt{\frac{2}{\mu_0\sigma_0\omega}}\,. \tag{2.59}$$

The general solution of the differential Eq. (2.57) is given by a linear combination:

$$\hat{E}_z^{(0)} = \tilde{A}_0 \cdot H_0^1(\lambda r) + \tilde{B} \cdot H_0^2(\lambda r)\,, \tag{2.60}$$

where H_0^1, and H_0^2 denote the first and second kind of Hankel functions of the zeroth order. The coefficient $\tilde{B}$ equals to zero in case of an infinite wall thickness.

Boundary conditions

The boundary conditions Eq. (2.51) for $\hat{E}_{0,z}$ and $\hat{B}_{0,\phi}$ are:

$$A_0 = \tilde{A}_0 \cdot H_0^1(\lambda b) \tag{2.61}$$

$$\frac{q_s Z_0}{2\pi b} - ik\, A_0 \frac{b}{2c} = \tilde{A}_0 \frac{ik}{\lambda c}\left(1 + \frac{\lambda^2}{k^2}\right) H_0^{1\prime}(\lambda b) \tag{2.62}$$

and resolved to the coefficient A one finds:

$$\Rightarrow \quad A_0(k) = \frac{q_s Z_0 c}{2\pi b} \cdot \frac{1}{\frac{ikb}{2} - \left(\frac{k}{\lambda} + \frac{\lambda}{k}\right)\frac{H_0^{1\prime}}{iH_0^1}} \,. \tag{2.63}$$

Here, $Z_0 \equiv \sqrt{\mu_0/\epsilon_0} = 120\,\pi\,\Omega$ is the impedance of "vacuum" and the prime at $H_0^{1\prime}$ means the derivative of Hankel function with respect to the argument.

Plane wall approximation ($|\lambda| b \gg 1$)

The radius is usually in the order of a few cm while the skin depth is in the range of nm to μm. Therefore the Hankel function is well approximated by its asymptotic expression for large arguments:

$$H_0^1(x) \sim \sqrt{\frac{2}{\pi x}}\left\{\frac{1-i}{\sqrt{2}} e^{ix}\right\} \qquad \text{for} \quad |x| \to \infty \tag{2.64}$$

and one can write for the ratio:

$$\frac{H_0^{1\prime}}{iH_0^1} \approx \left(1 + \frac{i}{2\lambda b}\right) \qquad (|\lambda| b \gg 1)\,. \tag{2.65}$$

The term $\propto 1/\lambda$ is a small correction, which is neglected in the following steps. Mathematically, the approximation means, that the first order derivative in the differential Eq. (2.57) has been dropped. The equation reads now:

$$(\partial_r^2 + \lambda^2)\hat{E}_z = 0 \tag{2.66}$$

where the curvature of the wall is neglected. The electromagnetic field in the wall can be written as:

$$\begin{aligned} \hat{E}_{0,z}(r,k) &= A_0\, e^{i\lambda(r-b)} \\ \hat{E}_{0,r}(r,k) &= -A_0 \tfrac{k}{\lambda}\, e^{i\lambda(r-b)} \\ \hat{B}_{0,\phi}(r,k) &= -A_0 \tfrac{k}{\lambda c}\left(1 + \tfrac{\lambda^2}{k^2}\right) e^{i\lambda(r-b)} \end{aligned} \tag{2.67}$$

with the coefficient A_0:

$$A_0(k) = \frac{q_s Z_0 c}{2\pi b} \cdot \frac{1}{\frac{ikb}{2} - \left(\frac{k}{\lambda} + \frac{\lambda}{k}\right)} \,. \tag{2.68}$$

2.2.2 Higher Multipoles

Solution in vacuum

The higher multipoles of the field components are derived in App. A.2. For $m > 0$ one finds:

$$\begin{aligned}
\hat{E}_{m,z} &= A_m(k) \cdot r^m \\
\hat{B}_{m,z} &= A_m(k) \cdot \tfrac{i}{c} r^m \\
\hat{E}_{m,r} &= B_m \cdot \tfrac{r^{m-1}}{2} + A_m \cdot \tfrac{1}{2}\left(\tfrac{m}{ikr} - \tfrac{ikr}{(m+1)}\right) r^m \\
\hat{B}_{m,r} &= B_m \cdot \tfrac{r^{m-1}}{2ic} - A_m \cdot \tfrac{1}{2ic}\left(\tfrac{m}{ikr} - \tfrac{ikr}{(m+1)}\right) r^m \\
\hat{E}_{m,\phi} &= -B_m \cdot \tfrac{r^{m-1}}{2i} - A_m \cdot \tfrac{1}{2i}\left(\tfrac{m}{ikr} + \tfrac{ikr}{(m+1)}\right) r^m \\
\hat{B}_{m,\phi} &= B_m \cdot \tfrac{r^{m-1}}{2c} - A_m \cdot \tfrac{1}{2c}\left(\tfrac{m}{ikr} + \tfrac{ikr}{(m+1)}\right) r^m
\end{aligned} \qquad (r < b)\,. \tag{2.69}$$

where the coefficients A_m and B_m are functions of the wave number k. The electromagnetic field components for $m < 0$ are obtained from the solutions in Eq. (2.69) by:

$$\begin{aligned}
(\hat{E}_{m,z}, \hat{E}_{m,r}, \hat{B}_{m,\phi}) &= (\hat{E}_{|m|,z}, \hat{E}_{|m|,r}, \hat{B}_{|m|,\phi}) \\
(\hat{E}_{m,\phi}, \hat{B}_{m,r}, \hat{B}_{m,z}) &= -(\hat{E}_{|m|,\phi}, \hat{B}_{|m|,r}, \hat{B}_{|m|,z})
\end{aligned} \qquad (m < 0)\,. \tag{2.70}$$

which is again a consequence of the parity of the fields for the replacement $\phi \to -\phi$. The coefficients $A_m(k)$ have the same meaning for the multipole modes as the coefficient A_0 for the monopole. They are related to the impedance per unit length of the n^{th} multipole according to Eq. (2.42) and Eq. (2.70) by:

$$\overline{Z}_{n,\parallel}(k) = -\frac{2}{q_s c} A_n(k)\, r^n \qquad (n \in \mathbb{N})\,. \tag{2.71}$$

Contrarily to the case $m = 0$ a second coefficient B_m appears which contributes only to the transverse field components. The corresponding Lorentz force vanishes, since the forces due to the electric fields cancel with those due to the magnetic fields.

In addition one observes that for perfectly conducting walls the longitudinal and the azimuthal electric field $\hat{E}_z$, $\hat{E}_\phi$ vanish at the wall $r = b$. Thus according to Eq. (2.69) the homogeneous solution of the electromagnetic field has to fulfill $A_m = 0$ and $B_m = 0$. As expected, in absence of a source electromagnetic fields can not exist in a beam pipe with perfectly conducting walls that are via construction ($\omega = ck$) of a phase (and group) velocity equal to the speed of light.

Solution in the metal

For wave numbers k, which satisfy

$$\left(\frac{m^2}{b^2 Z_0 \sigma_0}\right) \ll k \tag{2.72}$$

the electromagnetic field components can be written as:

$$\begin{aligned}
\hat{E}_{m,z} &= -ic\hat{B}_{m,z} = A_m \cdot b^m e^{i\lambda(r-b)} \\
\hat{E}_{m,r} &= -i\hat{E}_{m,\phi} = -A_m \cdot b^m \tfrac{k}{\lambda} e^{i\lambda(r-b)} \\
\hat{B}_{m,r} &= -A_m \cdot \tfrac{ib^m}{c}\left\{\tfrac{k}{\lambda} + \tfrac{im}{kr}\left(1 + \tfrac{k^2}{\lambda^2}\right)\right\} e^{i\lambda(r-b)} \\
\hat{B}_{m,\phi} &= -A_m \cdot \tfrac{b^m}{c}\left(\tfrac{k}{\lambda} + \tfrac{\lambda}{k} + \tfrac{imk}{r\lambda^2}\right) e^{i\lambda(r-b)} .
\end{aligned} \tag{2.73}$$

The plane wall approximation treated in the previous subsection has been used and hereby limits the validity of the solution for the long range wake fields. For instance, in a 1 mm copper pipe one finds that the calculations for the dipole wake fields (m =1) are valid for distances smaller than 22 km.

Coefficients

In order to obtain $\hat{B}^{(per)}_{m,\phi}$ make use of Eqs. (2.29) and (2.41):

$$\hat{B}^{(per)}_{m,\phi}(b^-) = \frac{q_s}{2\pi\epsilon_0 c}\frac{r_s^{|m|}}{b^{|m|+1}} \qquad m \in \mathbb{Z}/\{0\} . \tag{2.74}$$

Finally, one finds for the coefficients:

$$\begin{aligned}
A_m(k) &= \tfrac{q_s}{2\pi\epsilon_0}\tfrac{1}{b^{m+1}}\left(\tfrac{r_s}{b}\right)^m \cdot \left[\tfrac{m}{ikb} + \tfrac{ikb}{m+1} - \tfrac{\lambda}{k} - \tfrac{2k}{\lambda} - \tfrac{imk}{b\lambda^2}\right]^{-1} , \\
B_m(k) &= -b\left[\tfrac{m}{ikb} + \tfrac{ikb}{m+1} - \tfrac{2k}{\lambda}\right] \cdot A_m(k) ,
\end{aligned} \tag{2.75}$$

where the boundary conditions Eq. (2.51) and the electromagnetic field in vacuum as well as in metal have been used (see App. A.2).

2.2.3 Long-Range Approximation

In this subsection an approximation for the wake potential is presented. The so-called long-range approximation can be used for bunch lengths σ_z which are large in comparison to the characteristic length ζ_0 of the wake fields given by:

$$\zeta_0 = \left(\frac{2b^2}{Z_0\sigma_0}\right)^{1/3} . \tag{2.76}$$

In case of a copper pipe with 2 cm radius one finds $\zeta_0 = 33\,\mu$m.
The long-range approximation takes only the low-frequency behaviour of the impedance into account.

Monopole wake function

It is convenient to rewrite the impedance as a function of the dimensionless variable $\kappa = k\zeta_0$. According to Eq. (2.68) and Eq. (2.54) one finds:

$$\overline{Z}_{0,\parallel}(\kappa) = \frac{Z_0\zeta_0}{2\pi b^2}\cdot\left[\frac{1+i\,\mathrm{sign}(\kappa)}{\sqrt{|\kappa|}} - \frac{i\,\kappa}{2} + \left(\frac{\zeta_0}{b}\right)^2\frac{\sqrt{|\kappa|}}{1+i\,\mathrm{sign}(\kappa)}\right]^{-1} . \tag{2.77}$$

The term proportional to $|\kappa|^{-1/2}$ in the square bracket dominates the impedance for $\kappa \ll 1$ or distances $\zeta \gg \zeta_0$, correspondingly. Thus the impedance in the long-range approximation reads:

$$\overline{Z}_{0,\parallel}(\kappa) = \frac{Z_0\zeta_0}{4\pi b^2}\cdot\sqrt{|\kappa|}\,(1 - i\,\mathrm{sign}(\kappa)) . \tag{2.78}$$

Obviously, the above impedance diverges for $\kappa \to \infty$. Therefore the inverse Fourier transform does not exist in the conventional sense. If the wake function is understood as a "generalized" function and the impedance as the Fourier transform of such a "generalized function" then the inverse transform is well defined and exists [20]. One finds for the inverse Fourier transform of the signum function multiplied with $|k|^\alpha$ following formulas (see [20] $\alpha \in \mathbb{R}/\mathbb{Z}$):

$$|\zeta|^\alpha = \frac{1}{2\pi}\int_{-\infty}^{\infty} dk\left\{2\cos\left(\frac{\pi}{2}(\alpha+1)\right)\alpha!\,|k|^{-(\alpha+1)}\right\} e^{-ik\zeta} \tag{2.79}$$

$$|\zeta|^\alpha\mathrm{sign}(\zeta) = \frac{1}{2\pi}\int_{-\infty}^{\infty} dk\left\{2i\sin\left(\frac{\pi}{2}(\alpha+1)\right)\alpha!\,|k|^{-(\alpha+1)}\,\mathrm{sign}(k)\right\} e^{-ik\zeta} . \tag{2.80}$$

With $\alpha = -3/2$, $(-3/2)! = -2\sqrt{\pi}$ and $\kappa = k\zeta_0$ the wake function per unit length is written:

$$\begin{aligned} W^{\delta}_{0,\parallel}(\zeta) &= \frac{E_{0,z}(\zeta)}{q_s} = -\frac{c}{2\pi}\int_{-\infty}^{\infty} dk\, Z_{0,\parallel}(k)\, e^{-ik\zeta} \\ &= \frac{Z_0 c}{2\,(2\pi)^{3/2}b^2}\cdot\left(\frac{\zeta_0}{\zeta}\right)^{3/2}\cdot\left\{\frac{1+\mathrm{sign}(\zeta)}{2}\right\} . \end{aligned} \tag{2.81}$$

The above equation shows the well-known long-range behaviour of the monopole wake function, which decays proportionally to $\zeta^{-3/2}$. The sign of the force is such that the long-range resistive wall wake field accelerates a test charge. Due to the ratio $(\zeta_0/\zeta)^{3/2}$ the wake fields are usually small. The term in the curled brackets vanishes for $\zeta < 0$ and equals unity for $\zeta > 0$. For the rest of the section the bracket including the signum function in the space domain will be suppressed.

Longitudinal multi-bunch effect

The longitudinal wake fields due to a train of N bunches can be estimated. Consider a constant inter-bunch distance $\zeta_{bun} \gg \zeta_0$ and a bunch charge Q for each member of the

train. Then the longitudinal wake field acting on the last bunch is given by the wake fields generated by the $N-1$ bunches ahead and reads:

$$E_z(N) \;=\; C \cdot \sum_{j=1}^{N-1} \left(\frac{\zeta_0}{j\zeta_{bun}}\right)^{3/2} \;=\; C \cdot \left(\frac{\zeta_0}{\zeta_{bun}}\right)^{3/2} \sum_{j=1}^{N-1} j^{-3/2} \tag{2.82}$$

with

$$C \;=\; \frac{Z_0 c Q}{2\,(2\pi)^{3/2} b^2}\, L\,,$$

where L is length of the pipe. In the limit $N \to \infty$ the sum yields $\sum_{j=1}^{\infty} j^{-3/2} \approx 2.61$. Thus the amplitude for the wake fields has an upper boundary determined by the inter-bunch distance ζ_{bun}:

$$E_z(N \gg 1) \;\leq\; 2.61 \cdot C \cdot \left(\frac{\zeta_0}{\zeta_{bun}}\right)^{3/2}\,. \tag{2.83}$$

Higher multipole wake function

The impedances for the higher multipoles ($n \in \mathbb{N}$) (see Eq. (2.75)) as a function of κ are:

$$\begin{aligned} \overline{Z}_{n,\parallel}(\kappa) \;&=\; \frac{Z_0\zeta_0}{\pi b^2} \cdot \left(\frac{r r_s}{b^2}\right)^n \qquad (2.84)\\ &\times\; \left[\frac{1+i\,\mathrm{sign}(\kappa)}{\sqrt{|\kappa|}} - \frac{i\,\kappa}{(n+1)} + \left(\frac{\zeta_0}{b}\right)^2 \left\{\frac{\sqrt{|\kappa|}}{1+i\,\mathrm{sign}(\kappa)} + \frac{in}{\kappa} + \left(\frac{\zeta_0}{b}\right)^2 \frac{n}{2}\right\}\right]^{-1}\,. \end{aligned}$$

The terms in the curled brackets are strongly suppressed by the ratio $(\zeta_0/b)^2$ and are neglected in the following. The long-range approximation of the impedance restricted to wave numbers in the range $n^2(\zeta_0/b)^4 \ll \kappa \ll 1$ reduces to:

$$\overline{Z}_{n,\parallel}(\kappa) \;=\; \frac{Z_0\zeta_0}{2\pi b^2} \cdot \left(\frac{r r_s}{b^2}\right)^n \cdot \sqrt{|\kappa|}\,(1 - i\,\mathrm{sign}(k))\,. \tag{2.85}$$

As derived section 1.4 the amplitudes of the higher modes are proportional to the ratio $(r r_s/b^2)^n$. Note, that the behaviour of the impedances as a function of the wave number is independent of the multipole order. With the previously used inverse Fourier transform the wake function for the n^{th} mode is written:

$$\begin{aligned} \overline{W}^{\delta}_{n,\parallel}(\zeta) \;&=\; -\frac{c}{2\pi} \int_{-\infty}^{\infty} dk\, Z_{n,\parallel}(k)\, e^{-ik\zeta}\\ &=\; \frac{Z_0 c}{(2\pi)^{3/2} b^2} \cdot \left(\frac{r r_s}{b^2}\right)^n \cdot \left(\frac{\zeta_0}{\zeta}\right)^{3/2}\,. \end{aligned} \tag{2.86}$$

This expression differs by exactly a factor two from that of the monopole wake function.

Wake function including all multipoles

The wake field effect on a two particle system is obtained by summing over all multipole orders:

$$W_{\parallel}^{\delta}(\mathbf{r}, \mathbf{r}_{s\perp}, \zeta) \;=\; \frac{Z_0 c}{2(2\pi)^{3/2} b^2} \cdot g\left(\frac{r r_s}{b^2}, \phi\right) \cdot \left(\frac{\zeta_0}{\zeta}\right)^{3/2} , \tag{2.87}$$

where g is defined by:

$$g(r, r_s, \phi, b) \;\equiv\; \sum_{n=0}^{\infty} (2 - \delta_{0,n}) \left(\frac{r r_s}{b^2}\right)^n \cos(n\phi) \;=\; \frac{b^4 - r^2 r_s^2}{b^4 - 2b^2 r r_s \cos(\phi) + r^2 r_s^2} \,. \tag{2.88}$$

The azimuthal angle ϕ is measured between the transverse positions of the source and the test charge ($r r_s \cos(\phi) = \mathbf{r}_{\perp} \cdot \mathbf{r}_{s\perp}$). Note, that for a given angle ϕ the function g depends only on the ratio ($r r_s / b^2$). The function g is plotted for different values of ϕ in Fig. 2.3.

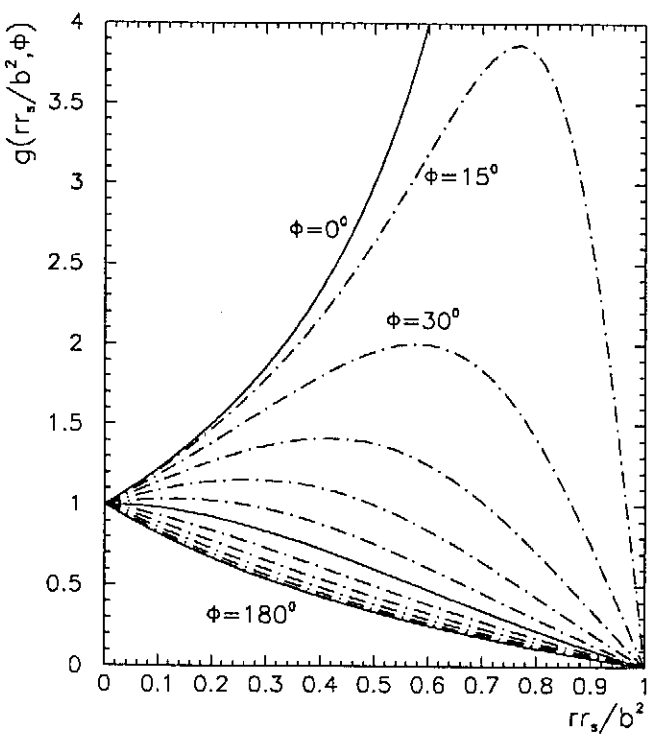

Figure 2.3: The function $g(r r_s/b^2, \phi)$ for different azimuthal angles $\phi = 0^0, 15^0, 30^0 \cdots 180^0$.

Transverse wake function

According to the Panofsky-Wenzel theorem Eq. (1.50) the transverse impedance can be written as:

$$\begin{aligned}\mathbf{Z}_{n,\perp}(k) &= \frac{1}{k}\nabla_\perp Z_{n,\|}(r,\phi,k) \\ &= \frac{Z_0\zeta_0^2}{2\pi b^2}\cdot\frac{n}{r}\left(\frac{rr_s}{b^2}\right)^n\cdot\frac{(\mathrm{sign}(\kappa)-i)}{\sqrt{|\kappa|}}\left(\cos(n\phi)\hat{\mathbf{e}}_r - \sin(n\phi)\hat{\mathbf{e}}_\phi\right) . \quad (2.89)\end{aligned}$$

With the transformations given in Eqs. (2.79-2.80) and $\alpha = -1/2$, $(-1/2)! = \sqrt{\pi}$ the transverse wake function yields:

$$\begin{aligned}\mathbf{W}_{n,\perp}(\zeta) &= \frac{ic}{2\pi}\int_{-\infty}^{\infty} dk\, Z_{n,\perp}(k)\, e^{-ik\zeta} \\ &= \frac{2Z_0\zeta_0}{(2\pi)^{3/2}b^2}\cdot\frac{n}{r}\left(\frac{rr_s}{b^2}\right)^n\cdot\left(\frac{\zeta_0}{\zeta}\right)^{1/2}\cdot\left(\cos(n\phi)\hat{\mathbf{e}}_r - \sin(n\phi)\hat{\mathbf{e}}_\phi\right) . \quad (2.90)\end{aligned}$$

In particular the transverse dipole wake function is:

$$\mathbf{W}_{1,\perp}(\zeta) = \frac{c}{\pi^{3/2}}\sqrt{\frac{Z_0}{\sigma_0}}\cdot\frac{\hat{\mathbf{r}}_{s\perp}}{b^3}\cdot\frac{1}{\sqrt{\zeta}} .$$

Thus the transverse dipole force deflects the test charge in direction of the source charge.

Transverse multi-bunch effect

In analogy to the longitudinal case, the last bunch in a train of N bunches suffers a momentum change of:

$$\Delta\mathbf{p}_\perp(N) = \frac{Q^2L}{\pi^{3/2}}\sqrt{\frac{Z_0}{\sigma_0\zeta_{bun}}}\cdot\frac{<\mathbf{r}>}{b^3}\cdot\sum_{j=1}^{N-1} j^{-1/2} \quad \text{with} \quad <\mathbf{r}> \equiv \frac{1}{N}\sum_{j=1}^{N-1}\mathbf{r}_j . \quad (2.91)$$

Here, it is assumed that the transverse extension of the beam and the relative offset of the individual bunches are small in comparison with the average displacement $< r >$ of the whole train*. Note, that the momentum change $\Delta\mathbf{p}_\perp(N)$ is unbounded for $N \to \infty$.

Fields in the wall

In the frequency domain the longitudinal electric field component in the metal wall is damped exponentially in radial direction (see Eq. (2.67)):

$$\hat{E}_{0,z}(r,k) = -\frac{Z_0 c}{4\pi b^2}\cdot\sqrt{|\kappa|}(1 - i\,\mathrm{sign}(\kappa))\, e^{i\lambda(r-b)} \qquad (r > b) . \quad (2.92)$$

*If the single bunch offset cannot be neglected one has to replace $<\mathbf{r}>\sum_{j=1}^{N-1} j^{-1/2}$ in Eq. (2.91) by $\sum_{j=1}^{N-1}\mathbf{r}_j\cdot(N-j)^{-1/2}$.

The inverse Fourier transform of $\hat{E}_{0,z}$ has been calculated in [12]:

$$E_{0,z}(r,\zeta) = \frac{Z_0 c q_s}{2(2\pi)^{3/2} b^2} \sqrt{\frac{b}{r}} \left(\frac{\zeta_0}{\zeta}\right)^{3/2} \cdot \left(1 - \frac{\alpha^2}{\zeta}\right) e^{-\alpha^2/(2\zeta)} \tag{2.93}$$

with

$$\alpha = \sqrt{\frac{Z_0\sigma_0}{2}}(r-b) = \frac{b}{\zeta_0^{3/2}}(r-b)\,. \tag{2.94}$$

Eq. (2.93) describes the penetration of the electric field into the walls. One can introduce a skin depth $\overline{\delta}_{skin}(\tau)$ as a function of time difference $\tau = \zeta/c$ between the leading and trailing particle, corresponding to the skin depth in the frequency domain:

$$\overline{\delta}_{skin}(\tau) = \sqrt{\frac{4\tau}{Z_0\sigma_0 c}} \quad \text{(time domain description)}\,, \tag{2.95}$$

$$\delta_{skin}(\omega) = \sqrt{\frac{2c}{Z_0\sigma_0\omega}} \quad \text{(frequency domain description)}\,. \tag{2.96}$$

Thus τ plays the role in $\overline{\delta}_{skin}$ as $c/2\omega$ plays in the skin depth δ_{skin}.

Longitudinal wake potential

In the low-frequency approximation the impedance $Z_{n,\parallel}(k)$ can be separated into the monopole impedance $Z_{0,\parallel}(k)$ and a function which depends on the offsets of the source and the test charge. This enables one to find a closed expression for the longitudinal wake potential. Using the impedances Eqs. (2.78), (2.85) and $\hat{\lambda}$, the Fourier transform of a Gaussian charge distribution, the wake potential reads [21]:

$$W_\parallel(r,\phi,\zeta) = -\frac{c}{2\pi}\sum_{n=0}^{\infty}\int_{-\infty}^{\infty} dk\, Z_{n,\parallel}(k)\,\hat{\lambda}(k)\,e^{-ik\zeta} \tag{2.97}$$

$$= -\frac{Z_0\, c\,\zeta_0^{3/2}}{8\pi^2\, b^2}\sum_{n=0}^{\infty}\left(\frac{r r_s}{b^2}\right)^n \cos(n\phi)(2-\delta_{n,0})\cdot\left(\int_{-\infty}^{\infty} dk\,(1 - i\,\mathrm{sign}(k))\sqrt{|k|}\cdot e^{-k^2\sigma_z^2/2}\,e^{-ik\zeta}\right)$$

$$= \frac{c}{4\pi\, b}\sqrt{\frac{Z_0}{\sigma_0}}\cdot\frac{1}{\sigma_z^{3/2}}\cdot g\left(\frac{r r_s}{b^2},\phi\right)\cdot\left|\frac{u}{2}\right|^{3/2}\cdot\left\{I_{1/4} - I_{-3/4} - \mathrm{sign}(u)(I_{-1/4} - I_{3/4})\right\} e^{-u^2/4}\,.$$

The argument of the Bessel functions I_ν are $u^2/4$; here u is a distance between the center of the bunch and the position of the test charge, normalized to σ_z:

$$u = -\frac{\zeta}{\sigma_z} = \frac{z-ct}{\sigma_z}\,. \tag{2.98}$$

The inverse Fourier transform is solved in App. A.3.
The amplitude of the wake potential on the radius b, the bunch length σ_z and the conductivity σ_0 is:

$$W_\parallel \propto b^{-1}\sigma_0^{-1/2}\sigma_z^{-3/2}\,. \tag{2.99}$$

The dependence on the transverse position of the test charge relative to the line charge distribution is described by the function g shown in Fig. 2.3. Finally, the shape of the wake potential is sketched Fig. 2.4.

The impedance is proportional to $|k|^{1/2}$, between a dominantly "inductive" and a dominantly "resistive" wake potential (see section 1.3.3).

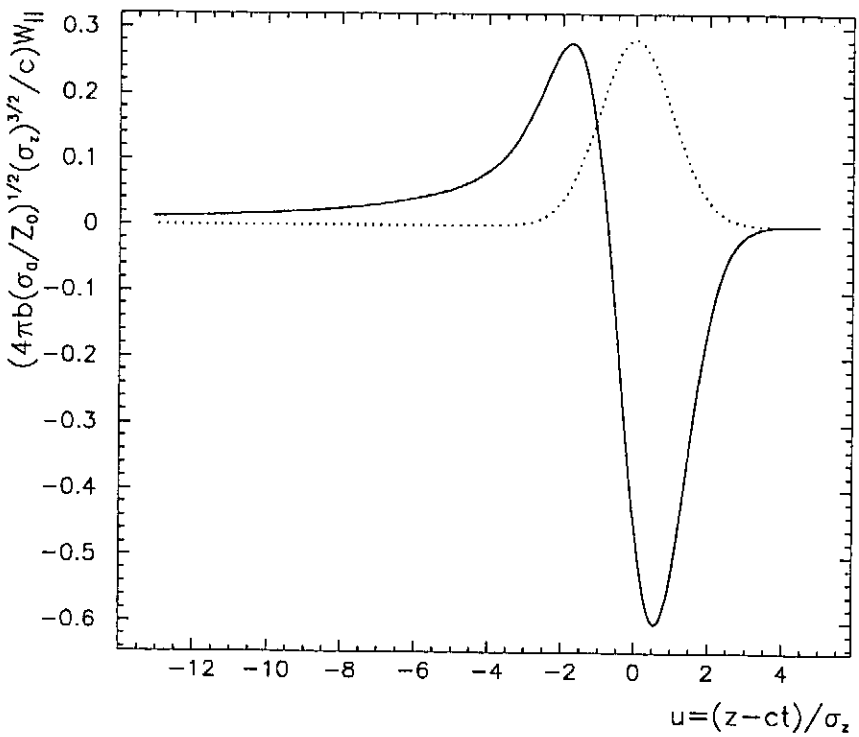

Figure 2.4: Longitudinal wake potential and charge distribution.

Transverse wake potential

The recurrence relation of the Bessel functions

$$I'_\nu(x) \;=\; I_{\nu+1}(x) + \frac{\nu}{x} I_\nu \;=\; I_{\nu-1}(x) - \frac{\nu}{x} I_\nu \tag{2.100}$$

and the relation between the partial derivatives $\partial_\zeta = -\sigma_z \partial_u$ can be used to prove the following result for the transverse wake potential:

$$\mathbf{W}_\perp(r,\phi,\zeta) \;=\; \frac{c}{4\pi\, b}\sqrt{\frac{Z_0}{\sigma_0}} \cdot \frac{1}{\sigma_z^{1/2}} \nabla_\perp g(r r_s/b^2,\phi) \cdot \left|\frac{u}{2}\right|^{1/2} \cdot \left\{ I_{-1/4} - \mathrm{sign}(u)\, I_{1/4} \right\} e^{-u^2/4} \,. \tag{2.101}$$

The argument of the modified Bessel functions is again $u^2/4$, with $u = -\zeta/\sigma_z$. The transverse gradient of the function g is:

$$\begin{pmatrix} \partial_r \\ \frac{1}{r}\partial_\phi \end{pmatrix} g(rr_s/b^2, \phi) = \frac{2x}{r} \frac{1}{(1-2x\cos(\phi)+x^2)^2} \cdot \begin{pmatrix} (1+x^2)\cos(\phi) - 2x \\ (x^2-1)\sin(\phi) \end{pmatrix}, \quad (2.102)$$

with $x = rr_s/b^2$. Equation (2.102) reduces for $\phi = 0$ and $r = r_s$ to:

$$g'(r_s, b) \equiv \frac{b^2}{2} \partial_r g(r = r_s, \phi = 0) = \frac{r_s b^4}{(b^2 - r_s^2)^2}. \quad (2.103)$$

The function g' is normalized to $g'(0, b)/r_s = 1$. The derivative of the radial forces with respect to the beam position ($r = r_s$) reads:

$$\frac{\partial W_r}{\partial r_s}(r_s, \zeta) = \frac{c}{2\pi b^3} \sqrt{\frac{Z_0}{\sigma_0}} \frac{1}{\sigma_z^{1/2}} \cdot \frac{\partial g'}{\partial r_s} \cdot \left|\frac{u}{2}\right|^{1/2} \cdot \left\{ I_{-1/4} - \mathrm{sign}(u)\, I_{1/4} \right\} e^{-u^2/4}, \quad (2.104)$$

with

$$\frac{\partial g'}{\partial r_s}(r_s/b) = \frac{1 + 3\,(r_s/b)}{\left(1 - (r_s/b)^2\right)^3}, \quad (2.105)$$

where the W_r denotes the radial wake potential. For small beam displacements the radial wake potential can be linearized with respect to the offset r_s:

$$\begin{aligned} W_r(r_s, \zeta) &= \left.\frac{\partial W_r}{\partial r_s}\right|_{r_s=0} \cdot r_s + \mathcal{O}(r_s^2) \quad (2.106) \\ &\approx \frac{c}{2\pi b^3} \sqrt{\frac{Z_0}{\sigma_0}} \frac{1}{\sigma_z^{1/2}} \cdot r_s \cdot \left|\frac{u}{2}\right|^{1/2} \cdot \left\{ I_{-1/4} - \mathrm{sign}(u)\, I_{1/4} \right\} e^{-u^2/4}. \end{aligned}$$

The amplitude of the radial wake potential is inversely proportional to the third power of the beam tube radius. The dependence on the bunch length is $\sigma_z^{-1/2}$ while the longitudinal wake fields behave like $\sigma_z^{-3/2}$ and are hence dominant for short bunches. The shape of the transverse wake potential is shown in Fig. 2.5.

Ohmic losses of the bunch

The total ohmic losses caused by the resistivity of the wall can be obtained by Eq. (2.97). According to the definition of the loss factor (per unit length) one finds for a line charge distribution $\rho(r, \phi, \zeta) = \lambda(\zeta)\delta(\phi)\delta(r - r_s)/r_s$ (see App. A.4):

$$\begin{aligned} k(r_s, b) &= -\int_{-\infty}^{\infty} d\zeta \int_{r=0}^{\infty} dr\, r \int_{\phi=0}^{2\pi} d\phi\, \rho(r, \phi, \zeta)\, W_\parallel(r, \phi, \zeta) \quad (2.107) \\ &= -\frac{c}{(4\pi\sigma_z)^{3/2} b} \sqrt{\frac{Z_0}{\sigma_0}} \cdot \frac{b^2 + r_s^2}{b^2 - r_s^2} \cdot \int_{-\infty}^{\infty} du\, |u|^{3/2} \cdot \left\{ I_{1/4} - I_{-3/4} \right\} e^{-3u^2/4} \\ &= \frac{c\Gamma(3/4)}{\pi^2 (2\sigma_z)^{3/2} b} \sqrt{\frac{Z_0}{\sigma_0}} \cdot \frac{b^2 + r_s^2}{b^2 - r_s^2} \quad \text{with} \quad \Gamma(3/4) \approx 1.2254. \end{aligned}$$

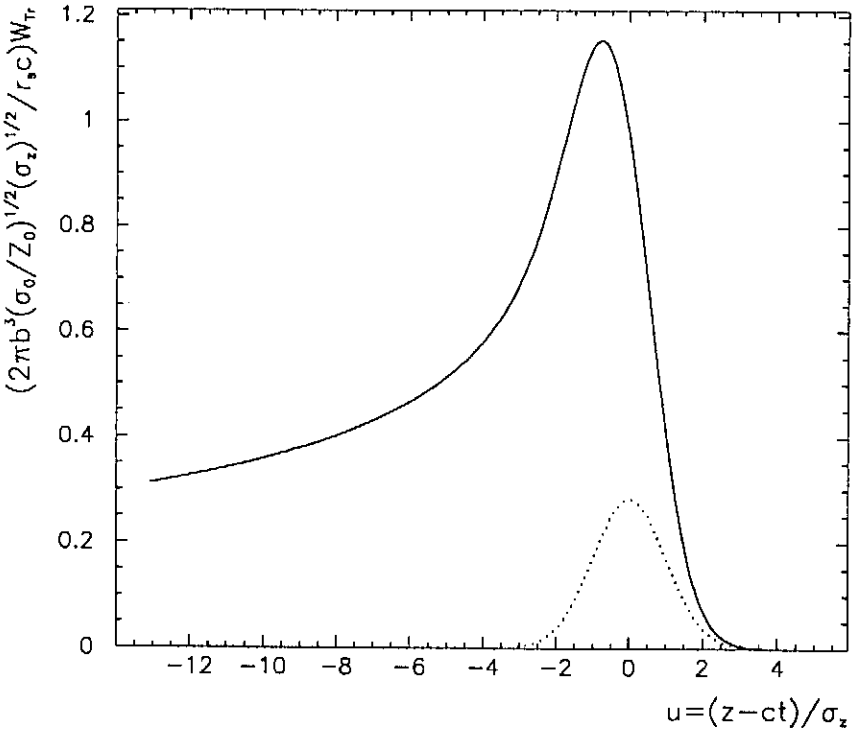

Figure 2.5: Transverse wake potential and charge distribution.

The ohmic power loss for a bunch with a charge Q (per unit time) is related to the loss factor by:

$$P^{(r)}(r_s, b) \;=\; Q^2 c\, k(r_s, b)\,. \tag{2.108}$$

Energy-spread

The rms energy-spread σ_E, induced in a Gaussian bunch by the resistive wall wake fields is written as (see [18]):

$$\sigma_E(\sigma_z) \;=\; Nq^2 \left(\int_{-\infty}^{\infty} d\zeta\, \lambda(\zeta)\, W_{\|}^2(\zeta, \sigma_z) \;-\; k_{\|}^2(\sigma_z) \right)^{1/2} \;=\; \frac{0.46 N q^2 c}{2\pi^2 b \sigma_z^{3/2}} \cdot \sqrt{\frac{Z_0}{\sigma_0}}\,. \tag{2.109}$$

Here N is the number of particles in the bunch, and it has been assumed that the bunch travels on the axis ($r = 0$) and $\sigma_z \gg \zeta_0$.

2.2.4 Short-Range Wake Function

The characteristic length $\zeta_0 = (2b/Z_0\sigma_0)^{1/3}$ has a fundamental meaning for the scaling of the resistive wall wake fields. Fig. 2.6 shows the characteristic length ζ as a function of the tube radius b for different metals.

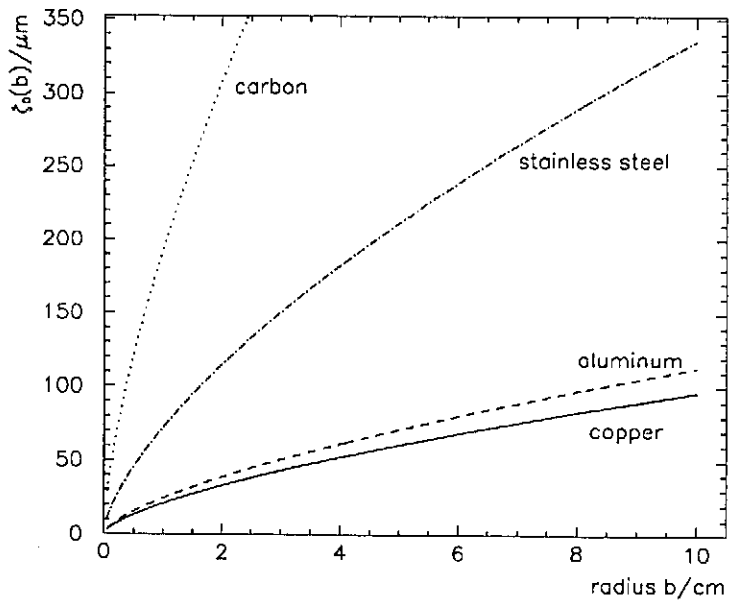

Figure 2.6: Characteristic length ζ_0 as a function of the radius for copper ($\sigma_0 = 5.88 \cdot 10^7\,\Omega^{-1}m^{-1}$), aluminum ($\sigma_0 = 3.65 \cdot 10^7\,\Omega^{-1}m^{-1}$), stainless steel ($\sigma_0 = 1.4 \cdot 10^6\,\Omega^{-1}m^{-1}$) and carbon ($\sigma_0 = 7.27 \cdot 10^4\,\Omega^{-1}m^{-1}$).

The wake potential for a bunch with rms-length σ_z behaves (1) dominantly long-range for $\sigma_z \gg \zeta_0$, (2) dominantly short-range for $\sigma_z \approx \zeta_0$, or (3) dominantly point-like for $\sigma_z \ll \zeta_0$. The long-range resistive wall wake potential has been treated in the previous section and shows a behaviour between an "inductive" and a "resistive" wake potential. The transitions of the wake potential from the cases (1) to (2) and (2) to (3) are discussed in the next section. The results can be clearly understood by the solution for the wake function. The relevant formulas are now developed following [22].

Monopole wake function

In the previous sections the impedance as a function of the dimensionless variable κ has been derived as:

$$Z_{0,\parallel}(\kappa) = \frac{Z_0\zeta_0}{2\pi b^2} \cdot \left[\frac{1 + i\,\mathrm{sign}(\kappa)}{\sqrt{|\kappa|}} - \frac{i\,\kappa}{2} + \left(\frac{\zeta_0}{b}\right)^2 \frac{\sqrt{|\kappa|}}{1 + i\,\mathrm{sign}(\kappa)} \right]^{-1} . \quad (2.110)$$

Obviously, the first term ($\propto |\kappa|^{-1/2}$) in the denominator of Eq. (2.110) is responsible for the low-frequency behaviour of the impedance ($\kappa \ll 1$). The second term in the denominator ($\propto \kappa$) dominates the imaginary part impedance at high frequency while the influence of the term ($\propto |\kappa|^{-1/2}$), which is caused by the radial component of the displacement current, and most effectively stopped by the surface charges, is suppressed

by the ratio $(\zeta_0/b)^2$.

However, in the case of wave numbers comparable to $Z_0\sigma_0$ the real part of the impedance $\mathrm{Re}(Z_0)$ changes its behaviour due to the radial displacement current and becomes proportional to $\kappa^{-3/2}$, while the imaginary part is not affected:

$$\begin{aligned} \mathrm{Re}(Z_{0,\|}(k)) &\propto \begin{cases} k^{-5/2} & \text{for} \quad 1/\zeta_0 \ll k \ll Z_0\sigma_0 \\ k^{-3/2} & \text{for} \quad Z_0\sigma_0 \ll k \end{cases} \\ \mathrm{Im}(Z_{0,\|}(k)) &\propto k^{-1} \quad \text{for} \quad 1/\zeta_0 \ll k\,. \end{aligned} \tag{2.111}$$

One finds that even for carbon the influence of the radial component of displacement current on the impedance is irrelevant for frequencies below the optical regime (see Fig. 2.7). Thus the approximation of the impedance by

$$Z_{0,\|}(\kappa) = \frac{Z_0\zeta_0}{2\pi b^2} \cdot \left[\frac{1 + i\,\mathrm{sign}(\kappa)}{\sqrt{|\kappa|}} - \frac{i\,\kappa}{2} \right]^{-1} \tag{2.112}$$

holds also for such a material*.

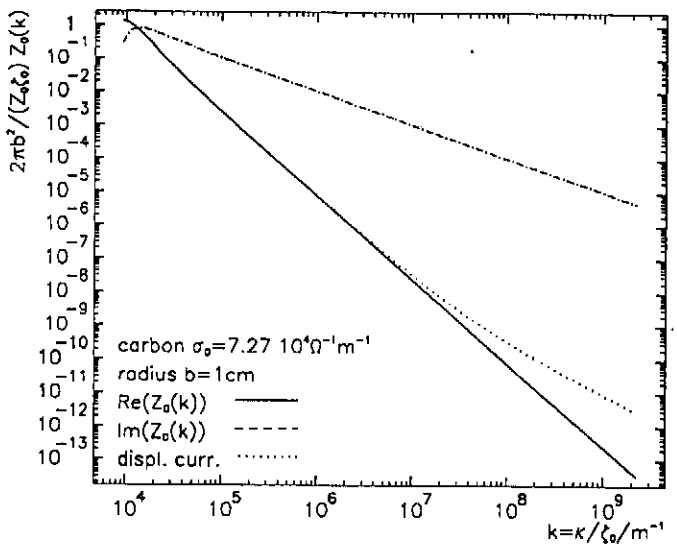

Figure 2.7: Behaviour of the impedance for a $b = 1\,\mathrm{cm}$ carbon pipe at high frequencies (real part: solid curve; imaginary part: dashes curve). Also shown is the effect due to the radial component of displacement current Eq. (2.110)(the dots).

In order to compute the wake function by performing the inverse Fourier transform of $Z_{0,\|}$, the impedance in Eq. (2.112) can be replaced by an analytic function $\mathcal{Z}_{0,\|}(\kappa)$ that

*Dielectric properties have not been taken into account.

equals $Z_{0,\|}(\kappa)$ on the real axis (see [22]):

$$Z_{0,\|}(\kappa) \;=\; \frac{Z_0\zeta_0}{2\pi b^2}\cdot\left[\frac{1+i}{\sqrt{\kappa}}-\frac{i\,\kappa}{2}\right]^{-1}\,. \tag{2.113}$$

In this equation κ is thought of as a complex variable. Because of the square root in Eq. (2.113) the complex plane has a branch-cut which can be chosen on the negative imaginary axis. Then the above function exists on two different Riemann sheets with an uniquely determined square root of the complex variable κ. By traversing the branch-cut one passes from one sheet to the other. The phase of the complex variable κ is counted from $\varphi = -\pi/2$ to $\varphi = 3\pi/2$ in the first Riemann sheet and from $\varphi = 3\pi/2$ to $\varphi = 7\pi/2$ in the second. The three poles of the impedance Eq. (2.113) are given by:

$$\kappa_1 = 2e^{-i\pi/6} = \sqrt{3}-i\,,\quad \kappa_2 = 2e^{i7\pi/6} = -\sqrt{3}-i\,,\quad \kappa_3 = 2e^{i15\pi/6} = 2i\cdot e^{2\pi i}\,,$$

sketched in Fig. 2.8. The original impedance $Z_{0,\|}(\kappa)$ is recovered only on the real axis at

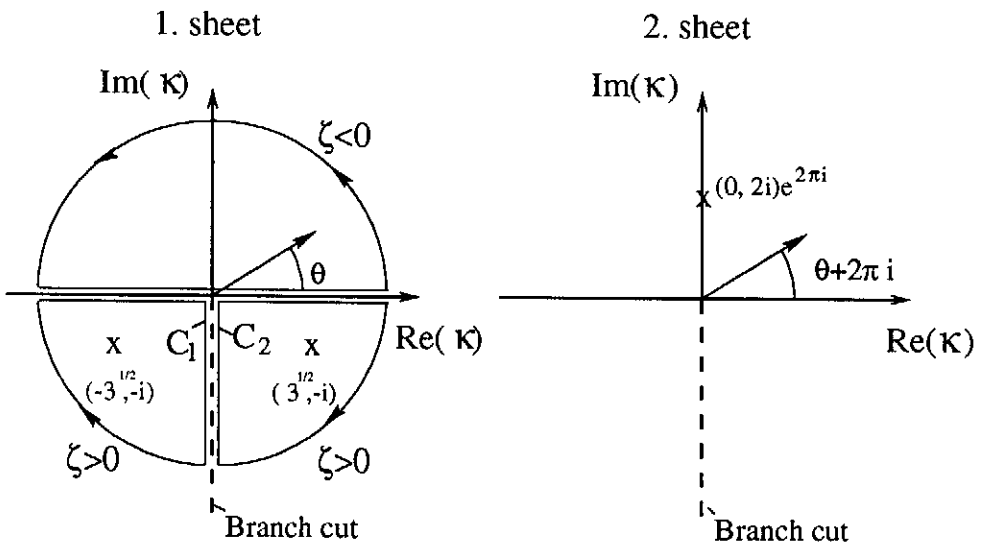

Figure 2.8: Scheme of the Riemann sheets. The poles of the impedance are signed by 'x'. Also shown are the integration contours for the inverse Fourier transform obtaining the wake function for $\mp\zeta < 0$.

the first Riemann sheet.

The inverse Fourier transform is computed using the integration paths shown in Fig. 2.8. The integral along the arcs vanishes by means of $\exp(i\mathrm{Im}(\kappa)\,\zeta) \to 0$ for $\pm\zeta > 0$ and $|\kappa| \to \infty$. The integrals around the paths for $\pm\zeta > 0$ equal $(\mp 2\pi i)$ times the sum of the residuals at the enclosed poles. No poles are present in the upper half plane, hence $W^{\delta}_{0,\|} \equiv 0$ for $\zeta < 0$, that is for particles moving in front of the source charge. Because of the branch-cut the integration path for $\zeta > 0$ splits into a path in the third quadrant and a path in the fourth quadrant. The integrals along C_1 and C_2 lead to an additional term that has to be subtracted from the sum of the residues. Using the substitution $\alpha = \kappa^{1/2}$,

the resonance part of the wake function caused by the poles of the impedance yields:

$$W_{0,\parallel}^{res}(\zeta) = -\frac{Z_0 c}{2\pi b^2}\frac{1}{2\pi}(-2\pi i)\sum_{j=1,2}\frac{4i\alpha_j^2\, e^{-i\alpha_j^2\zeta/\zeta_0}}{\prod_{k\neq j}^{3}(\alpha_j-\alpha_k)}$$
$$= -\frac{4Z_0 c}{3\pi b^2}\, e^{-\zeta/\zeta_0}\cos(\sqrt{3}\zeta/\zeta_0)\,. \qquad (2.114)$$

with $\alpha_j = \kappa_j^{1/2}$. For the integrals along $\mathcal{C}_1$ and $\mathcal{C}_2$ one finds the following expression:

$$W_{0,\parallel}^{pen}(\zeta) = -\frac{Z_0 c}{2\pi b^2}\frac{1}{2\pi}\int_{\tilde{\mathcal{C}}_1+\tilde{\mathcal{C}}_2} d\alpha\,\frac{4i\alpha^2\, e^{-i\alpha^2\zeta/\zeta_0}}{(\alpha^3-2(1-i))}$$
$$= \frac{4Z_0 c}{\pi b^2}\frac{\sqrt{2}}{\pi}\int_0^\infty dx\,\frac{x^2\, e^{-x^2\zeta/\zeta_0}}{x^6+8}\,, \qquad (2.115)$$

where $\tilde{\mathcal{C}}_1, \tilde{\mathcal{C}}_2$ are the integration paths obtained from $\mathcal{C}_1, \mathcal{C}_2$ by using the above substitution. The superscript *pen* indicates that the integral in Eq. (2.115) describes the long-range wake fields ($\propto \zeta^{-3/2}$), hence the penetration of the electromagnetic field into the wall. The value of the integral at $\zeta = 0^+$ is given by:

$$\int_0^\infty dx\,\frac{x^2}{x^6+8} = \frac{\pi}{12\sqrt{2}}\,. \qquad (2.116)$$

Taking this result into account it is convenient to write the wake function as the sum of the resonance and the penetration term in the following way:

$$W_{0,\parallel}(\zeta) = -\frac{Z_0 c}{\pi b^2}\left(\frac{4}{3}\, e^{-\zeta/\zeta_0}\cos(\sqrt{3}\zeta/\zeta_0) - \frac{12\sqrt{2}}{3\pi}\int_0^\infty dx\,\frac{x^2\, e^{-x^2\zeta/\zeta_0}}{x^6+8}\right) \quad (\zeta>0)\,. \qquad (2.117)$$

Note that the wake function only depends on the ratio (ζ/ζ_0). For $\zeta \to 0$ the term in the parentheses is unity. Hence, the amplitude of longitudinal wake function immediately behind the source charge is:

$$W_{0,\parallel}(0^+) = -\frac{Z_0 c}{\pi b^2}\,. \qquad (2.118)$$

The force is decelerating with an amplitude inversely proportional to the square of the pipe radius b and independent of the conductivity of the metal.
The shape of the short-range wake function is dominated by the high-frequency broad band resonator $W_{0,\parallel}^{res}$, with a resonance wave number $k_{res} = \sqrt{3}/\zeta_0$ and a damping factor $\Gamma_{res} = 1/\zeta_0$. In terms of a quality factor Q, introduced in the section 1.3.3, one finds $Q = k_{res}/(2\Gamma_{res}) = \sqrt{3}/2$. An impedance representing these values $(k_{res}, \Gamma_{res}, Q)$ is correspondingly written [23]:

$$Z_{0,\parallel}^{res}(\kappa) = \frac{4Z_0\zeta_0}{3\pi b^2}\,\frac{1-i\kappa}{4-2i\kappa-\kappa^2}\,. \qquad (2.119)$$

The impedance and the wake function are plotted in Fig 2.9 and Fig 2.10.

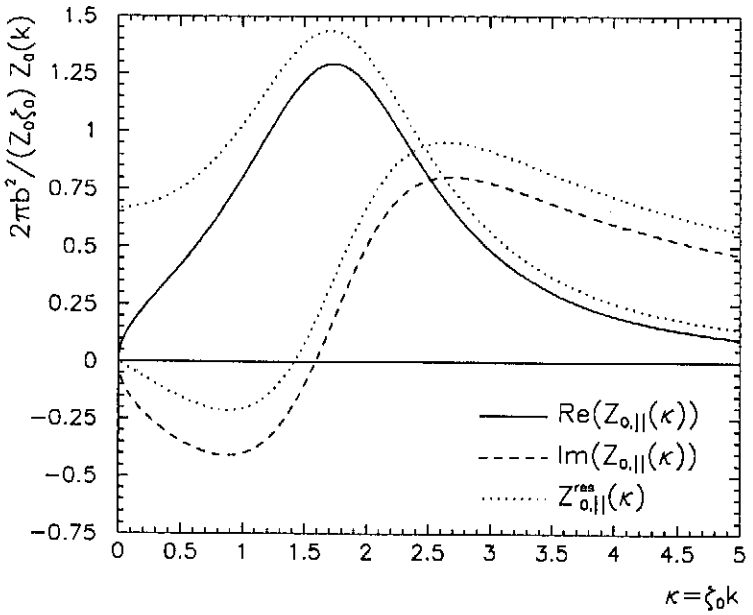

Figure 2.9: Real and imaginary part of the impedance $Z_{0,\|}$ Eq. (2.112) as a function of $\kappa = k\zeta_0$. The impedance of the resonance $Z^{res}_{0,\|}$ is given by the dots.

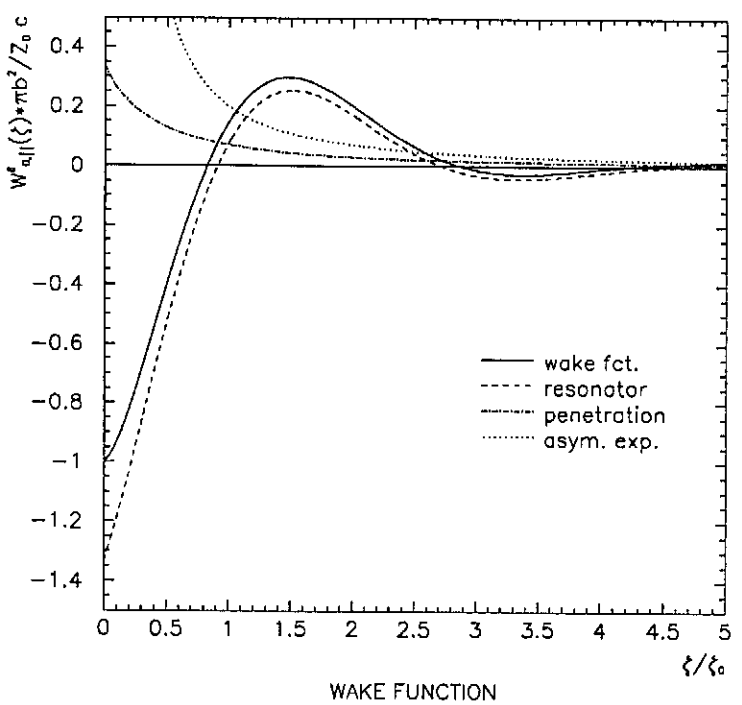

Figure 2.10: The solid curve is the longitudinal short-range resistive wall wake function. Also shown are the oscillator component (dashed), the penetration term (dot-dashed) and the long-range solution of the wake fields (dotted).

Higher modes

In order to calculate the wake functions for higher multipoles the same steps can be repeated as for the monopole wake function. From Eq. (2.84) the impedance for $n > 0$ can be written:

$$\overline{Z}_{n,\parallel}(\kappa) = \frac{Z_0\zeta_0}{\pi b^2}\cdot\left(\frac{rr_s}{b^2}\right)^n\cdot\left[\frac{1+i\,\mathrm{sign}(\kappa)}{\sqrt{|\kappa|}}-\frac{i\,\kappa}{(n+1)}\right]^{-1}, \tag{2.120}$$

where the terms in the curled bracket in the denominator of the impedance have been dropped. The impedance $\overline{Z}_{n,\parallel}$ can be replaced by an analytic function $\mathcal{Z}_{n,\parallel}$. The relevant poles of $\mathcal{Z}_{n,\parallel}$ are:

$$\kappa_{n,1/2} = \left(\frac{n+1}{2}\right)^{2/3}(\pm\sqrt{3}-i)\,. \tag{2.121}$$

Therefore, the resonance wave number and the damping factor of the oscillator component of the wake function increases with the multipole order n proportional to $(n+1)/2$, while the quality factor $Q_n = \sqrt{3}/2$ remains constant. With the same integration paths used for the monopole impedance one obtains the wake function of the n^{th} mode. Using the substitutions $\alpha = \kappa_n^{1/2}\gamma_n^{-1/3}$ with $\gamma_n = (n+1)/2$ the calculation yields:

$$\overline{\overline{W}}_{n,\parallel}(\zeta) = -\frac{Z_0 c}{\pi b^2}\,2\gamma_n\left(\frac{4}{3}\,e^{-\gamma_n^{2/3}\zeta/\zeta_0}\cos\left(\sqrt{3}\gamma_n^{2/3}\zeta/\zeta_0\right)-\frac{12\sqrt{2}\gamma_n}{3\pi}\int_0^\infty dx\,\frac{x^2\,e^{-x^2\zeta/\zeta_0}}{x^6+8\gamma_n^2}\right). \tag{2.122}$$

The amplitude of the n^{th} wake function at $\zeta = 0^+$ is given by $(n+1)W_0(0^+)$. The resistive wall wake function can be written in a compact form as:

$$W_\parallel^\delta(r_\perp, r_{s\perp}, \zeta) = \sum_{n=0}^{\infty}\left(\frac{rr_s}{b^2}\right)^n\overline{\overline{W}}_{n,\parallel}(\zeta)\cos\left(n(\phi-\phi_s)\right). \tag{2.123}$$

The wake functions $\overline{\overline{W}}_{n,\parallel}$ for higher modes are shown in Fig. 2.11.

Transverse wake function

Using the Panofsky-Wenzel theorem and the result given in Eq. (2.123) the transverse wake function is evaluated to:

$$\mathbf{W}_\perp^\delta(\mathbf{r}_\perp, \mathbf{r}_{s\perp}, \zeta) = \sum_{n=1}^{\infty} n\left(\frac{rr_s}{b^2}\right)^{n-1}\left(\frac{r_s}{b^2}\right) \times\left[\cos\left(n(\phi-\phi_s)\right)\hat{\mathbf{e}}_r-\sin\left(n(\phi-\phi_s)\right)\hat{\mathbf{e}}_\phi\right]\cdot\overline{\overline{\mathbf{W}}}_{n,\perp}(\zeta) \tag{2.124}$$

with

$$\overline{\overline{\mathbf{W}}}_{n,\perp}(\zeta) = \frac{Z_0\,c}{\pi\,b^2}\,\zeta_0\cdot\left\{\gamma_n^{1/3}e^{-\gamma_n^{2/3}\zeta'}\cdot\left[\frac{2}{\sqrt{3}}\sin\left(\sqrt{3}\gamma_n^{2/3}\zeta'\right)-\frac{2}{3}\cos\left(\sqrt{3}\gamma_n^{2/3}\zeta'\right)\right]+\frac{24\sqrt{2}\gamma_n^2}{3\pi}\int_0^\infty dx\frac{e^{-x^2\zeta'}}{x^6+8\,\gamma_n^2}\right\}, \tag{2.125}$$

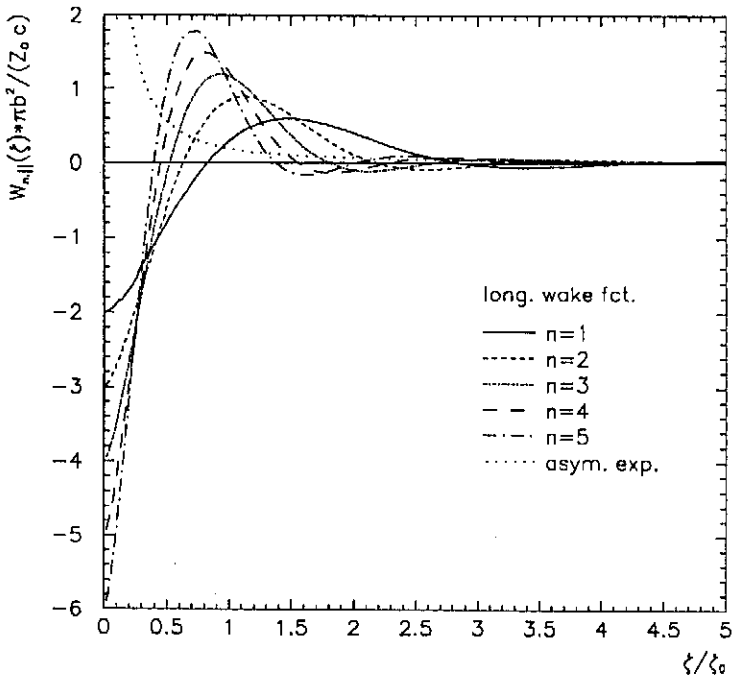

Figure 2.11: Longitudinal wake functions $\overline{\overline{W}}_{n,\parallel}$ of higher multipoles modes ($n = 1, \ldots, 5$).

where $\zeta' = \zeta/\zeta_0$ is the normalized distance. The first five multipoles beginning with the dipole mode of the transverse wake functions are plotted in Fig. 2.12.

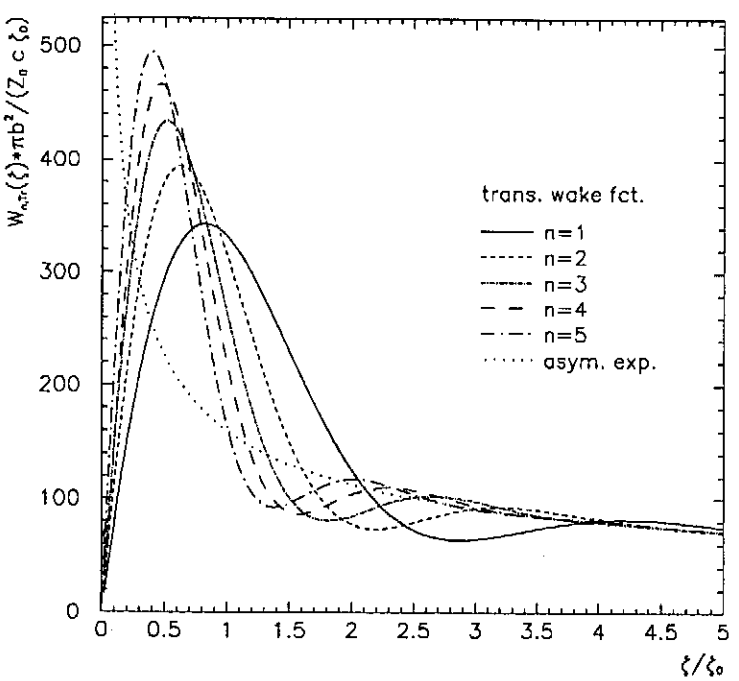

Figure 2.12: Transverse wake functions $\overline{\overline{W}}_{n,\perp}$ of higher multipoles ($n = 1, \ldots, 5$).

Wake potential for a uniform beam

The wake potential for a longitudinally uniform beam ($\lambda = 1$) is obtained by integrating the wake function with respect to ζ':

$$W_{\parallel}^{uni}(\zeta) \;=\; \int_{-\infty}^{\infty} d\zeta'\, \lambda(\zeta' - \zeta)\, W_{\parallel}^{\delta}(\zeta') \;=\; \int_{0}^{\infty} d\zeta'\, W_{\parallel}^{\delta}(\zeta')\,. \tag{2.126}$$

Calculations show that the last integral in Eq. (2.126) vanishes for all multipoles $W_{n,\parallel}^{\delta}$. Hence, the wake potential of a uniform beam in a resistive tube equals zero independent of the beam position $\mathbf{r}_{s\perp}$:

$$W_{\parallel}^{uni} \;\equiv\; 0 \qquad \Leftrightarrow \qquad \int_{0}^{\infty} d\zeta'\, \overline{\overline{W}}_{n,\parallel}(\zeta') \;=\; 0 \qquad \forall\, n \in \mathbb{N}\,. \tag{2.127}$$

Wake function at $\zeta = 0$

Since the integral $\int_{-\infty}^{\infty} d\zeta' W_{n,\parallel}^{\delta}(\zeta')$ is absolutely convergent and the wake function satisfies Dirichlet's condition* for $-\infty < \zeta < \infty$ one can use Fourier's integral theorem obtaining

$$\overline{\overline{W}}_{n,\parallel}^{\delta}(0) \;=\; \frac{1}{2}\left[\overline{\overline{W}}_{n,\parallel}(0^-) + \overline{\overline{W}}_{n,\parallel}(0^+)\right] \;=\; \frac{Z_0 c\,(n+1)}{2\pi b^2}\,. \tag{2.128}$$

This result can also be derived by performing the inverse Fourier transform of the impedance at $\zeta = 0$.

2.2.5 Short-Range Wake Potential

The wake potential of a Gaussian-charge distribution in case of a frequency independent conductivity has been derived in [18]. The results are summarized and compared to the results of the last sections.

Impedance

The impedance for two point-like particles has been found as:

$$Z_{\parallel}(r, r_s, \phi)(k) \;=\; \sum_{n=0}^{\infty} \frac{1}{1+\delta_{0,n}} \left(\frac{r r_s}{b^2}\right)^n \overline{\overline{Z}}_{n,\parallel}(k) \cos(n\phi) \tag{2.129}$$

with

$$\begin{aligned} \overline{\overline{Z}}_{n,\parallel}(k) \;&=\; \frac{Z_0}{i\pi}\,(n+1)\,k\,H_n^1(\lambda b)\Big[\left(n(n+1) - k^2 b^2\right) \\ &+\; 2(n+1)\frac{k^2 b^2}{\lambda} H_{n+1}^1(\lambda b) + \frac{n+1}{2-\delta_{0,n}} \lambda b \left(H_{n+1}^1(\lambda b) - H_{n-1}^1(\lambda b)\right)\Big]^{-1}\,. \end{aligned} \tag{2.130}$$

*A function f(x) satisfies Dirichlet's conditions in the interval (a,b) if

1. f(x) has only a finite number of maxima and minima in (a,b).
2. f(x) has only a finite number of finite discontinuities in (a,b) - and no infinite discontinuities.

The above equation describes the impedance up to any multipole order over the whole frequency range where Ohm's law with a constant conductivity is still applicable. If the Hankel functions of first kind H^1 are replaced by their asymptotic expression for large arguments and the very high and very low-frequency terms are dropped the impedance of the previous section is recovered:

$$\overline{\overline{Z}}_{n,\|}(k) \;=\; \frac{Z_0}{\pi b}\left[(1+\delta_{0,n})\frac{i\lambda}{k} - \frac{ikb}{(n+1)}\right]^{-1} . \tag{2.131}$$

Longitudinal wake potential per unit length

The wake potential has been calculated by the inverse Fourier transform of the impedance multiplied by the frequency spectrum of the bunch. One can expand the longitudinal wake potential* in the following way [18]:

$$W_{\|}(r,\phi,\zeta,\sigma_z) \;=\; -\frac{Z_0 c}{\pi b^2}\sum_{n=0}^{\infty}\left(\frac{r r_s}{b^2}\right)^n \cos(n\phi)\, w_{n,\|}(\zeta/\zeta_0,\sigma_z/\zeta_0)\,, \tag{2.132}$$

where the dimensionless function $w_{n,\|}$ is given by the integral

$$w_{n,\|}(u,v) \;=\; \frac{2(n+1)}{3\pi}\int_{-1}^{\infty} dx\, e^{-\phi_n^2/2}\,\frac{x\sin(\theta_n)\;+\;\cos(\theta_n)}{x^2\;+\;1} \tag{2.133}$$

with

$$\theta_n \;=\; u\left[(n+1+\delta_{0,n})(x+1)\right]^{2/3}\,, \qquad \phi_n \;=\; v\left[(n+1+\delta_{0,n})(x+1)\right]^{2/3}\,. \tag{2.134}$$

For distances $\zeta \gg \zeta_0$† the asymptotic behaviour of $w_{n,\|}$ is

$$w_{n,\|}(u,v) \;\overset{u\gg(1,v)}{\simeq}\; -\frac{1}{(1+\delta_{0,n})\sqrt{8\pi}}\,u^{-3/2}\,, \tag{2.135}$$

in agreement with Eq. (2.81), Eq. (2.86) for the behaviour of the long-range wake function.

Transverse wake potential per unit length

A parameterization of the transverse wake potential suitable for numerical calculation has been derived in [18]:

$$\begin{aligned}\mathbf{W}_{\perp}(r,\phi,\zeta,\sigma_z) \;=\; & -\frac{Z_0 c\zeta_0}{\pi b^3}\sum_{n=0}^{\infty} n\left(\frac{r}{b}\right)^{n-1}\left(\frac{r_s}{b}\right)^n\left(\cos(n\phi)\mathbf{e}_r - \sin(n\phi)\mathbf{e}_\phi\right)\\ & \times w_{n,r}(\zeta/\zeta_0,\sigma_z/\zeta_0)\,,\end{aligned} \tag{2.136}$$

where the dimensionless function $w_{n,r}$ is given by the integral

$$w_{n,r}(u,v) \;=\; \frac{2(n+1)^{1/3}}{3\pi}\int_{-1}^{\infty} dx\, e^{-\phi_n^2/2}\,\frac{\sin(\theta_n)\;-\;x\cos(\theta_n)}{(x+1)^{2/3}(x^2+1)}\,. \tag{2.137}$$

*In [18] the opposite sign for the longitudinal wake potential is used.

†The characteristic length s_0 introduced in [18] differs by a factor $2^{-1/3}$ from ζ_0.

For distances ζ much larger than the characteristic length ζ_0 the above integral expression yields:

$$w_{1,r}(u,v) \overset{u\gg(1,v)}{\sim} \frac{1}{\sqrt{2\pi}}\, u^{-1/2}\,, \tag{2.138}$$

which corresponds to the solution given in Eq. (2.104) for the transverse wake function of a dipole in the long-range approximation.

Numerical results

The numerical results* of the integral representation Eqs. (2.133, 2.137) for the wake potentials are in agreement with the corresponding solutions for the wake potential obtained by convolving the wake functions with a Gaussian charge distribution. The longitudinal wake potential per unit length for different values of $v = \sigma_z/\zeta_0$ for a line-charge traveling on-axis is shown in Fig. 2.13. The behaviour of the corresponding transverse dipole wake function per unit offset is plotted in Fig. 2.14.

The dimensionless parameter $v = \sigma_z/\zeta_0$ is a measure for a dominantly long-range ($\sigma_z \gg \zeta_0$), a dominantly short-range ($\sigma_z \approx \zeta_0$) or a dominantly point-like ($\sigma_z \ll \zeta_0$) wake potential. For $v \to \infty$ one finds the solution given in Eq. (2.97) and Eq. (2.101) as the long-range limit for the wake potentials. As the parameter v decreases the wake potential becomes "resistive", and for $v \ll 1$ it is purely "capacitive". Then the wake potential of the bunch approaches the integral over the charge distribution. In the limit $v \to 0$ the potential yields the wake function for a point-like charge. The origin of the discontinuity at $\zeta = 0$ is shown in Fig. 2.15.

Longitudinal loss factor for Gaussian charge distribution

The longitudinal loss factor of a Gaussian line-charge distribution can be written [18]:

$$k_{\|}(r,\sigma_z) \;=\; \frac{Z_0 c}{\pi b^2} \sum_{n=0}^{\infty} \left(\frac{r}{b}\right)^{2n} k_{n,\|}(\sigma_z/\zeta_0)\,, \tag{2.139}$$

where the dimensionless function $k_{n,\|}$ reads

$$k_{n,\|}(v) \;=\; \frac{2(n+1)}{3\pi} \int_{-1}^{\infty} dx\, e^{-\phi_n^2} \frac{1}{x^2+1}\,, \tag{2.140}$$

with ϕ_n given in Eq. (2.134). For $\sigma_z \gg \zeta_0$ the above integral is approximately given by:

$$k_{n,\|}(v) \overset{v\gg 1}{\simeq} \frac{\Gamma(3/4)}{2(1+\delta_{0,n})\pi}\, v^{-3/2}\,. \tag{2.141}$$

Therefore the loss factors of the multipoles in the long distance limit become proportional to $\sigma_z^{-3/2} b^{-1} \sigma_0^{-1/2}$ in agreement to the result in Eq. (2.107). For a point charge ($\sigma_z = 0$) the integral in Eq. (2.141) can be calculated analytically and one finds

$$k_{n,\|}(v=0) \;=\; \frac{(n+1)}{2}\,. \tag{2.142}$$

*A numerical code written by O. Napoly has been used.

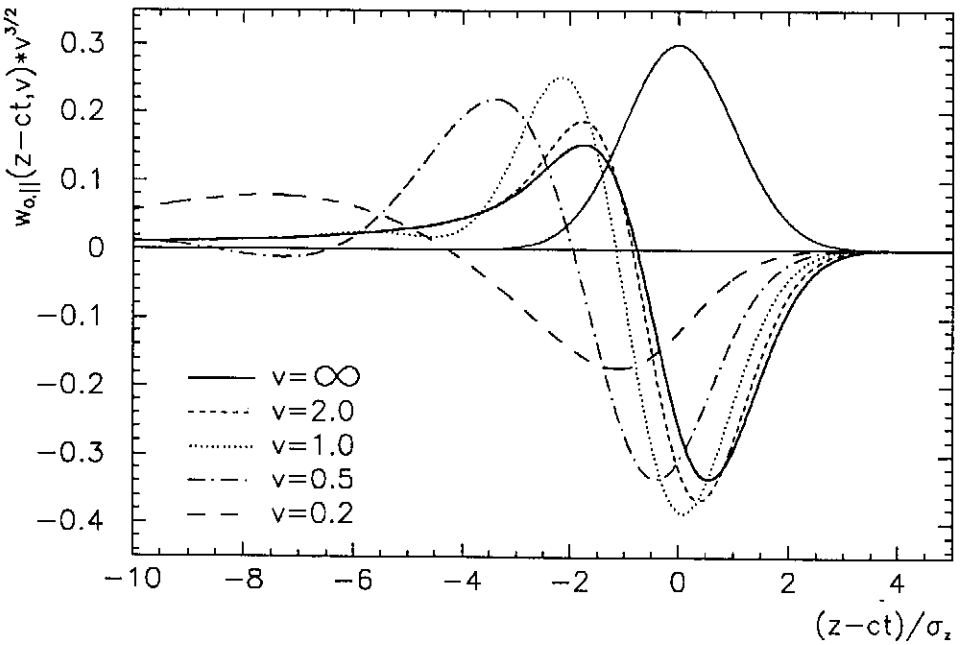

Figure 2.13: Transition of the Gaussian longitudinal wake potential ($n = 0$) from the long-range to the short-range dominated regime described by the dimensionless parameter $v = \sigma_z/\zeta_0$.

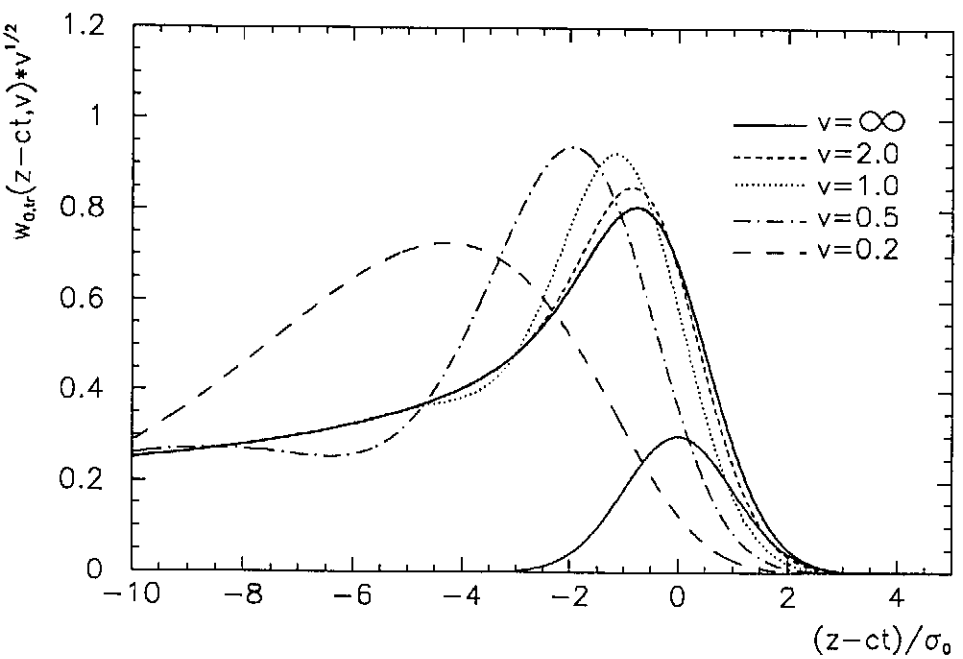

Figure 2.14: Transition of the Gaussian transverse wake potential ($n = 1$) per unit displacement r from the long-range to the short-range dominated regime described by the dimensionless parameter $v = \sigma_z/\zeta_0$.

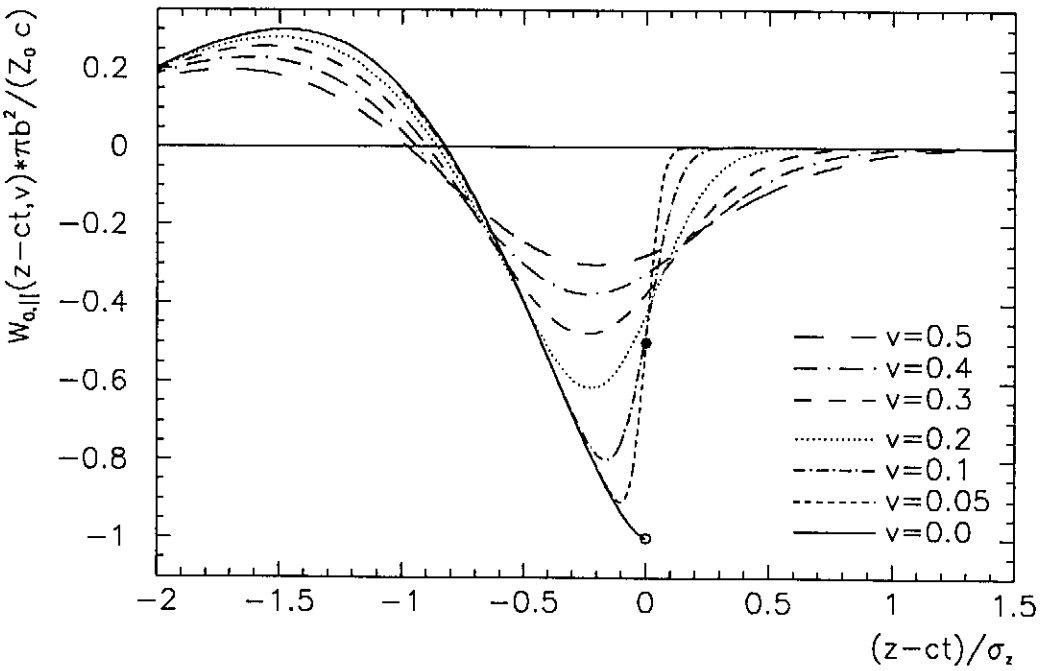

Figure 2.15: Transition for the longitudinal wake potential for short bunches ($\sigma < \zeta_0$) to a point-like charge. The origin of the discontinue is clearly seen. The wake potential along a Gaussian charge distribution is approximately given by the **error** function.

As a consequence, by evaluating Eq. (2.139) the longitudinal loss factor of point charge moving off-axis is:

$$k_z(\sigma_z = 0) \;=\; -\frac{Z_0 c}{2\pi b^2}\cdot\frac{b^4}{(b^2 - r^2)^2}\,. \tag{2.143}$$

Transverse loss factor of a Gaussian charge distribution

The corresponding equation for the radial loss factor ($\phi = 0$) is written as:

$$k_r(r,\sigma_z) \;=\; \frac{Z_0 c\zeta_0}{\pi b^3}\sum_{n=1}^{\infty}\left(\frac{r}{b}\right)^{2n-1} k_{n,r}(\sigma_z/\zeta_0)\,, \tag{2.144}$$

where the integral representation for $k_{n,r}$ is given by:

$$k_{n,r}(v) \;=\; -\frac{2(n+1)^{1/3}}{3\pi}\int_{-1}^{\infty} dx\, e^{-\phi_n^2}\frac{x}{(x+1)^{2/3}(x^2+1)} \tag{2.145}$$

with the asymptotic expressions

$$k_{n,r}(v) \;\overset{v\gtrsim 1}{\simeq}\; \frac{\Gamma(1/4)}{2^{5/3}\pi}\,v^{-1/2}\,. \tag{2.146}$$

2.2.6 Physical Interpretation of the Resistive Wall Wake Fields

A physical interpretation of the mechanism that can account for the high-frequency resonance has been given in [22].

An electromagnetic wave propagating down a tube with perfectly conducting walls cannot interact with a particle, that is, in a dispersion diagram the speed of light line representing the phase (and group) velocity of the bunch never crosses the dispersion curve of the wave. When the tube has a finite but high conductivity the dispersion curve is slightly different.

In this case the wave number can be approximated by:

$$k_\lambda \approx k_\lambda^{(0)} + \alpha_\lambda + i\,\beta_\lambda \qquad \text{and} \quad k_\lambda^{(0)} = \frac{\omega}{c}\sqrt{1-\left(\frac{\omega_\lambda}{\omega}\right)^2} \tag{2.147}$$

with α_λ, β_λ small real numbers, and $k_\lambda^{(0)}$ the wave number of the λ^{th} mode in a perfectly conducting pipe. By the method of perturbed boundary conditions it can be shown [3] that $\alpha_\lambda = \beta_\lambda$ for TM-modes in a cylindrical tube. The phase velocity is reduced by the additional real part, and for a sufficiently high frequency it crosses the dispersion line of light. Hence, a beam with $v \approx c$ can couple to the electromagnetic waves excited in a resistive tube.

The frequency ω satisfying the equation

$$\frac{\omega}{c} = k_\lambda^{(0)}(\omega) + \alpha_\lambda(\omega) \tag{2.148}$$

for the first TM-mode in a cylindrical pipe is in good agreement with the resonance frequency $\omega_{res} = ck_{res}$ obtained for the oscillator part of the wake function [22].

The damping of the wave is described by β_λ, and leads to a width of the resonance $\delta k_\lambda \approx \beta_\lambda \ll k_\lambda$. This is schematically drawn in Fig. 2.16 by two - rather than one - dispersion lines.

The low Q-factor of the broad-band resonator derived for the wake function cannot be understood by looking at the damping of the waves, but by studying the spread in frequencies $\delta\omega$ in the waves excited (see Fig. 2.16) [22].

2.3 Wake Fields for Frequency-Dependent Conductivity

The short-range wake fields have to be modified if the frequencies of the excited electromagnetic waves approach the inverse of the relaxation time τ of the metal. An extension to this regime has been derived in [22]. By introducing a dimensionless variable Γ

$$\Gamma = \left(\frac{\tau\, c}{\zeta_0}\right), \tag{2.149}$$

the following cases can be distinguished:

- $\Gamma \ll 1$: The wake function obtained from a constant conductivity is a sufficient approximation;

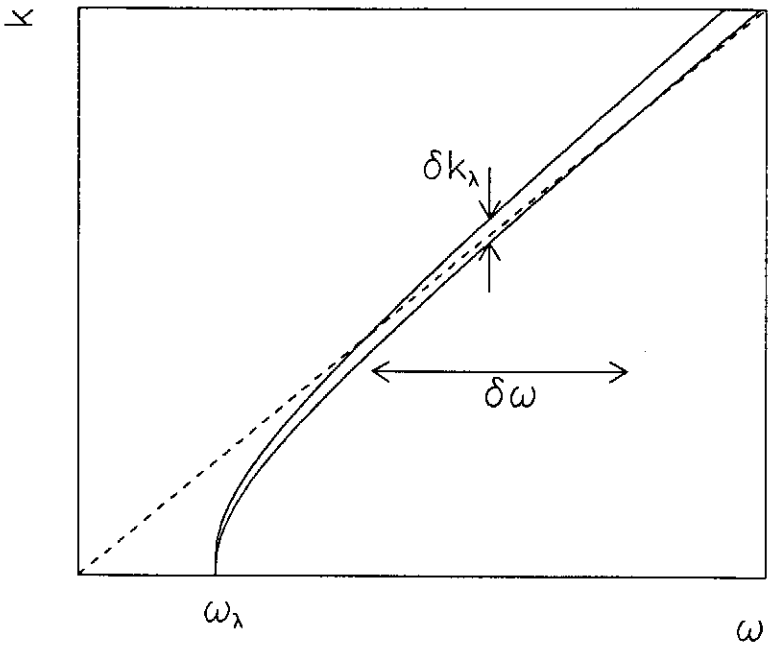

Figure 2.16: A sketch of one band of the dispersion curve for a resistive pipe. The light line is given by the dashed line.

- $\Gamma \simeq 1$: The wake function obtained from a frequency-dependent conductivity has to be used;
- $\Gamma \gg 1$: An approximation for the wake function can be considered.

Typical values for the relaxation time τ and the dimensionless parameter Γ are given in Tab. 2.1. Since the relation between the electric field and the current differs from that

materials	relaxation time τ	conductivity σ_0	parameter Γ		
T = 300 K	$\times 10^{-14}$ sec.	$\times 10^7\ \Omega^{-1}m^{-1}$	b=0.1 cm	b=0.5 cm	b=2.0 cm
Ag	3.76	5.93	2.52	0.87	0.34
Cu	2.46	5.88	1.64	0.56	0.22
Al	0.71	3.65	0.40	0.13	0.05
Fe	0.23	1.10	0.08	0.03	0.01

Table 2.1: Normalized relaxation time Γ for different pipe radii and materials.

used before, the monopole impedance given by Eq. (2.112) is rewritten as:

$$Z_{0,\parallel}(k) \;=\; \frac{Z_0}{2\pi b}\cdot\left[\frac{\lambda}{k}-\frac{ikb}{2}\right]^{-1} \qquad \text{with} \qquad \lambda^2 \;=\; ikZ_0\sigma(\omega)\,, \tag{2.150}$$

where now the conductivity σ depends in addition on the frequency ω.

2.3.1 Frequency-Dependence of Conductivity

If the time variation of an electric field is of the order of the collision time τ of the conducting electrons then the current $\mathbf{j}$ and the electric field $\mathbf{E}$ are related by (see [19]):

$$\mathbf{j} = \frac{\sigma_0 \mathbf{E}}{1 - i\omega\tau} \quad \text{with} \quad \sigma_0 = \frac{ne^2\tau}{m}, \tag{2.151}$$

where n denotes the number of conducting electrons per unit volume, and m the electron mass. The result is usually written as:

$$\mathbf{j} = \sigma(\omega)\mathbf{E}, \tag{2.152}$$

where $\sigma(\omega)$, known as the frequency-dependent (or **AC**) conductivity, reads:

$$\sigma(\omega) = \frac{\sigma_0}{1 - i\omega\tau}. \tag{2.153}$$

Equation (2.153) reduces to the constant electrical conductivity σ_0 if $\omega\tau \ll 1$.

2.3.2 The High Γ Limit

Expressing Eq. (2.153) in terms of Γ and the normalized wave number $\kappa = k\zeta_0$, the frequency-dependent conductivity reads:

$$\sigma(\kappa) = \frac{\sigma_0}{1 - i\kappa\Gamma}. \tag{2.154}$$

For $\kappa\Gamma \gg 1$ the conductivity can be approximated by

$$\sigma \approx \frac{\sigma_0}{\kappa\Gamma}\left(i + \frac{1}{\kappa\Gamma}\right). \tag{2.155}$$

Using this approximation the square root of λ^2 Eq. (2.150) can be written as:

$$\lambda = \frac{b}{\zeta_0^2}\sqrt{\frac{2}{\Gamma}}\left(i + \frac{\mathrm{sign}(\kappa)}{2\kappa\Gamma} + \mathcal{O}\left(\frac{1}{(\kappa\Gamma)^2}\right)\right). \tag{2.156}$$

The positive imaginary part of λ guarantees a vanishing electromagnetic field* for $r \to \infty$. The impedance obtained by inserting λ in Eq. (2.150) can be replaced by an analytic function $\mathcal{Z}_{0,\|}$ yielding:

$$\mathcal{Z}_{0,\|}(\kappa) = \frac{Z_0\zeta_0}{2\pi b^2}\left(\sqrt{\frac{2}{\Gamma}}\frac{1}{\kappa}\left(i + \frac{1}{2\kappa\Gamma}\right) - \frac{i\kappa}{2}\right)^{-1}. \tag{2.157}$$

The longitudinal wake function calculated from $\mathcal{Z}_{0,\|}$ reads [22]:

$$W_{0,\|}(\zeta) = -\frac{Z_0 c}{\pi b^2} e^{-\zeta/(4\Gamma\zeta_0)} \cos\left((8/\Gamma)^{1/4}\zeta/\zeta_0\right). \tag{2.158}$$

*In analogy to the derivation of the electromagnetic field in metal section 2.2.1 the dependence of the field components have been chosen $\propto e^{i\lambda r}$.

Hence, the wake function is represented by a weakly damped resonator with a resonance wave number $k_{res} = (8/\Gamma)^{1/4}/\zeta_0$ and a damping factor $\Gamma_{res} = 1/(4\tau c)$. One can express the wake function in terms of the plasma frequency of the metal $\omega_p = \sqrt{ne^2/(\epsilon_0 m)}$ by:

$$W_{0,\parallel}(\zeta) \approx -\frac{Z_0 c}{\pi b^2} \cos\left(\sqrt{\frac{2\omega_p}{cb}}\zeta\right), \tag{2.159}$$

where the damping term has been dropped. For example, the values for the plasma frequency and the resonance wave length $\lambda_{res} = 2\pi/k_{res}$ for a silver and a copper pipe of a radius $b = 1\,\mathrm{mm}$ are listed in Tab. 2.2.

material	plasma frequency $\nu_p = \omega_p/2\pi$	wave length λ_{res}
T = 300 K	$\times 10^{15}$ Hz	$b = 1\,\mathrm{mm}$
Ag	2.12	$21.0\,\mu\mathrm{m}$
Cu	2.61	$20.0\,\mu\mathrm{m}$

Table 2.2: Plasma frequency of a metal and the resonance wave length $\lambda_{res} = 2\pi/k_{res}$ of the wake function for a silver and a copper tube of 1 mm tube radius.

The above calculation can be repeated within the metal walls. By dropping again the weak damping term the longitudinal electric fields in the wall are found as:

$$E_{0,z}(\zeta) \approx -\frac{qZ_0 c}{\pi b^2}\sqrt{\frac{b}{r}}e^{-k_p(r-b)}\cos\left(\sqrt{\frac{2k_p}{b}}\zeta\right) \qquad (r > b). \tag{2.160}$$

Contrary to the long-range behaviour of the wake fields, where a penetration of the electromagnetic field into the wall is observed, the fields for short distances are limited to a thin layer at the surface. The depth $(r - b)$ for which the amplitude of the fields drops to $1/e$ of its maximum is just $1/k_p$, i.e. for copper one finds $\delta r \approx 18\,\mathrm{nm}$. In addition the electric field $E_{0,z}$ has a longitudinal cosine modulation.

2.3.3 General Case

Impedance

In order to calculate the resistive wall wake function for arbitrary Γ, one can use:

$$\lambda = \frac{b}{\zeta_0^2}\frac{|\kappa|^{1/2}}{(1+\kappa^2\Gamma^2)^{1/4}}\left(i\sqrt{1+t_\lambda} + \mathrm{sign}(\kappa)\sqrt{1-t_\lambda}\right) \tag{2.161}$$

where

$$t_\lambda = \frac{|\kappa|\Gamma}{\sqrt{1+\kappa^2\Gamma^2}}. \tag{2.162}$$

Inserting this expression in Eq. (2.150), the impedance for a frequency-dependent conductivity is given by:

$$Z_{0,\parallel}(\kappa) = \frac{Z_0\zeta_0}{2\pi b^2}\left[\sqrt{\frac{t_\lambda}{\Gamma\kappa^2}}\left(i\sqrt{1+t_\lambda} + \mathrm{sign}(\kappa)\sqrt{1-t_\lambda}\right) - \frac{i\kappa}{2}\right]^{-1}. \tag{2.163}$$

The real and the imaginary part of the impedance Eq. (2.163) as a function of the

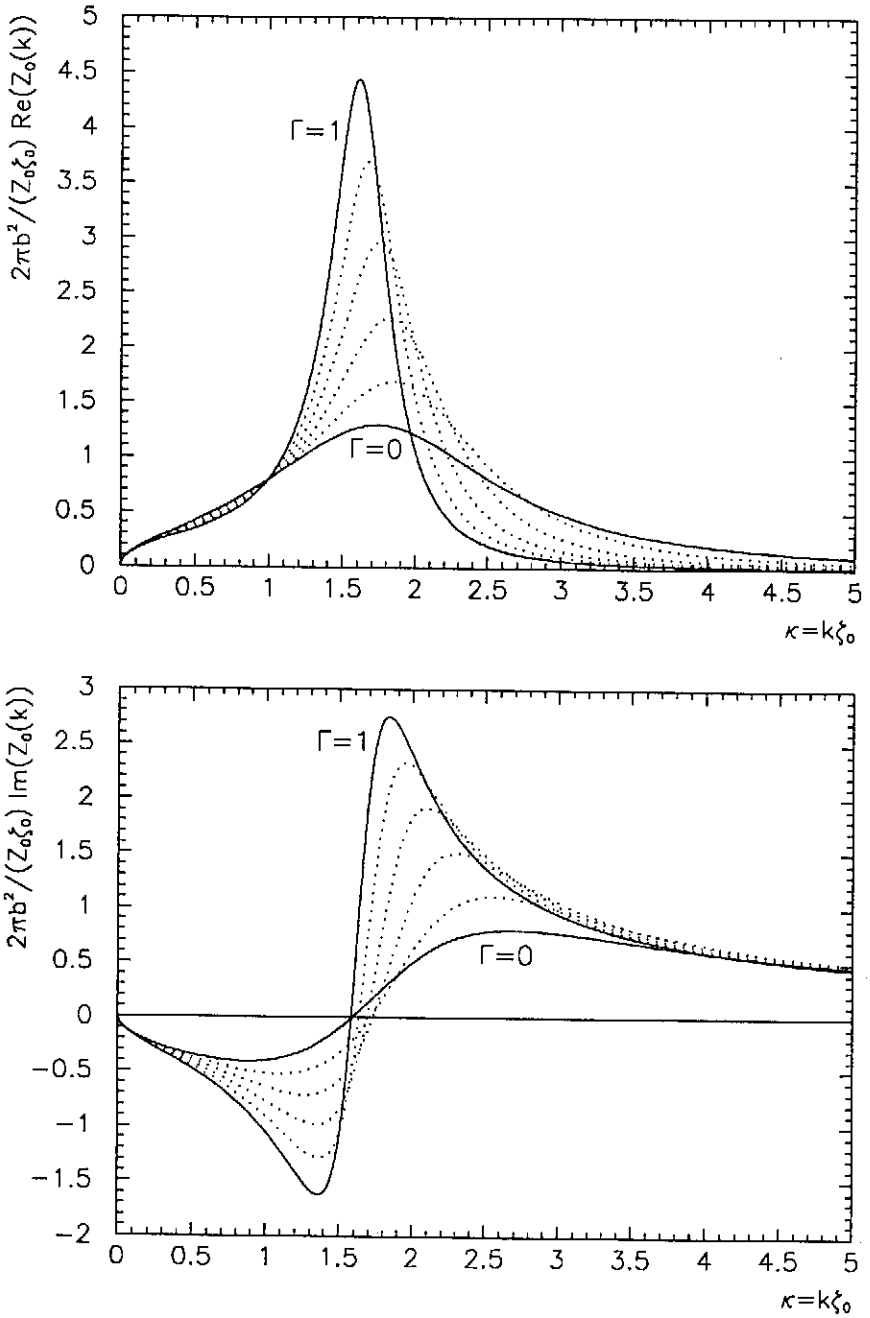

Figure 2.17: Real and imaginary part of the impedance for $\Gamma = 0$, 0.2, 0.4, 0.6, 0.8 and 1.

normalized variable κ for different values of Γ is shown in Fig. 2.17.

The impedance for $\Gamma \neq 0$ differs significantly from the case $\Gamma = 0$ only in the range $0.5 < \kappa = \zeta k < 4.5$. With increasing Γ the resonance of the impedance becomes narrower and the corresponding Q-factors are larger.

Obviously, the short-range behaviour of the wake fields is also dominated by an high frequency oscillator. This oscillator term is associated with two simple poles of an analytic

function $\mathcal{Z}_{0,\|}$. The poles are located in the lower half of the complex plane, symmetrically with respect to the imaginary axis.

In order to find the resonance frequency, the damping, and the strength of the resonance, the locations and the residue of the poles have to be calculated. As discussed in section 2.2.4 the square root of the variable κ leads to a branch-cut in the complex plane where the relevant Riemann sheet can again be defined for $-\pi/2 < \theta < 3\pi/2$.

The movement of the fourth quadrant pole of the impedance is shown in Fig. 2.18 when Γ varies from 0 to 5. The asterisks ($*$) in this plot are related to the pole positions for half integer values of Γ.

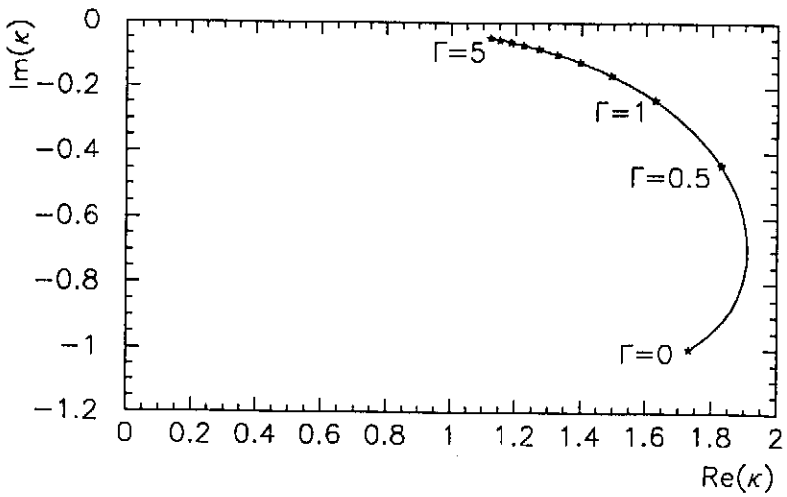

Figure 2.18: Position of the poles in the complex κ-plane of the impedance given in Eq. (2.18) for $\Gamma = 0, 0.5, \ldots, 5$

Wake function

In Fig. 2.19 the longitudinal wake functions for different values of the parameter Γ are plotted. As expected, the number of oscillations of the wake function until it remains positive (long-range behaviour) increases for larger Γ. The resonance frequency reaches a maximum at $\Gamma \approx 0.3$ and degreases at higher values for Γ. Finally, for high Γ, one finds for the resonance wave number $k_{res} = (8/\Gamma)^{1/4}/\zeta_0$ as derived in the previous subsection.

Wake potential

From the behaviour of the wake function for a frequency-dependent conductivity $\sigma(\omega)$, described above, it is obvious that the wake potential differs only significantly from the case of a constant conductivity σ_0 if the bunch length σ_z is of the order of the characteristic length ζ_0. For $\sigma_z \ll \zeta_0$ the wake potential is mainly influenced by the wake function at ultra-short distances, with an approximately constant amplitude given by $W_{0,\|} = -Z_0 c/(\pi b^2)$. Hence, the results given in subsection 2.2.5 for the transition between a dominantly short-range to a dominantly point-like wake potential are independent of Γ. In the opposite case $\sigma_z \gg \zeta_0$ the variation of the charge distribution $\lambda(\zeta)$ over one period of the short-range wake function ($\propto 1/k_{res}$) is small and therefore the positive and negative contributions of the wake function to the wake potential cancel. In this case the

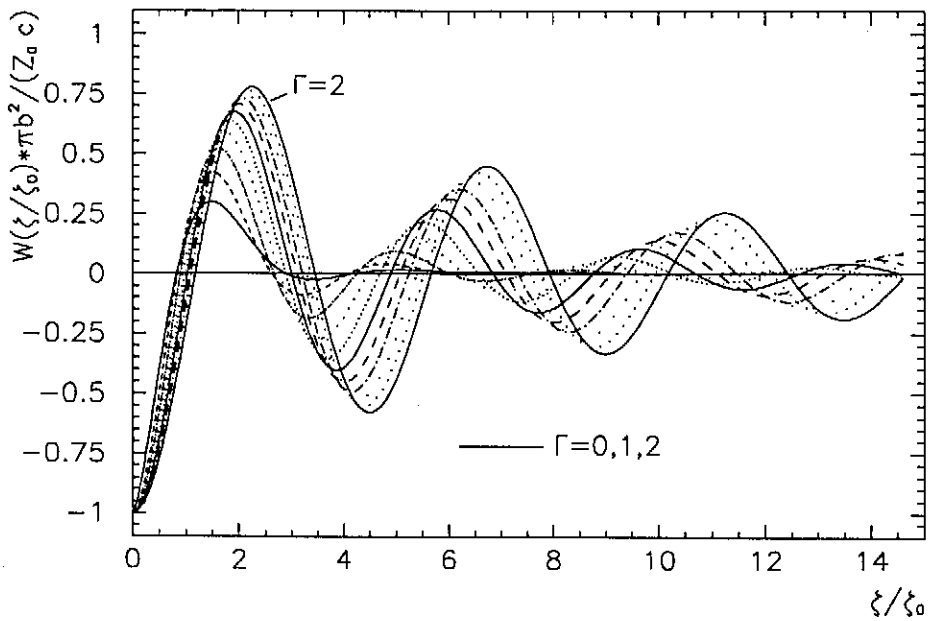

Figure 2.19: Wake function for different values of the dimensionless parameter $\Gamma = 0, 0.2, \ldots, 1.8, 2.0$.

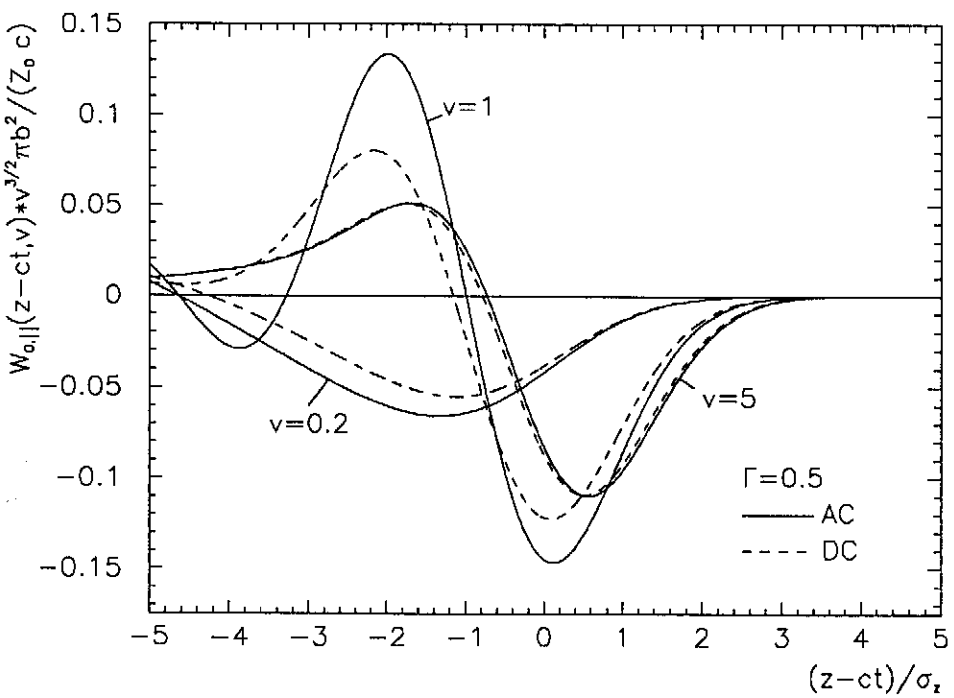

Figure 2.20: Longitudinal wake potential of a Gaussian bunch in case of a constant (**DC**) conductivity (dashed line) and a frequency-dependent (**AC**) conductivity (solid line); $\Gamma = 0.5, v = \sigma_z/\zeta_0$.

wake potential is well described by the long-range approximation. An example of this behaviour is shown in Fig. 2.20 for $\Gamma = 0.5$ for several values of $v = \sigma_z/\zeta_0$.

2.4 Domain of Validity

In the previous section an extension to the frequency-dependent conductivity $\sigma(\omega)$ has been given. The results presented in this section are limited by the assumption leading to Eq. (2.163) for large values of $\zeta = ct - z$, and, for small values of ζ or σ_z. The long-range part of the wake fields is restricted to distances

$$\zeta \ll \max(b^2, 1/n^2) Z_0 \sigma_0 \,. \tag{2.164}$$

This equation is practically always fulfilled.

The constraints for small values of the distance ζ or bunch length σ_z is given by the validity of the local Ohm's law which relies on the assumption that the penetration-depth $\delta = \sqrt{2c/Z_0\sigma_0\omega}$ is much larger than the mean free-path $l = v_F \tau$ of the conducting electrons in the metal, where v_F is the Fermi velocity [18, 22].

In the case of $\delta \simeq l$ the anomalous skin effect begins to dominate the behaviour of the conducting electrons and Ohm's law has to be extended to non-local theories. The condition sets an upper bound on the frequency ω. Translating these bounds into lower bounds for either of the parameters ζ or σ_z one finds [18]:

$$\zeta \,,\, \sigma_z \;>\; \zeta_0' = \frac{1}{2}\left(\frac{l}{\sigma_0}\right)^2 Z_0\, \sigma_0^3 \tag{2.165}$$

where the ratio (l/σ_0) is a characteristic constant independent of the temperature:

$$\frac{l}{\sigma_0} \;=\; \frac{v_F\,\tau}{\sigma_0} \;=\; \frac{v_F\, m}{n\, e^2} \,. \tag{2.166}$$

For copper at $T = 300\,\mathrm{K}$, with $v_F = 1.57{\cdot}10^6\,\mathrm{m/s}$ and $(l/\sigma_0) = 6.6{\cdot}10^{-16}\,\Omega\mathrm{m}^2$ this leads to $\zeta_0' = 16.5\mu\mathrm{m}$. This value is comparable to the characteristic length ζ_0 used in the previous sections for small pipe radii. Therefore, the examples of the short-range wake fields as given in the previous section may not accurately correspond to reality.

Assuming that for characteristic length $\zeta_0 \gg \zeta_0'$ the influence of the anomalous skin effect on the imaginary part of the impedance (see Eq. (2.111) and Fig. 2.7) that dominates at $k \gg 1/\zeta_0$ can be neglected, the transition from a short-range to a point-like dominated wake potential, exhibited for instance in Fig. 2.15, is physical.

Finally, one should point out that the impedance given in Eq. (2.163) is derived for an infinite beam energy. In the case of $\zeta \sim b/\gamma$ the spread in the electric field pattern of the pan-cake term modifies the impedance for wave numbers $k \sim \gamma/b$ and leads to a continuous wake function at $\zeta = 0$. The monopole impedance in case of finite γ can be written*:

$$Z_{0,\parallel}(k) \;=\; \frac{Z_0}{2\pi b} \cdot \left(\frac{I_0(\alpha r) I_0(\alpha r)}{I_0(\alpha b)^2}\right) \cdot \left[\frac{\sqrt{\lambda^2 - \alpha^2}}{k} - \frac{i\beta^2 kb}{2}\left(\frac{2}{\alpha\beta}\frac{I_0'(\alpha b)}{I_0(\alpha b)}\right)\right]^{-1} \tag{2.167}$$

with $\alpha^2 = k^2/\gamma^2$. I_0 is the modified Bessel function of zeroth order and the prime denotes the derivative with respect to the argument. In the limit $\gamma \to \infty$ the impedance given in Eq. (2.163) is recovered.

*The impedance can be obtained from the solution derived in [21].

2.5 Influence of Wake Fields on Beam-Parameters

In the following section the influence on a beam due to wake fields is summarized by the longitudinal loss factor $k_{||}$, the energy-spread σ_E and the transverse loss factor $k_\perp$.

Simple analytical formulas can be derived in case of bunch lengths σ_z that are much smaller or larger than the characteristic length $\zeta_0 = (2b^2/Z_0\sigma_0)^{1/3}$. For bunch lengths between the two above cases only numerical solutions can be given. The code "RWAC" [17] has been used for calculating the wake functions. The results are in agreement with the solution derived in earlier sections.

The wake fields for a constant and frequency-dependent conductivity have been investigated, and the results $k_{||}, \sigma_E$, and $k_\perp$, can be compared. The calculation uses the stationary solution for the wake fields, which assumes that the beam pipe is infinitely long and longitudinally uniform. The longitudinal line-charge distribution is of Gaussian shape and travels with the speed of light, which is justified for bunch length σ_z much larger than the ratio (b/γ) between the beam pipe radius b and the Lorentz factor γ.

Furthermore, in order to describe the longitudinal wake fields by the monopole wake potential and the transverse wake fields by the dipole wake potential the beam offset r_s is considered to be small $(r_s \ll b)$.

2.5.1 Longitudinal Loss Factor

The longitudinal loss factor $k_{||}$ is related to the average energy loss $\triangle E$ per particle by

$$\triangle E \;=\; Nq^2 k_{||} \tag{2.168}$$

where N denotes the number of particles in the bunch, and $Nq = Q$ the bunch charge. The longitudinal loss factor is obtained from the longitudinal wake potential according to (see section 1.2):

$$k_{||} \;=\; - < W_{||} >_\lambda \qquad \text{with} \qquad < W_{||} >_\lambda \equiv \int_{-\infty}^{\infty} d\zeta \, \lambda(\zeta) \cdot W_{||}(\zeta) \quad . \tag{2.169}$$

For long bunches $\sigma_z \gg \zeta_0$ (long-range approximation) the loss factor can be written as:

$$k_{0,||} \;=\; \frac{\Gamma(3/4)c}{\pi^2(2\sigma_z)^{3/2}b}\sqrt{\frac{Z_0}{\sigma_0}} \;=\; 2.522\,[\mathrm{V\,m/\Omega^{1/2}\,nC}] \cdot b^{-1}\,\sigma_z^{-3/2}\,\sigma_0^{-1/2} \,. \tag{2.170}$$

For sufficiently short bunches $\sigma_z \ll \zeta_0$ (ultra-short range approximation) the loss factor of a bunch is proportional to the energy loss of a point-like particle:

$$k_{0,||} \;=\; \frac{Z_0 c}{2\pi b^2} \;=\; 17.987\,[\mathrm{Vm/nC}] \cdot b^{-2} \,. \tag{2.171}$$

The dependence of the longitudinal monopole loss factor on the beam pipe radius for different bunch length and materials is shown in Fig. 2.21.

2.5.2 Energy-Spread

The energy-spread σ_E is defined by:

$$\sigma_E \equiv N q^2 \left(< W_{\|}^2 >_\lambda - k_{\|}^2 \right)^{1/2} . \tag{2.172}$$

In the long-range approximation of a wake potential the energy-spread (see Eq. (2.109)) is calculated as:

$$\sigma_E = \frac{0.46 N q^2 c}{2\pi^2 b \sigma_z^{3/2}} \cdot \sqrt{\frac{Z_0}{\sigma_0}} = 0.136\,[\mathrm{eVm}/\Omega^{1/2}\mathrm{nC}] \cdot N q\, b^{-1} \sigma_z^{-3/2} \sigma_0^{-1/2} \quad (\sigma_z \gg \zeta_0) . \tag{2.173}$$

In the ultra-short range approximation for $\sigma_z \ll \zeta_0$ one can use the error-function instead of the longitudinal wake potential of a Gaussian-charge distribution:

$$W_{0,\|} \simeq -\frac{Z_0 c}{\pi b^2} \cdot \mathbf{erf}(-\zeta/\sigma_z) \quad \text{with} \quad \mathbf{erf}(z) \equiv \frac{1}{\sqrt{2\pi}} \int_{-\infty}^{z} dt\, e^{-t^2/2} \tag{2.174}$$

$$\Rightarrow \sigma_E = 0.289 \frac{N q^2 Z_0 c}{\pi b^2} = 10.4\,[\mathrm{eV\,m}/\Omega^{1/2}\mathrm{nC}] \cdot N q\, b^{-2} \quad (\sigma_z \ll \zeta_0) . \tag{2.175}$$

Note, that for $\sigma_z \ll \zeta_0$ the energy-spread σ_E and longitudinal loss-factor $k_{\|}$ are independent on the bunch length σ_z and the wall material. This behaviour is observed for large radii and metals of poor conductivity.

2.5.3 Transverse Loss Factor

The azimuthal force vanishes for a line charge distribution traveling in a cylindrical pipe. The radial loss factor is defined as the average radial wake potential:

$$k_r \equiv < W_r >_\lambda \tag{2.176}$$

The leading term is given by the dipole wake potential:

$$k_{1,r} \equiv < W_{1,r} >_\lambda . \tag{2.177}$$

In the long range approximation Eq. (2.144) has been found ($\Gamma(1/4) = 3.624$):

$$k_r(r, \sigma_z) = \frac{\Gamma(1/4) c}{2^{3/2}\pi^2 b^3} r \sqrt{\frac{Z_0}{\sigma_z \sigma_0}} = 0.756\,[\mathrm{Vm}/\Omega^{1/2}\mathrm{nC}] \cdot r \sigma_z^{-1/2} b^{-3} \sigma_0^{-1/2} \quad (\sigma_z \gg \zeta_0) . \tag{2.178}$$

In the opposite limit the ultra-short range approximation the transverse loss factor yields:

$$k_r(r, \sigma_z) = \frac{2 Z_0 c \sigma_z}{\pi^{3/2} b^4} = 0.406\,[\mathrm{Vm/nC}] \cdot r \sigma_z b^{-4} \quad (\sigma_z \ll \zeta_0) \tag{2.179}$$

which is also independent of the resistivity of the wall material. The transverse kick per unit length suffered by the bunch vanishes linearly with the bunch length. In Fig. 2.23 the transverse loss factor together with its asymptotic approximation is shown.

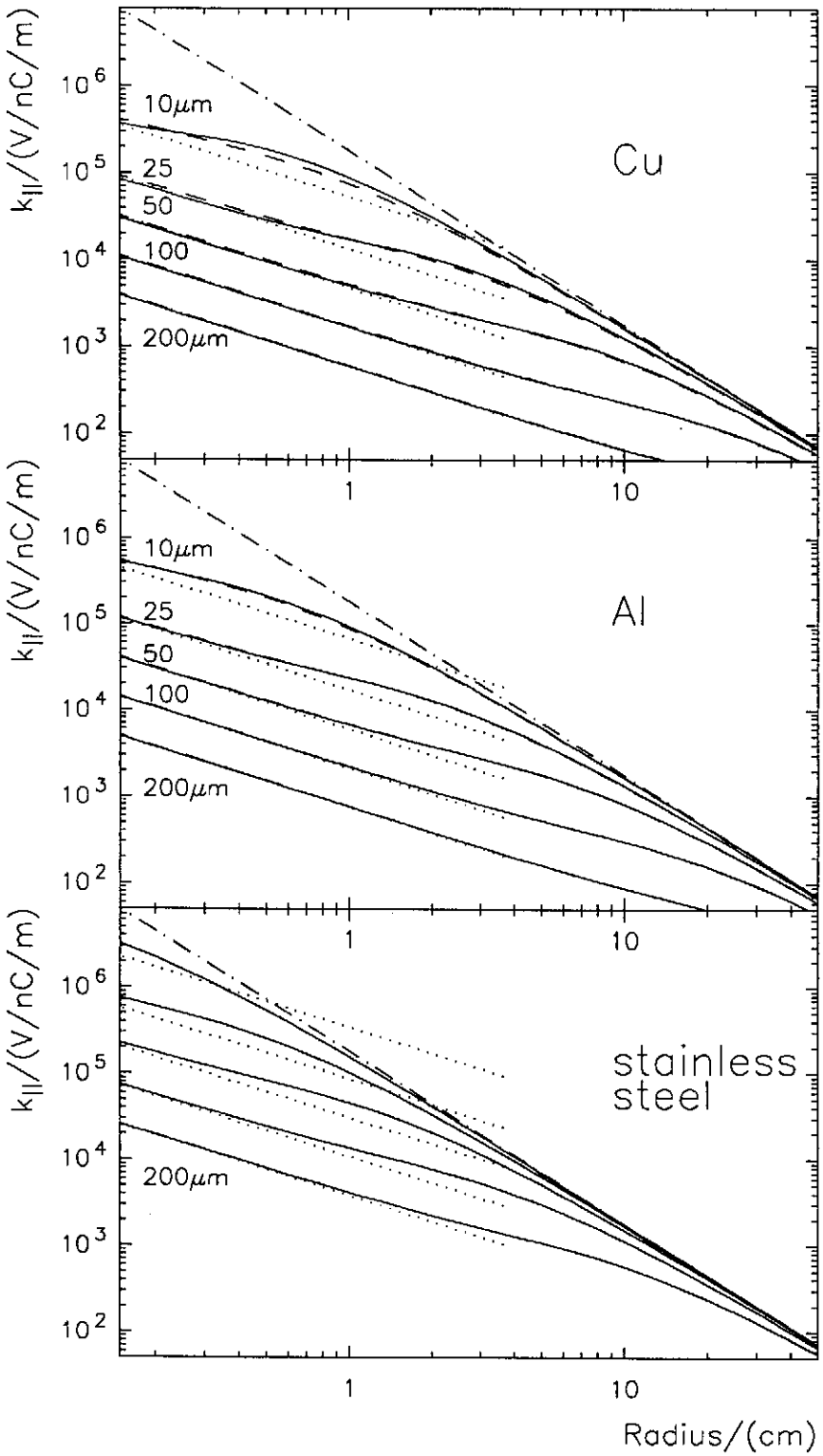

Figure 2.21: Longitudinal loss factor for copper ($\sigma_0 = 5.88 \cdot 10^7\,\Omega^{-1}\mathrm{mm}^{-1}$), aluminum ($\sigma_0 = 3.65{\cdot}10^7\,\Omega^{-1}\mathrm{mm}^{-1}$) and stainless steel ($\sigma_0 = 0.14{\cdot}10^7\,\Omega^{-1}\mathrm{mm}^{-1}$). The loss-factor for a frequency-dependent conductivity (solid line) and for a constant conductivity (dashed line) are plotted for different bunch length $\sigma_z = 10, 25, 50, 100, 200\,\mu$m. The long-range approximation Eq. (2.170) (dotted) and the ultra-short range approximation Eq. (2.171) (dashed-dotted) are also shown.

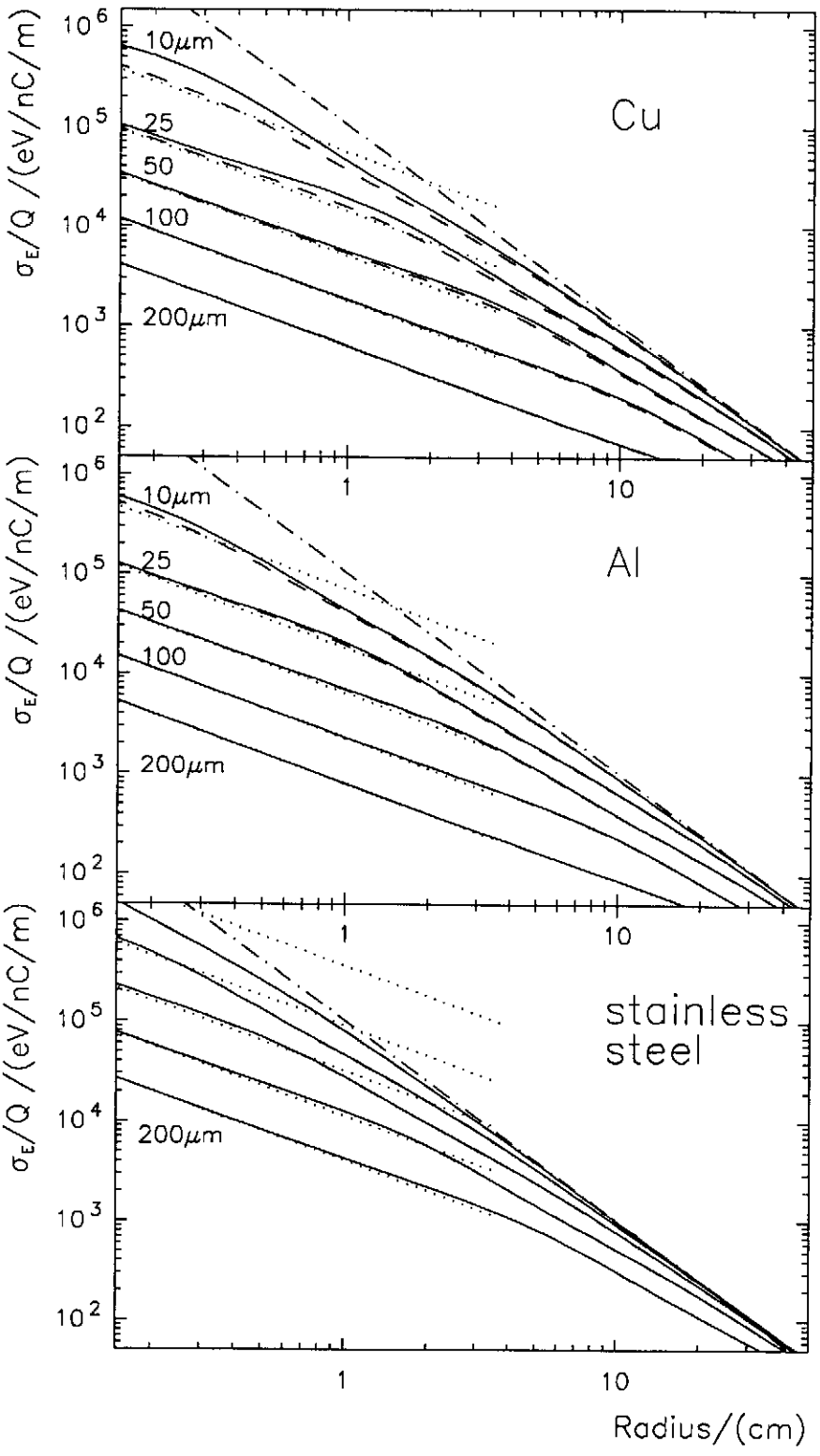

Figure 2.22: Energy-spread per unit bunch charge, unit pipe length for copper ($\sigma_0 = 5.88 \cdot 10^7\,\Omega^{-1}\mathrm{mm}^{-1}$), aluminum ($\sigma_0 = 3.65 \cdot 10^7\,\Omega^{-1}\mathrm{mm}^{-1}$) and stainless steel ($\sigma_0 = 0.14 \cdot 10^7\,\Omega^{-1}\mathrm{mm}^{-1}$). The energy-spread for a frequency-dependent conductivity (solid line) and for a constant conductivity (dashed line) are plotted for different bunch lengths $\sigma_z = 10, 25, 50, 100, 200\,\mu\mathrm{m}$. The long-range approximation Eq. (2.173) (dotted) and the ultra-short range approximation Eq. (2.174) (dashed-dotted) are also shown.

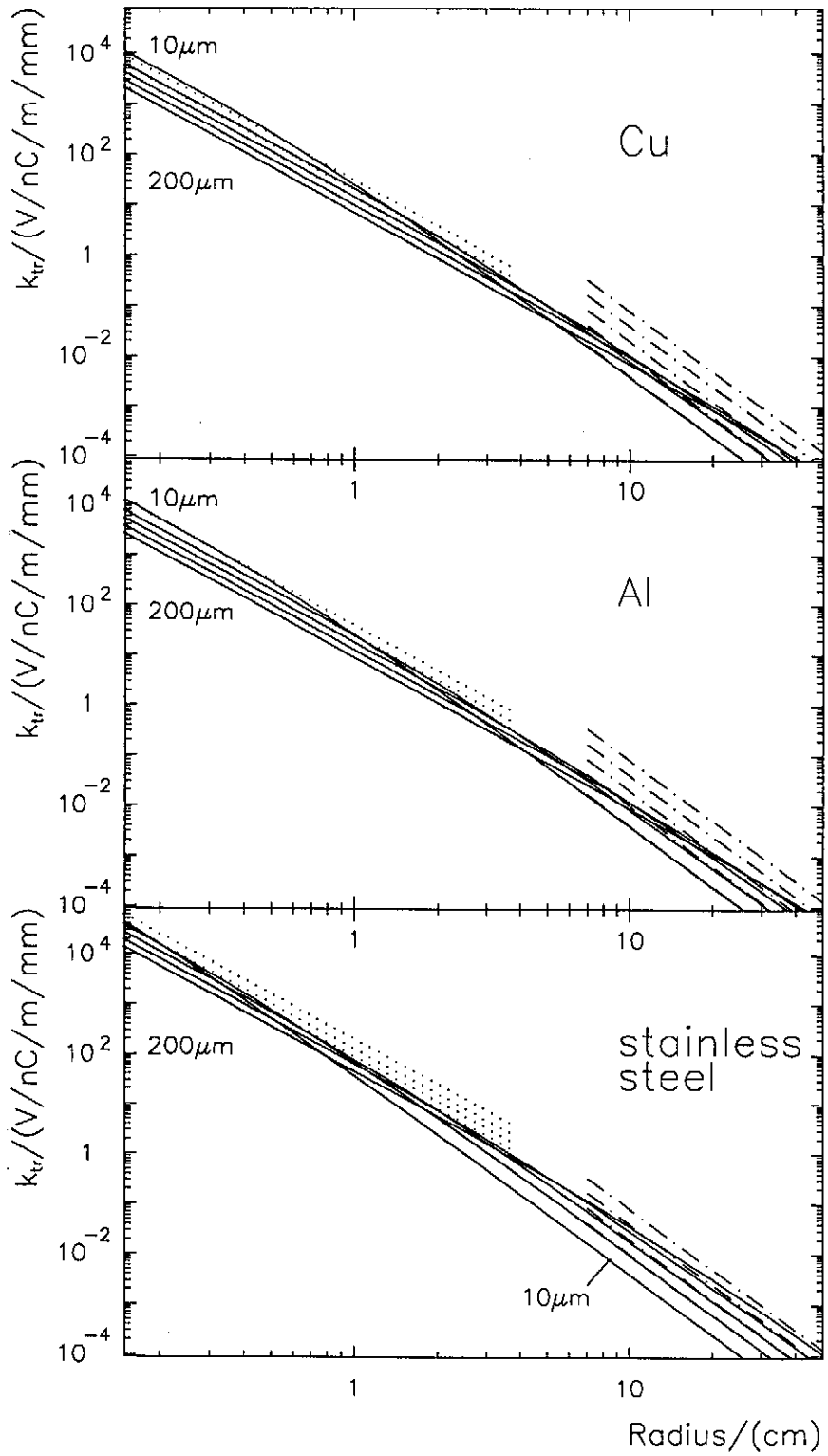

Figure 2.23: Transverse loss factor per unit length, unit charge, and unit offset for a frequency-dependent conductivity (solid line) is plotted for different bunch length $\sigma_z = 10, 25, 50, 100, 200\,\mu$m. The long-range approximation Eq. (2.178) (dotted) and the ultra-short range approximation Eq. (2.179) (dashed-dotted) are also shown.

Chapter 3

Resistive Wall Wake Fields in the Undulator Vacuum Chamber

A high gain FEL operation is a achieved when the undulator length L is much large than the gain length l_g, i.e. the e-folding length of the radiated power [1]:

$$G = \frac{L}{l_g} \gg 1 . \tag{3.1}$$

G is known as the exponential gain parameter of the FEL. The gain length l_g can be deduced from the one dimensional Lorentz-Maxwell equation. It is related to the beam and the undulator parameter as [1]:

$$l_g \propto \left(\frac{\epsilon^n E_0}{I_{peak}}\right)^{1/3} \cdot \left(\frac{\beta}{B_u^2 \lambda_u}\right) . \tag{3.2}$$

Here, $\epsilon^n = 2\,\pi$ mm mrad is the normalized transverse emittance, $E_0 = 1$ GeV is the beam energy and I_{peak} the peak current. The relevant undulator parameters are the undulator period λ_u, the peak undulator magnetic field B_u and the average beta-function $\beta = 3$ m. Assuming NdFeB/hybrid permanent magnet technology, then the peak field B_u can be described by a function depending on the ratio g/λ_u of the undulator gap g to the undulator periods λ_u. Calculations show, that for an undulator length of $L = 30$ m, and an undulator period of $\lambda_u = 27.3$ mm the undulator gap g has an upper boundary of approximately 12 mm in order to achieve a sufficiently strong peak magnetic field [1]. With this parameters the saturation length for SASE-FEL is about 1 m.

Since the FEL process depends strongly on the good beam quality (small energy spread and emittance), the material and the shape of the cross section of the undulator pipe must be chosen carefully to reduce the amplitude of the wake fields in order to preserve the beam parameters while it propagates through the undulator pipe.

At the present time, the perturbation of the SASE-FEL due to wake fields has not be completely in-corporated in the numerical codes so far. First simulations show that an introduced coherent energy-spread smaller than the initial energy-spread still produces an acceptable result of the FEL-performance [24].

In addition, the difference between the optical axis of the undulator defined by the quadrupoles and the geometrical axis defined by the undulator vacuum chamber causes an offset of the beam which leads to an emittance grow due to the deflecting forces of the

wake fields. A simple model for the emittance dilution based on a beam with a constant small transverse offset $\mathbf{r}_\perp$ is used in order to estimated this effect.

The largest contribution of the various sources of wake fields is expected to be from the resistive walls. The wake fields generated by surface roughness of the pipe, beam position monitors (coupling windows and cavities), pumping holes, etc. have to be treated separately. In the following a uniform perfectly smooth pipe is considered.

The relevant parameters for the calculation of the resistive wall wake fields at the TESLA FEL (phase 2) are listed in Tab. 3.1*†[1], [25].

variable		units	values
beam energy	E_0	GeV	1.0
number of electrons per Gaussian bunch	N		$6.24{\cdot}10^9$
bunch charge	Q_0	nC	1.0
peak electron beam current	I_{peak}	A	2391.9
rms bunch length	σ_z	μm	50.0
normalized emittance in the undulator	ϵ^n	π mrad mm	2.0
rms bunch size	$\sigma_\perp$	μm	50.0
relative energy spread	σ_γ/γ	10^{-3}	1.0
bunch train length		μs	800
number of bunches per train	N_{train}		up to 7200
inter-bunch distance	ζ_{bun}	m	33.3
undulator length	L	m	28.7
undulator gap	g	mm	12.0
pipe thickness (minimum)	t	mm	1.25
beam optics beta function	$\bar{\beta}$	m	3
FODO period length	L_{FODO}	m	0.96
Number of FODO periods per module	N_{FODO}		5
Length of the FODO quad		mm	136.5
Required field Gradient		T/m	18.3

Table 3.1: Relevant parameters for the wake field calculations of the TESLA Test Facility FEL (phase two).

3.1 Round Vacuum Chamber

In the present design the vacuum chamber shape is cylindrically with a radius of $b = 4.75\,\mathrm{mm}$. Different materials for the undulator vacuum chamber have been considered. The results for the average energy loss per electron $\triangle E$, the energy broadening σ_E/E_0 and the average transverse kick $Ne^2Lk_\perp$ (per unit offset) for an undulator vacuum chamber of copper, aluminum and stainless steel are listed in Tab. 3.2.

*σ_γ denotes the initially dominantly uncorrelated energy-spread of the beam at the entrance of the undulator, while σ_E designates the along the undulator induced correlated energy-spread.

†For I_{peak} a longitudinal Gaussian distributed bunch with rms-value σ_z has been considered.

vacuum chamber material	$\triangle E = Ne^2Lk_{\parallel}$	σ_E/E_0	$Ne^2Lk_{\perp}$
	MeV	10^{-3}	MeV/m
copper	0.296	0.338	4.023
aluminum	0.394	0.421	5.008
stainless steel	2.569	2.246	24.541

Table 3.2: Effect of the resistive wall wake fields on the beam parameters for a beam pipe radius of $b = 4.75\,\mathrm{mm}$.

The energy broadening in a copper pipe as well as in an aluminum pipe is below the initial relative energy-spread of the beam σ_γ/γ. In case of a stainless steel beam pipe the induced energy broadening exceeds 0.1%.

The longitudinal energy distribution of a beam traversing the vacuum chamber is shown Fig. 3.1. The values and the positions of the minima and maxima of the longitudinal wake potential can be obtained from Tab. 3.3.

vacuum chamber material	$W_{\parallel}^{min}$	z^{min}	$W_{\parallel}^{max}$	z^{max}
units	MV/nC	μm	MV/nC	μm
copper	-0.683	28.4	0.321	-82.6
aluminum	-0.865	25.1	0.411	-86.0
stainless steel	-4.839	7.8	3.044	-101.8

Table 3.3: Minima and maxima of the longitudinal wake potentials for a vacuum chamber radius of $b = 4.75\,\mathrm{mm}$.

The wake potentials for copper and aluminum can be described by the long bunch (long-range) approximation for the wake potential and vary mainly in amplitude rather than in shape. This approximation can not be applied to the wake potential for a stainless steel pipe since the characteristic length ζ_0 of the wake fields is in the order of the bunch length σ_z (see Tab. 3.4).

vacuum chamber material	$\zeta_0 = \left(\frac{2b^2}{Z_0\sigma_0}\right)^{1/3}$
copper	12.7 μm
aluminum	14.9 μm
stainless steel	44.1 μm

Table 3.4: Characteristic length of the wake fields for an cylindrical undulator vacuum chamber ($b = 4.75\,\mathrm{mm}$) for different metals.

The energy broadening for different beam pipe radii b is plotted in Fig. 3.2 and depends for copper and aluminum inversely proportional to b.

The longitudinal multi-bunch effect leads to an additional electric field, which accelerates the trailling bunches in a train. This additional electric field seen by a bunch has an

upper boundary, which is independent of the number of bunches in a train (see section 2.2.3):

$$E_z \;<\; 1.24 \cdot 10^7 [V/m] \cdot \left(\frac{\zeta_0}{\zeta_{bun}}\right)^{3/2} \qquad (b \,=\, 4.75\,\mathrm{mm})\,. \tag{3.3}$$

Since the inter-bunch distances ζ_{bun} are large in comparison with the characteristic length ζ_0 the longitudinal electric field is extremely small. For aluminum one finds 3.7 mV.

While the longitudinal multi-bunch effect is bounded, the transverse multi-bunch effect grows with the number of bunches in the train N_{train}. Assume a constant average offset $\mathbf{r}_\perp$ from the symmetry axis of undulator vacuum chamber for all members of the train. Then the momentum change $\triangle \mathbf{p}_\perp$ per electron in the N^{th} bunch of the train can be written (see Eq. (2.91)):

$$\triangle \mathbf{p}_\perp \;=\; 8.45 \cdot 10^{11} [(eV/c)m^{-2}] \cdot \frac{\zeta_0^{3/2}}{\zeta_{bun}^{1/2}} \cdot <\mathbf{r}_\perp> \cdot \sum_{j=1}^{N-1} j^{-1/2} \qquad (b \,=\, 4.75\,\mathrm{mm})\,. \tag{3.4}$$

For the last bunch $N = N_{train}$ the sum yields $\sum_{j=1}^{N_{train}} j^{-1/2}$ =168.24. The slope $|\triangle \mathbf{p}_\perp c|/E_0$ of the last bunch in the train at the exit of the undulator with an aluminum vacuum chamber for a beam with an offset of 0.1 mm is 0.14 μrad. Thus the displacement from the origin trajectory is below 5 μm (below 5 % of the offset).

Note that the undulator length L =28.7 m is much smaller than the length of the train ζ_{train} =240 km. Calculations for the resistive wall wake fields of a finite beam pipe length may lead to different results. Therefore, the above results can only give rough estimations for the multi-bunch effects. In addition one should point out that the train length ζ_{train} is in the order of $b^2 Z_0 \sigma_0$ the upper boundary for the validity of the long-range transverse wake fields of a dipole calculated for an infinite beam pipe. For example, one finds for an aluminum beam pipe with a radius of b =4.75 mm an upper boundary of $b^2 Z_0 \sigma_0$ =310 km*.

The transverse wake potentials per unit offset are shown in Fig. 3.3. The values of the position and the amplitude of the maxima are listed in Tab. 3.5.

vacuum chamber material	$Ne^2 L W_\perp^{max}$	z^{max}
units	MeV/m	μm
copper	5.655	-35.1
aluminum	7.192	-38.5
stainless steel	40.452	-50.3

Table 3.5: Position and amplitude of the maxima for the transverse wake potential (per unit offset).

*The impedance for an infinite beam pipe including lower frequencies has been derived in section 2.2.2.

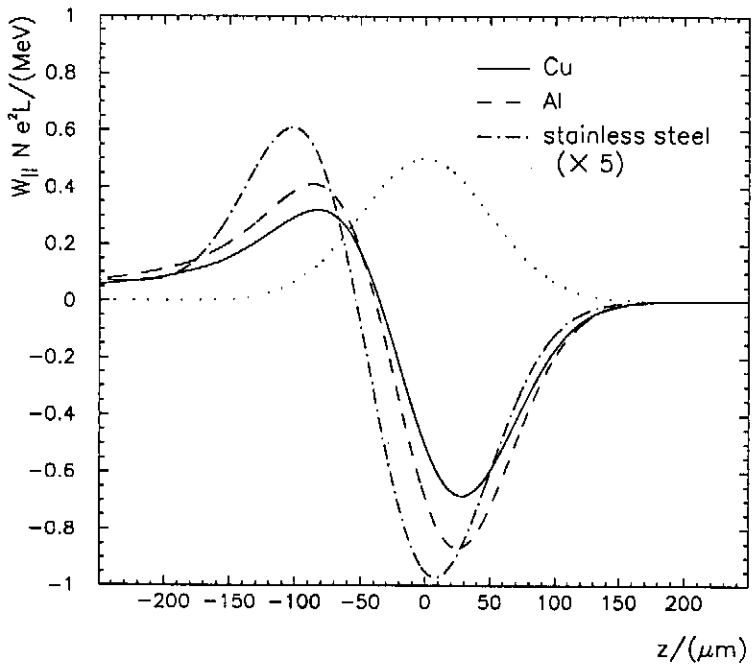

Figure 3.1: Longitudinal energy distribution of a bunch after passing an undulator vacuum chamber made of copper (solid line), aluminum (dashed line) and stainless steel (dashed-dotted line). The dotted line is the charge distribution (arbitrary units); (beam tube radius is 4.75 mm).

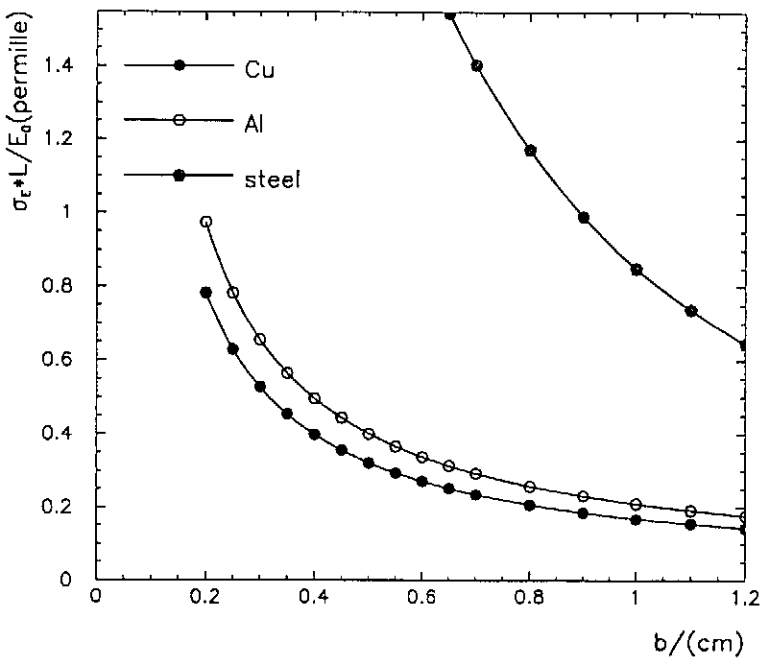

Figure 3.2: Energy broadening for copper, aluminum, and stainless steel for different radii b of a cylindrical vacuum chamber.

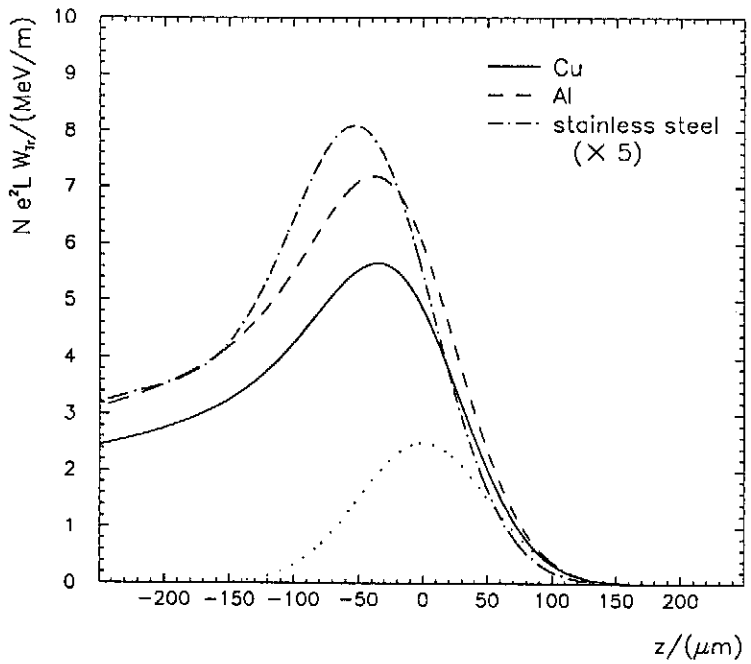

Figure 3.3: Transverse wake potential per unit offset of a Gaussian bunch after passing the undulator vacuum chamber made of copper (solid), aluminum (dashed), and stainless steel (dashed-dotted). The dotted line shows the charge distribution; (beam tube radius is 4.75 mm).

3.1.1 Emittance Growth

An emittance growth due to the transverse wake forces occurs if the beam is displaced from the symmetry axis of the vacuum chamber. The displacement can have two possible sources: first a betatron oscillation of the beam due to an initial offset* x_{off} of the bunch at the entrance of the undulator, second a displacement x_{geo} of the symmetry axis of the vacuum chamber from the optical axis defined by the quadrupoles of the FODO-cells.

The emittance growth using an average beta function $\overline{\beta}$ has been calculated to (see App. B.1):

$$\begin{aligned}\frac{\delta\epsilon_x(s)}{\epsilon_x} \approx\ & \frac{1}{2\epsilon_x}\cdot\left(\frac{Ne^2}{E_0}\right)^2\cdot\left(<W_\perp^{\lambda^2}>_\lambda - k_\perp^2\right) \\ \times\ & \left\{\left(\frac{x_{off}\sqrt{\overline{\beta}}}{2}\, s\,\sin\left(k_{\overline{\beta}}\, s\right) - x_{geo}\,\overline{\beta}^{3/2}\left[1-\cos\left(k_{\overline{\beta}}\, s\right)\right]\right)^2\right. \\ & \left. + \left(\frac{x_{off}\sqrt{\overline{\beta}}}{2}\left[s\,\cos\left(k_{\overline{\beta}}\, s\right) + \overline{\beta}\sin\left(k_{\overline{\beta}}\, s\right)\right] - x_{geo}\,\overline{\beta}^{3/2}\sin\left(k_{\overline{\beta}}\, s\right)\right)^2\right\}.\end{aligned} \tag{3.5}$$

*The offset is defined with respect to the average beta function (see App. B.1 $x_{off} = \overline{x}$).

with $< W_\perp^{\lambda^2} >_\lambda = \int \lambda W_\perp^{\lambda^2}$ †, ϵ_x is the initial transverse emittance of the beam in the x-plane and $k_{\overline{\beta}} = 1/\overline{\beta}$ is the betatron wave number. The coordinate s describes the position along the undulator ($s = 0$ corresponds to the entrance).

A misalignment of the quadrupoles and an orbit correction by steerers has not been taken into account. The displacement x_{geo} of the vacuum chamber is considered to be constant along the undulator.

The formula for the emittance growth has to be modified if $\delta\epsilon_x(s)$ is comparable with the beam emittance at the entrance of the undulator $\epsilon_x(0)$ (see App. B.1).

The development of the emittance growth for an aluminum chamber in three different situations are given in Fig. 3.4: first a beam with initial offset x_{off} of 100 μm, but vanishing x_{geo}; second a beam with vanishing initial offset x_{off}, but a misaligned vacuum chamber $x_{geo} = 100\,\mu$m and third a beam with initial offset in direction of the misaligned of the chamber $x_{off} = 100\,\mu$m and $x_{geo} = 100\,\mu$m are plotted in Fig. 3.4.

In all three cases the emittance growth $\delta\epsilon_x/\epsilon_x$ is in the order of 10^{-5}. Even in the case of a stainless steel pipe with the very large offsets of 1 mm one finds an emittance growth below 3 % (see Fig. 3.5).

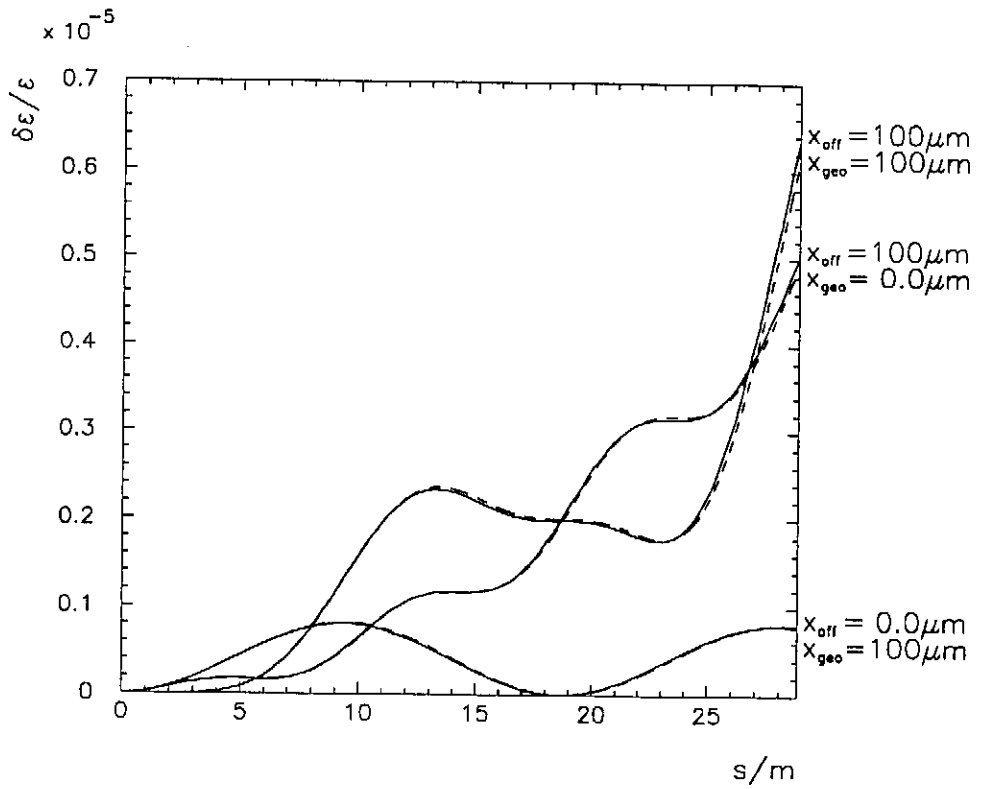

Figure 3.4: Emittance growth along the undulator for an aluminum vacuum chamber with a radius of 4.75 mm: numerical simulation including the beta function of the undulator FODO-cell structure (solid line); the analytical formula Eq. (3.5) for an average constant beta function (dashed line).

†The bars for the wake potentials have been suppressed in the formulas.

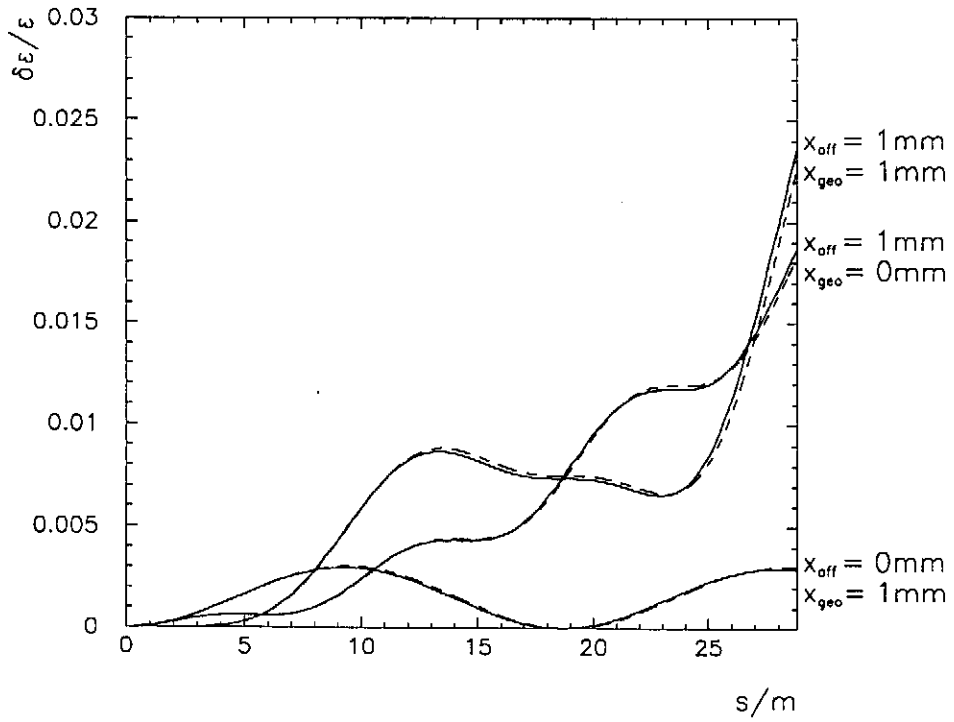

Figure 3.5: Emittance growth along the undulator for a stainless steel vacuum chamber with a radius of 4.75 mm: numerical simulation (solid line); analytical solution (dashed line).

3.2 Elliptic and Rectangular Cross Sections

The code "RWAC" written by K. Yokoya allows to calculate the wake functions for beam pipes with an elliptic and a rectangular cross section. For further details about the calculation method and the properties of the wake functions in non-cylindrically symmetric structures see [17].

The length of the horizontal and the vertical semi-axis are denoted by a and b. The geometry of the cross sections are illustrated in Fig. 3.6. The energy broadening for

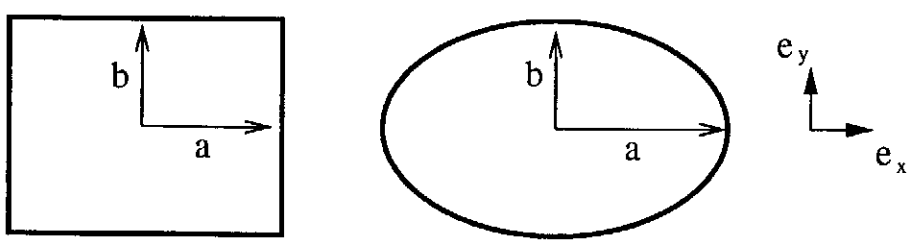

Figure 3.6: Alternative cross sections for the undulator vacuum chamber.

a given vertical semi-axis of $b = 4.75$ mm in a copper and an aluminum chamber as a function of the parameter $\epsilon = (a - b)/(a + b)$ is shown in Fig. 3.7. The values for

an elliptical (rectangular) cross section are indicated by circles (squares). A vanishing $\epsilon = 0$ corresponds to a cylindric (quadratic) cross section. For $\epsilon = 1$ the vacuum chamber is given by two parallel plates in the horizontal plane distanced by $2b = 9.5\,\mathrm{mm}$. A

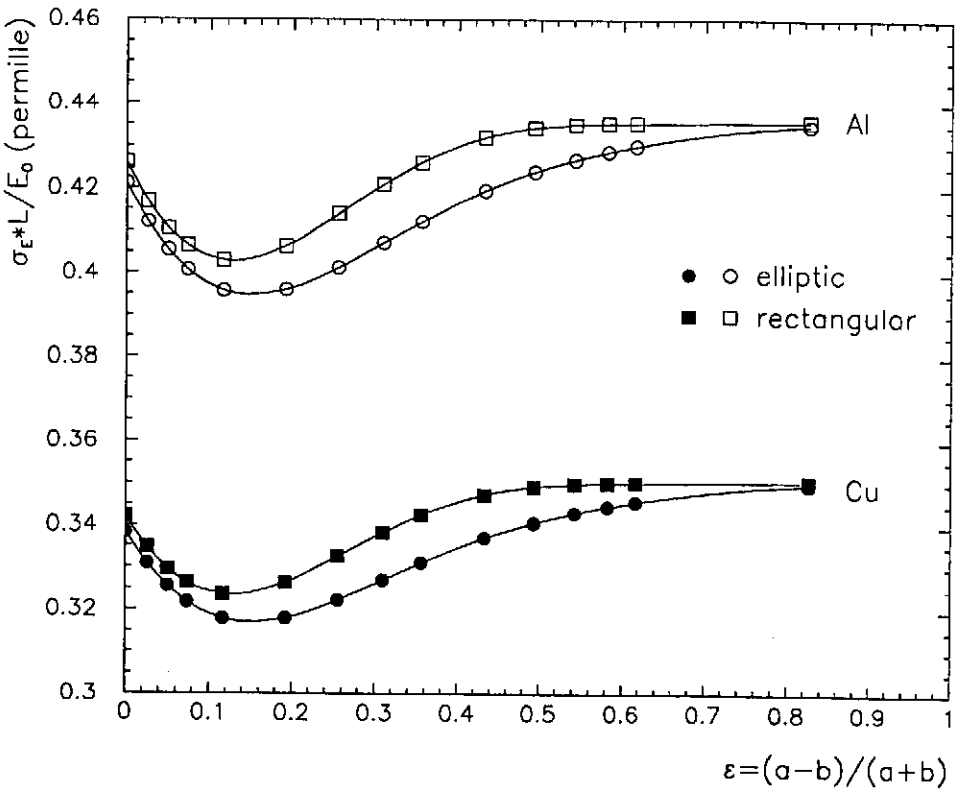

Figure 3.7: Energy broadening of the beam passing a vacuum chamber of an elliptic or an rectangular cross section for different values of the parameter $\epsilon = (a-b)/(a+b)$.

minimum energy broadening for an elliptic pipe is approximately given at $\epsilon \approx 0.15$, which corresponds to a ratio $(a/b) \approx 1.35$ between the horizontal and the vertical semi-axis. However, for one given semi-axis due to the limited gab of the undulator, the energy broadening by using an elliptical cross section can only be reduced by 6% in comparison with a cylindrical pipe.

Conclusion

The basic concept of wake fields, wake functions and wake potentials have been introduced. General properties of the time and the frequency domain description of the interaction between the bunch and the wake fields are summarized.

An analytical treatment of the wake fields caused by the resistivity of metal for a constant and a frequency-dependent conductivity has been given and compared with the results of the publications about resistive wall wake fields.

The transition of bunch lengths much larger to bunch lengths much smaller than the characteristic length of the wake fields has been observed in detail.

The transition shows a behaviour between an "inductive" and a "resistive" wake potential for the long range approximation ($\propto \omega^{1/2}$) and turns to be purely "capacitive" for the ultra-short range approximation ($\propto \omega^{-1}$). The latter induces a linear correlation between the electron energies and their longitudinal positions at the center of the bunch. This correlation scales inversely proportional to the square of the beam pipe radius independent on the conductivity of the metal and independent on the bunch length. Based on these results, a promising method for a new future μm-bunch length compressor system installed in a long beam transfer line has been found [26].

The longitudinal and transverse loss factors as well as the energy spread for ultra-short bunches -as relevant for drive beams of FEL's- have been treated numerically and asymptotic expressions are given.

In particular for the TTF-undulator it has been found that copper and aluminum are proper choices for the vacuum chamber material, while stainless steel has to be excluded. In case of copper and aluminum the dependence of the amplitude for the wake fields on the beam pipe radius b, the bunch length σ_z and the conductivity σ_0 is well described by the long range approximation of the wake potential It scales $\propto b^{-1}\sigma_z^{-3/2}\sigma_0^{-1/2}$ for the longitudinal wake fields and $\propto b^{-3}\sigma_z^{-1/2}\sigma_0^{-1/2}$ for the transverse wake fields.

An estimate of the transverse multi-bunch effect shows that the large inter-bunch distance in a bunch train of the TTF-FEL leads to very small values for the deflecting forces of the trailing bunches. For example, the displacement of a bunch from the original trajectory due to the transverse wake forces of a train travelling with a constant offset of $100\,\mu$m through the undulator is below $5\,\mu$m.

In order to calculate the emittance growth of the beam caused by the transverse wake fields, a multi-slice model has been developed. The dynamics of the slices have been analyzed numerically and analytically in first order perturbation theory. The resulting emittance growth along the undulator due to the slice motions is restricted to a few percent even for a beam-offset of 1 mm.

In addition, undulator chambers of elliptical and rectangular cross section have been studied. The result for the energy-spread differs only weakly from that of a round pipe of

a radius given by the smaller semi-axis. Thus the performance of an undulator cannot be significantly increases by using a non-cylindrical beam pipe. The energy spread is mainly determined by the undulator gap, the vacuum chamber material and the bunch length.

What has not been studied, but should be taken into account in further studies are the wake fields induced at geometrical changes in the cross section of the undulator, i.e. the contribution due to the surface roughness of the vacuum chamber and the various interruptions and coupling windows for the diagnostic elements. In particular, the wake fields caused by the surface roughness may lead to a significant contribution to the wake fields that are comparable with the resistive wall wake fields.

In order to in-corporate wake fields in the numerical simulations of the SASE-FEL process the beam-wake fields interaction distance should be studied in more details.

Bibliography

[1] A VUV Free Electron Laser at the TESLA Test Facility at DESY, Conceptual Design Report. Technical Report TESLA-FEL 95-03, Deutsches Elektronen-Synchrotron,DESY, June 1995.

[2] Conceptual Design of a 500 e^+e^- Linear Collider with Intergrated X-ray Laser Facility. Technical Report DESY 1997-048, DESY, ECFA, May 1997.

[3] J. D.Jackson. *Classical Electrodynamics.* New York, John Wiley & Sons,Inc., 2 edition, 1975.

[4] For example, TBCI (T. Weiland, DESY 82-015,1982), DBCI (A. Aharonian, R. Meller, and R. H. Siemann, CLNS 82/535,1982), XWAKE (F. Harfoush, CERN SL/Note 94-07,1994) ABCI (Y. H. Chin, CERN SL/94-02 (AP)).

[5] S.A. Heifets. Diffractive model of the high-frequency impedance. *Physical Review D*, 40(9):3097–3106, 1989.

[6] A. Novokhatski. Private communication.

[7] A.Novokhatski and A.Mosnier. Short bunch wake potential for a chain of tesla cavities. Technical Report DAPNIA/SEA-96-08, DAPHIA, November 1996.

[8] S.A. Kheifets and S.A. Heifets. Radiation of a charge in a perfectly conducting cylindrical pipe with a jump in its cross section. *Proceedings of the Linear Accelerator Conference (LINAC86), Stanford,California*, pages 493–495, 1986.

[9] V.G. Vaccaro L. Palumbo and M. Zobov. Wake fields and impedance. Technical Report LNF-94/041(P), Laboratori Nationali di Frascati, September 1994.

[10] R. Wanzenberg. The impedances of selected components of the HERA proton ring. Technical Report DESY HERA-95-07, Deutsches Elektronen-Synchrotron,DESY, November 1995.

[11] W.K.H. Panofsky and W.A. Wenzel. Some consideration concerning the transverse deflecion of charge particles in radio-frequency fields. *Rev. Sci. Instrum.*, 27:947, 1956.

[12] A. W. Chao. *Physics of Collective Beam Instabilities in High Energy Accelerator.* New York, John Wiley & Sons,Inc., 1993.

[13] K. Bane and M. Sands. Wakefields of very short bunches in an accelerating cavity. *Particle Accelerators*, 25:73–95, 1990.

[14] T. Weiland and R.Wanzenberg. Wake fields and impedances. Technical Report DESY M-91-06, Deutsches Elektronen-Synchrotron,DESY, May 1991.

[15] Yong Ho Chin Olivier Napoly and Bruno Zotter. A generalized method for calculating wake potentials. *Nuclear Instruments and Methodes in Physics Research A*, 334:255–265, 1993.

[16] N. Napoly. Private communication.

[17] K. Yokoya. Resistive wall impedance of beam pipes of general cross section. *Particle Accelerators*, 41:221–248, 1993.

[18] O.Henry and O.Napoly. The resistive pipe wake potentials for short bunches. *Particle Accelerators*, 35:235–247, 1991.

[19] N.W. Ashcroft and N.D. Mermin. *Solid State Physics.* Holt, Rinehart and Winston, 1 edition, 1976.

[20] M.J. Lighthill. *An introduction to Fourier analysis and generalised functions.* Press Syndicate of the University of Cambridge, 1 edition, 1958.

[21] A. Piwinski. Wake fields and ohmic losses in round vaccum chambers. Technical Report DESY HERA 92-11, Deutsches Elektronen-Synchrotron,DESY, May 1992.

[22] Karl L.F. Bane. The short range resistive wall wakefields. Technical Report SLAC-AP-87, Stanford Linear Accelerator Center, 1991.

[23] Karl L.F. Bane. The short-range resistive wall wakefields. Technical Report SLAC-PUB-95/7074, Stanford Linear Accelerator Center, 1995.

[24] S. Reiche. Private communication.

[25] Contribution to the FEL'96 converence, August 26-31, 1996 in Rome, Italy. Technical Report TESLA-FEL 96-13, Deutsches Elektronen-Synchrotron,DESY, Sept. 1996.

[26] H. Schlarb and R. Brinkmann. Ultra-short bunches by using a quasi-continuous compressor scheme in a long beam transver line. In *Particle Accelerator Conferences*, Vancover, 1997.

[27] M.Abramowitz and I.A.Stegun. *Handbook of Mathematical Functions.* Number 55. Department of Commerce, 2 edition, 1964. pp.358-364.

[28] I.S. Gradshteyn and I.M. Ryzhik. *Tabel of Intergals, Series, and Products.* Academic Press Inc., 4 edition, 1965.

[29] M. Drevlak. On the Preservation of single- and multi-bunch emittance in the linear accelerators. Technical Report DESY 95-225, Deutsches Elektronen-Synchrotron,DESY, November 1995.

Appendix A

A.1 Integrals involving the Bessel function

Solution of the integral

$$\Phi_m^{(sp)}(r,\phi,\zeta) \;=\; \frac{q_s}{2\pi\epsilon_0}\,\delta(\zeta)\,e^{im(\phi-\phi_s)}\int_0^\infty dq\,\frac{1}{q}\,J_m(qr)\,J_m(qr_s)\,. \tag{A.1}$$

The integral for m and $(-m)$ can be treated together by means of the relation for the Bessel function [27]:

$$J_{-m}(x) \;=\; (-1)^m\,J_m(x) \qquad m\in\mathbb{Z}\,. \tag{A.2}$$

For $m>0$ make use of [27]

$$J_{m-1}(x)\;+\;J_{m+1}(x) \;=\; \frac{2m}{x}\,J_m(x) \tag{A.3}$$

in order to split the above integral into two parts:

$$\int_0^\infty dq\,\frac{1}{q}\,J_m(qr)\,J_m(qr_s) \;=\; \frac{r}{2m}\left\{\int_0^\infty dq\,J_{m-1}(qr)\,J_m(qr_s)\;+\;\int_0^\infty dq\,J_{m+1}(qr)\,J_m(qr_s)\right\}. \tag{A.4}$$

The integrals involving the Bessel function can be solved by using the following formula [27]:

$$\int_0^\infty dz\;J_\mu(az)\,J_{\mu-1}(cz) \;=\; \begin{cases} c^{\mu-1}/a^\mu & (a>c>0)\\ 1/2c & (a=c>0)\\ 0 & (c>a>0)\end{cases} \tag{A.5}$$

and reads:

$$\int_0^\infty dq\,\frac{1}{q}\,J_m(qr)\,J_m(qr_s) \;=\; \frac{r}{2m}\left\{\begin{array}{ccc} r^{m-1}/r_s^m & + & 0\\ 1/2r & + & 1/2r\\ 0 & + & r_s^m/r^{m+1}\end{array}\right\}\begin{array}{l}(r_s>r>0)\\(r_s=r>0)\\(r>r_s>0)\end{array} \tag{A.6}$$

The result of the potential for $m\neq 0$ can be summarized to:

$$\Phi_m(r,\phi,\zeta) \;=\; \frac{q_s}{2\pi\epsilon_0}\,\delta(\zeta)\,e^{im(\phi-\phi_s)}\,\frac{1}{2|m|}\left(\frac{r_<}{r_>}\right)^{|m|}\,. \tag{A.7}$$

The case of $m=0$ has to be treated separately, since the integral

$$\lim_{\epsilon\to 0}\int_\epsilon^\infty dq\,\frac{1}{q}\,J_0(qr)\,J_0(qr_s) \tag{A.8}$$

diverges logarithmically. One can overcome the problem by using the integral [27]:

$$\int_0^\infty dz\,\frac{J_0(ax)}{x}\,[J_0(cx)-1] \;=\; \begin{cases} 0 & (a\geq c>0)\\ \ln(a/c) & (c\geq a>0)\end{cases} \tag{A.9}$$

and a constant $A(\epsilon)$ depending on a "cut-off" parameter $\epsilon \ll \min(1/r, 1/r_s)$ as

$$A(\epsilon) \equiv \int_{\epsilon}^{\infty} dq \, \frac{J_0(qr_s)}{q} . \tag{A.10}$$

With $a = r_s$ and $c = r$ one can write

$$\Phi_0^{(sp)}(r, \phi, \zeta) \approx \frac{q_s}{2\pi\epsilon_0} \delta(\zeta) \left(A(\epsilon) + \ln\left(\frac{r_s}{r}\right) \theta(r - r_s) \right) . \tag{A.11}$$

For $\epsilon \rightarrow 0$ the constant $A(\epsilon)$ becomes infinite.

Monopole term for a perfectly conducting pipe

Finally, the solution for the scalar potential of the monopole multipole in a perfectly conducting pipe is derived. A scalar potential $\Phi_0^{(per)}$ which fulfills the inhomogeneous Bessel equation for $m = 0$ and vanishes at $r = b$ can be written as:

$$\Phi_0^{(per)}(r, \phi, \zeta) = \frac{q_s}{2\pi\epsilon_0} \delta(\zeta) \int_0^{\infty} dq \, \frac{J_0(qr_s)}{q} \left[J_0(qr) - J_0(qb) \right] . \tag{A.12}$$

Thus the constant $A(\epsilon)$ only occurs in absence of boundary conditions. The integral for $\Phi_0^{(per)}$ can be solved using Eq. (A.9) once with $a = r_s$, $c = r$ and once with $a = r_s$, $c = b$ where the results are subtracted. This reads:

$$\begin{aligned} \Phi_0^{(per)}(r, \phi, \zeta) &= \frac{q_s}{2\pi\epsilon_0} \delta(\zeta) \cdot \left[\ln\left(\frac{r_s}{r}\right) \theta(r - r_s) - \ln\left(\frac{r_s}{b}\right) \theta(b - r_s) \right] \\ &= \frac{q_s}{2\pi\epsilon_0} \delta(\zeta) \cdot \ln\left(\frac{b}{r_>}\right) , \end{aligned} \tag{A.13}$$

which justifies the method use for $\Phi_0^{(sp)}$.

A.2 Electromagnetic Fields of Higher Multipoles

For $m \neq 0$ six equations of the system Eqs. (2.43) -(2.50) are non-redundant.

Solution in vacuum

In vacuum ($r < b$) the source-less Maxwell equations reduce to:

$$\begin{aligned}
\partial_r \hat{E}_{m,z} &= -\tfrac{imc}{r}\hat{B}_{m,z} \\
\partial_r \hat{B}_{m,z} &= \tfrac{im}{cr}\hat{E}_{m,z} \\
\tfrac{1}{r}\partial_r(r\hat{E}_{m,r}) - \tfrac{imc}{r}\hat{B}_{m,r} &= -ik\left(1 + \tfrac{m^2}{k^2r^2}\right)\hat{E}_{m,z} \\
\tfrac{1}{r}\partial_r(r\hat{B}_{m,r}) + \tfrac{im}{cr}\hat{E}_{m,r} &= -ik\left(1 + \tfrac{m^2}{k^2r^2}\right)\hat{B}_{m,z} \qquad (m \in \mathbb{Z}). \\
\hat{E}_{m,\phi} &= -c\hat{B}_{m,r} + \tfrac{m}{kr}\hat{E}_{m,z} \\
\hat{B}_{m,\phi} &= \tfrac{1}{c}\hat{E}_{m,r} + \tfrac{m}{kr}\hat{B}_{m,z}
\end{aligned} \tag{A.14}$$

With the transformation:

$$\left\{ \begin{array}{l} (\hat{E}_{m,\phi}, \hat{B}_{m,r}, \hat{B}_{m,z}) \\ (\hat{E}_{m,z}, \hat{E}_{m,r}, \hat{B}_{m,\phi}) \end{array} \right\} \rightarrow \left\{ \begin{array}{l} (\hat{E}_{-m,\phi}, \hat{B}_{-m,r}, \hat{B}_{-m,z}) \\ -(\hat{E}_{-m,z}, \hat{E}_{-m,r}, \hat{B}_{-m,\phi}) \end{array} \right\} \tag{A.15}$$

$$m \rightarrow -m \tag{A.16}$$

the system of differential equations remains equal. Hence, one can restrict the calculations to the solution for $m > 0$. The corresponding fields for $m < 0$ are obtained by the above transformation. The longitudinal electromagnetic field components are derived easily from the first two Eq. (A.14) yielding:

$$\begin{aligned}
\hat{E}_{m,z} &= A_m(k) \cdot r^m \\
\hat{B}_{m,z} &= A_m(k) \cdot \tfrac{i}{c} r^m \,.
\end{aligned} \tag{A.17}$$

The second independent solution is proportional to r^{-m} and diverges for $r \rightarrow 0$; the coefficient must vanish for an electromagnetic field that can be interpreted physically. Taking the results for $\hat{E}_{m,z}$ and $\hat{B}_{m,z}$ into account the homogeneous solutions of the Maxwell's equations in vacuum for the other components are given by:

$$\begin{aligned}
\hat{E}_{m,r} &= B_m \cdot \tfrac{r^{m-1}}{2} + A_m \cdot \tfrac{1}{2}\left(\tfrac{m}{ikr} - \tfrac{ikr}{(m+1)}\right) r^m \\
\hat{B}_{m,r} &= B_m \cdot \tfrac{r^{m-1}}{2ic} - A_m \cdot \tfrac{1}{2ic}\left(\tfrac{m}{ikr} - \tfrac{ikr}{(m+1)}\right) r^m \\
\hat{E}_{m,\phi} &= -B_m \cdot \tfrac{r^{m-1}}{2i} - A_m \cdot \tfrac{1}{2i}\left(\tfrac{m}{ikr} + \tfrac{ikr}{(m+1)}\right) r^m \\
\hat{B}_{m,\phi} &= B_m \cdot \tfrac{r^{m-1}}{2c} - A_m \cdot \tfrac{1}{2c}\left(\tfrac{m}{ikr} + \tfrac{ikr}{(m+1)}\right) r^m \,.
\end{aligned} \tag{A.18}$$

Solution in the metal

From Eqs. (2.43-2.50) one finds the following reduced system of equations for the electromagnetic field in a metal:

$$\begin{aligned}
\tfrac{1}{r}\partial_r(r\partial_r\hat{E}_{m,z}) + \left(\lambda^2 - \tfrac{m^2}{r^2}\right)\hat{E}_{m,z} &= 0 \\
\tfrac{1}{r}\partial_r(r\partial_r\hat{B}_{m,z}) + \left(\lambda^2 - \tfrac{m^2}{r^2}\right)\hat{B}_{m,z} &= 0 \\
\hat{E}_{m,r} &= \tfrac{ik}{\lambda^2}\left(\partial_r\hat{E}_{m,z} + \tfrac{imc}{r}\hat{B}_{m,z}\right) \\
\hat{B}_{m,r} &= \tfrac{ik}{\lambda^2}\partial_r\hat{B}_{m,z} + \tfrac{m}{ckr}\left(1 - \left(\tfrac{ik}{\lambda}\right)^2\right)\hat{E}_{m,z} \\
\hat{E}_{m,\phi} &= \tfrac{ik}{\lambda^2}\left(\tfrac{im}{r}\hat{E}_{m,z} - c\partial_r\hat{B}_{m,z}\right) \\
\hat{B}_{m,\phi} &= -\tfrac{mk}{r\lambda^2}\hat{B}_{m,z} + \left(\tfrac{ik}{\lambda^2 c} - \tfrac{1}{ikc}\right)\partial_r\hat{E}_{m,z}\,.
\end{aligned} \tag{A.19}$$

The solutions of the first pair of equations for $\hat{E}_{m,z}$ and $\hat{B}_{m,z}$ imply the solutions for the remaining electromagnetic field components using the last four equations. Consider an infinite wall thickness. With respect to Eq. (2.69) the longitudinal field components can be written:

$$\hat{B}_{m,z} = \frac{i}{c}\hat{E}_{m,z} = A_m(k)\cdot b^m\,\overline{H}_m \qquad \text{with} \quad \overline{H}_m = \frac{H_m^1(\lambda r)}{H_m^1(\lambda b)}\,. \tag{A.20}$$

where H_m^1 denotes the Hankel function of first kind and the m^{th} order. The other components read:

$$\begin{aligned}
\hat{E}_{m,r} &= -i\,\hat{E}_{m,\phi} = A_m(k)\cdot b^m\,\tfrac{ik}{\lambda}\left\{\overline{H}' - \tfrac{m}{r\lambda}\overline{H}_m\right\} \\
\hat{B}_{m,r} &= -A_m(k)\cdot b^m\left\{\tfrac{k}{c\lambda}\overline{H}'_m - \tfrac{m}{ckr}\left(1 - \left(\tfrac{ik}{\lambda}\right)^2\right)\overline{H}_m\right\} \\
\hat{B}_{m,\phi} &= -A_m(k)\cdot b^m\,\tfrac{1}{c}\left\{\tfrac{imk}{r\lambda^2}\overline{H}_m - \left(\tfrac{ik}{\lambda} - \tfrac{\lambda}{ik}\right)\overline{H}'_m\right\}\,.
\end{aligned} \tag{A.21}$$

The prime denotes the derivative with respect to (λr). For large arguments the Hankel function H_m^1 can be replaced by its' asymptotic expansion [27]:

$$H_m^1(x) \approx \sqrt{\frac{2}{\pi x}}\,e^{i(x - m\pi/2 - \pi/4)} \qquad \text{for} \quad (x \gg m) \tag{A.22}$$

thus for the ratios of Hankel function $\overline{H}_m$ and $\overline{H}'_m$ one can write:

$$\begin{aligned}
\overline{H}_m &\simeq \sqrt{\tfrac{b}{r}}\cdot e^{i\lambda(r-b)} \simeq e^{i\lambda(r-b)} \\
\overline{H}'_m &\simeq \left\{-\tfrac{1}{2\lambda}\sqrt{\tfrac{b}{r^3}} + i\sqrt{\tfrac{b}{r}}\right\}e^{i\lambda(r-b)} \simeq ie^{i\lambda(r-b)}\,.
\end{aligned} \qquad \text{for} \quad (|\lambda|b \gg m) \tag{A.23}$$

As shown in section 2.2.1 the approximation corresponds to a replacement of a curvilinear wall by a plane one. However, the estimation limits the validity of the calculation for large distances. For wave numbers above

$$\left(\frac{m^2}{b^2 Z_0 \sigma_0}\right) \ll k \tag{A.24}$$

the electromagnetic field can be written:

$$\begin{aligned}
\hat{E}_{m,z} &= -ic\,\hat{B}_{m,z} = A_m(k)\cdot b^m\, e^{i\lambda(r-b)} \\
\hat{E}_{m,r} &= -i\,\hat{E}_{m,\phi} = -A_m(k)\cdot b^m\,\tfrac{k}{\lambda}\, e^{i\lambda(r-b)} \\
\hat{B}_{m,r} &= -A_m(k)\cdot \tfrac{ib^m}{c}\left\{\tfrac{k}{\lambda} + \tfrac{im}{kr}\left(1+\tfrac{k^2}{\lambda^2}\right)\right\} e^{i\lambda(r-b)} \\
\hat{B}_{m,\phi} &= -A_m(k)\cdot \tfrac{b^m}{c}\left(\tfrac{k}{\lambda} + \tfrac{\lambda}{k} + \tfrac{imk}{r\lambda}\right) e^{i\lambda(r-b)}\,.
\end{aligned} \tag{A.25}$$

Coefficients

Two equations of the boundary conditions (see Eq. (2.51)) are redundant. The longitudinal electric field $\hat{E}_{m,z}$ is automatically matched on the surface ($r = b$). The remaining equations are given by:

$$\begin{aligned}
\tfrac{q_s}{2\pi\epsilon_0 c}\tfrac{r_s^m}{b^{m+1}} + B_m\cdot\tfrac{b^{m-1}}{2c} - A_m\cdot\tfrac{1}{2c}\left(\tfrac{m}{ikb} + \tfrac{ikb}{(m+1)}\right) b^m &= -A_m(k)\cdot\tfrac{b^m}{c}\left(\tfrac{k}{\lambda} + \tfrac{\lambda}{k} + \tfrac{imk}{r\lambda^2}\right) \\
-B_m\cdot\tfrac{b^{m-1}}{2i} - A_m\cdot\tfrac{1}{2i}\left(\tfrac{m}{ikb} + \tfrac{ikb}{(m+1)}\right) b^m &= A_m(k)\cdot b^m\,\tfrac{ik}{\lambda}
\end{aligned} \tag{A.26}$$

where the first is obtained from the azimuthal magnetic field component and the second from the azimuthal electric, correspondingly. If one resolves the Eq. (A.26) to the coefficients A_m and B_m one finds:

$$\begin{aligned}
A_m(k) &= \tfrac{q_s}{2\pi\epsilon_0}\tfrac{1}{b^{m+1}}\left(\tfrac{r_s}{b}\right)^m\cdot\left[\tfrac{m}{ikb} + \tfrac{ikb}{m+1} - \tfrac{\lambda}{k} - \tfrac{2k}{\lambda} - \tfrac{imk}{b\lambda^2}\right]^{-1} \\
B_m(k) &= -b\left[\tfrac{m}{ikb} + \tfrac{ikb}{m+1} - \tfrac{2k}{\lambda}\right]\cdot A_m(k)\,.
\end{aligned} \tag{A.27}$$

A.3 Wake Potential in the Long-Bunch Approximation

Longitudinal wake potential

The integral in Eq. (2.97) can be expand as

$$\int_{-\infty}^{\infty} dk\,(1 - i\,\mathrm{sign}(k))\sqrt{|k|}\cdot e^{-k^2\sigma_z^2/2}\,e^{-ik\zeta} = (1-i)\int_0^{\infty} dk\,\sqrt{|k|}\cdot e^{-k^2\sigma_z^2/2}\,e^{-ik\zeta} + (1+i)\int_0^{\infty} dk\,\sqrt{|k|}\cdot e^{-k^2\sigma_z^2/2}\,e^{+ik\zeta}\,. \tag{A.28}$$

It is shown [21] that:

$$\int_0^{\infty} dk\,\frac{e^{-ak^2-ik\zeta}}{\sqrt{k}} = \frac{\pi\sqrt{|\zeta|}}{\sqrt{8a}}\left\{I_{-1/4}(b) - i\,\mathrm{sign}(\zeta)\,I_{1/4}(b)\right\}e^{-b}\,. \tag{A.29}$$

with

$$a = \frac{\sigma_z^2}{2}\,, \qquad b = \frac{\zeta^2}{8a}\,. \tag{A.30}$$

The derivative of Eq. (A.29) with respect to ζ is given by:

$$\int_0^{\infty} dk\,\sqrt{k}\,e^{-ak^2-ik\zeta} = \tag{A.31}$$

$$-\frac{\pi|\zeta|^{3/2}}{4a\sqrt{8a}}\left\{I_{1/4}(b) - I_{-3/4}(b) + i\,\mathrm{sign}(\zeta)\,\left(I_{-1/4}(b) - I_{3/4}(b)\right)\right\}e^{-b}\,. \tag{A.32}$$

where the recurrence relation

$$I'_\nu(b) = I_{\nu+1}(b) + \frac{\nu}{b}I_\nu(b) = I_{\nu-1}(b) - \frac{\nu}{b}\,I_\nu(b) \tag{A.33}$$

has been used. Inserting this result in Eq. (A.28) one obtains

$$\int_{-\infty}^{\infty} dk\,(1 - i\,\mathrm{sign}(k))\sqrt{|k|}\cdot e^{-k^2\sigma_z^2/2}\,e^{-ik\zeta} = \tag{A.34}$$

$$-\frac{\pi|\zeta|^{3/2}}{2\sigma_z^3}\left\{I_{1/4}(b) - I_{-3/4}(b) + \mathrm{sign}(\zeta)\,\left(I_{-1/4}(b) - I_{3/4}(b)\right)\right\}e^{-b}\,.$$

With $u = -\zeta/\sigma_z$ and $b = u^2/4$ one gets the result in Eq. (2.97).

A.4 Integrals Involving the Modified Bessel Functions

Longitudinal loss factor

Following the derivation given in [21] one can substitute $x = u^2/4$ in the integral Eq. (2.107) yielding:

$$\int_{-\infty}^{\infty} du\ |u|^{3/2} \cdot \left\{ I_{1/4} - I_{-3/4} \right\} e^{-3u^2/4} = 2^{5/2} \int_0^{\infty} dx\, x^{1/4} \cdot \left\{ I_{1/4}(x) - I_{-3/4(x)} \right\} e^{-3x} . \quad \text{(A.35)}$$

With [28] p.712 one obtains

$$\int_0^{\infty} dx\, x^{\nu}\, I_{\nu}(bx)\, e^{-ax} = \frac{(2b)^{\nu}\Gamma(\nu + 1/2)}{\sqrt{\pi}(a^2 - b^2)^{\nu+1/2}} \quad \text{(A.36)}$$

and by the derivation respectively a

$$\int_0^{\infty} dx\, x^{\nu+1}\, I_{\nu}(bx)\, e^{-ax} = \frac{2a(2b)^{\nu}\Gamma(\nu + 1/2)}{\sqrt{\pi}(a^2 - b^2)^{\nu+3/2}} , \quad \text{(A.37)}$$

the above integral yields:

$$\int_{-\infty}^{\infty} du\ |u|^{3/2} \cdot \left\{ I_{1/4} - I_{-3/4} \right\} e^{-3u^2/4} = -\frac{2\sqrt{2}}{\sqrt{\pi}}\Gamma(3/4) . \quad \text{(A.38)}$$

Appendix B

B.1 Emittance Growth due to Wake Fields

B.1.1 Multi-Slice Emittance Growth Model

The bunches, containing a large number of electrons ($N = 6.24 \cdot 10^9$ for TTF-FEL), are of finite extension both in the longitudinal and in the transverse direction. Each electron contributing to the bunch is said to be distributed in the 6-dimensional coordinate space $\{x, x', y, y', z, E_z\}$. Here, the coordinate z defines the position of the electrons with respect to the bunch center at $z = 0$, where $z > 0$ indicates electrons ahead of the center.

In the following, the variation of the electron energies caused by longitudinal wake fields and due to the coupling of the electrons to the photon beam while passing through the undulator is neglected.

Furthermore it is assumed, that the degrees of freedom in the x, y and z directions are decoupled and therefore each can be described by itself. The calculations in this sections are restricted to the x-direction, analogous formulas can be found for the y-direction.

The projected transverse emittance of a bunch in x-direction is defined as:

$$\epsilon_x \equiv \sqrt{<\Delta x^2><\Delta x'^2> - <\Delta x \Delta x'>^2} \tag{B.1}$$

with

$$\Delta x_i \equiv x_i - <x> \quad \text{and} \quad <x> \equiv \frac{1}{N}\sum_{i=1}^{N} x_i \tag{B.2}$$

where N is the number of electrons in the bunch. The prime denotes the derivative with respect to s, the coordinate along the undulator. The entrance of the undulator is defined at $s = 0$, where $s = L$ ($L = 28.8\,\mathrm{m}$ for the TTF-FEL undulator) is the exit.

The bunch can be divided longitudinal into equidistant "slices" given by the intervals $[z_\nu - \Delta z/2, z_\nu + \Delta z/2]$, where Δz the length of the interval is chosen much smaller than the bunch length σ_z. For each slice the following definitions for the mean values

$$x_\nu = \frac{1}{N_\nu}\sum_{j=1}^{N_\nu} x_{j,\nu}\,, \qquad x'_\nu = \frac{1}{N_\nu}\sum_{j=1}^{N_\nu} x'_{j,\nu}\,, \tag{B.3}$$

and for the variances $\sigma_{xx\nu}$, $\sigma_{xx'\nu}$ and $\sigma_{x'x'\nu}$

$$\begin{aligned} \sigma_{xx\nu} &= \tfrac{1}{N_\nu}\sum_{j=1}^{N_\nu}(\Delta x_{j,\nu})^2\,, \\ \sigma_{xx'\nu} &= \tfrac{1}{N_\nu}\sum_{j=1}^{N_\nu}(\Delta x_{j,\nu})(\Delta x'_{j,\nu})\,, \\ \sigma_{x'x'\nu} &= \tfrac{1}{N_\nu}\sum_{j=1}^{N_\nu}(\Delta x'_{j,\nu})^2 \end{aligned} \tag{B.4}$$

are used. The sums are extended over the N_ν electrons contained in the ν-slice of the bunch. The emittance ϵ_x Eq. (B.1) can be rewritten as:

$$\begin{aligned} \epsilon_x = \Bigg\{ &\left[\sum_\nu \lambda_\nu \left\{\sigma_{xx\nu} + (x_\nu - x)^2\right\}\right]\left[\sum_\nu \lambda_\nu \left\{\sigma_{x'x'\nu} + (x'_\nu - x')^2\right\}\right] \\ &- \left[\sum_\nu \lambda_\nu \left\{\sigma_{xx'\nu} + (x_\nu - x)(x'_\nu - x')\right\}\right] \Bigg\}^{1/2} \end{aligned} \tag{B.5}$$

with

$$\lambda_\nu \equiv \frac{N_\nu}{N} \qquad \text{and} \qquad \sum_\nu \lambda_\nu = 1\,, \tag{B.6}$$

the average longitudinal charge density in the interval $[z_\nu - \triangle z/2, z_\nu + \triangle z/2]$. For sufficiently small $\triangle z$, the longitudinal charge distribution $\lambda_{\|}$ at z_ν is approximated by λ_ν.

The bunch emittance ϵ_x can be thought of as being composed of two different contributions, namely the finite extension of the individual slices in the $\{x, x'\}$-space, which are referred to as the self emittances $\epsilon_{x\nu}$, and secondly the relative offsets between the individual slices in that space, which is called the centroid emittance [29]. The centroid emittance is defined as:

$$\epsilon_{xC} \equiv \sqrt{\sigma_{xxC}\sigma_{x'x'C} - \sigma_{xx'C}^2} \tag{B.7}$$

with

$$\begin{aligned} \sigma_{xxC} &= \sum_\nu \lambda_\nu (x_\nu - x)^2\,, \\ \sigma_{x'x'C} &= \sum_\nu \lambda_\nu (x'_\nu - x')^2\,, \\ \sigma_{xx'C} &= \sum_\nu \lambda_\nu (x_\nu - x)(x'_\nu - x')\,, \end{aligned} \tag{B.8}$$

and gives the area over which the center of the bunch-slices are scattered.

As derived in section 1.4 the largest contribution of the transverse wake fields for small beam offsets is given by the transverse dipole wake fields. For cylindrically symmetric structures the transverse dipole wake fields depend only on the displacement of the mean position of the source slice from the center of the structure. Hence, for sufficiently small $\triangle z$ the development of the slice-variances are determined by the optic of the undulator and are not influenced by the transverse wake fields. Therefore, in the following, the slice emittances $\epsilon_{x\nu}$ are considered to be constant.

Furthermore it is assumed, that the variation of the slice-emittances over the individual slices of a bunch is small ($\epsilon_{x\nu} \approx \epsilon_x^s$).

Consider the case that at the entrance of the undulator the individual slices center in the $\{x, x'\}$-space are equal. Then the variances (σ_{xx}^s, ...) and the slice-emittance ϵ_x^s coincide with the bunch variances (σ_{xx}, ...) and the bunch emittance ϵ_x at $s = 0$. With these assumptions the bunch emittance as a function of the coordinate s reduces to:

$$\epsilon_x(s) = \sqrt{\epsilon_x^2(0) + \sigma_{xx}(s)\sigma_{x'x'C}(s) - 2\,\sigma_{xx'}(s)\sigma_{xx'C}(s) + \sigma_{x'x'}(s)\sigma_{xxC}(s) + \epsilon_{xC}^2(s)}\,. \tag{B.9}$$

The development of the variances along the undulator can be described by the twist parameters $\beta_x(s)$, $\alpha(s)$ and $\gamma(s)$ according to:

$$\sigma_{xx}(s) = \epsilon_x(0)\beta(s)\,, \qquad \sigma_{x'x}(s) = -\epsilon_x(0)\alpha(s)\,, \qquad \sigma_{x'x'}(s) = \epsilon_x(0)\gamma(s)\,, \tag{B.10}$$

with $\alpha = -\beta'/2$ and $\gamma = (1 + \alpha^2)/\beta$. Finally, one can express the emittance growth $\delta\epsilon_x(s) = \epsilon_x(s) - \epsilon_x(0)$ as:

$$\frac{\delta\epsilon_x(s)}{\epsilon_x(0)} = \left(\sqrt{1 + \frac{1}{\epsilon_x(0)}\left[\beta_x\sigma_{x'x'C} + 2\,\alpha_x\sigma_{xx'C}(s) + \gamma_x\sigma_{xxC}\right] + \frac{\epsilon_{xC}^2}{\epsilon_x^2(0)}} - 1\right) \tag{B.11}$$

In the case of small centroid variances, as expected for sufficiently small offset of the initial beam, the emittance growth can be written as:

$$\frac{\delta\epsilon_x(s)}{\epsilon_x(0)} = \frac{1}{2\epsilon_x(0)}\left[\beta_x\sigma_{x'x'C} + 2\,\alpha_x\sigma_{xx'C}(s) + \gamma_x\sigma_{xxC}\right] + \frac{\epsilon_{xC}^2}{2\epsilon_x^2(0)}\,. \qquad \text{(B.12)}$$

B.1.2 Beam Distortion due to Transverse Wake Fields

As mentioned above, for small beam offsets the dynamics of the beam slices can be represented by macro particles, where the ν-slice is now given by a macro particle at (x_ν, x'_ν) charged with $Ne\lambda_\nu$.

In absence of wake fields the macro particles execute a free betatron oscillation:

$$x_\nu(s) = \tilde{x}\sqrt{\frac{\beta_x(s)}{\beta_x(0)}}\cos\left(\Psi(s)\right) \qquad \text{with} \qquad \Psi(s) \equiv \int_0^s ds'\frac{1}{\beta_x(s')} \qquad \text{(B.13)}$$

where Ψ is the phase of the macro particle.

The undulator optic consists of a number of FODO-cells. For convenience $s = 0$ is defined at the center of the first quadrupole, with a vanishing α. Therefore, the slope of the beam at the center of the quadrupole is considered to be zero, and $\tilde{x}$ defines the initial offset.

In presence of wake fields the equation of motion for the ν-macro particle reads* †:

$$x''_\nu - k(s)\,x_\nu = \frac{Ne^2}{E_0}\sum_\mu \lambda_\mu \overline{\overline{W}}^{\delta}_{\perp}(z_\mu - z_\nu)\,x_\mu\,. \qquad \text{(B.14)}$$

Since the wake function vanishes for $z_\mu \leq z_\nu$ the sum is restricted to the macro particles in front of the ν^{th} one. Therefore, the motion of the head of the bunch influences the motion of the bunch tail.

In order to solve the differential Eq. (B.14) consider a perturbation expansion

$$x_\nu(s) = \sum_{n=0}^{M_\nu} x_\nu^{(n)}(s)\,, \qquad \text{(B.15)}$$

where M_ν are the number of slices downstream. The leading term ($n = 0$) is given by the free betatron oscillation Eq. (B.13). The n^{th} term $x_\nu^{(n)}$ is $(n-1)^{th}$ order in the wake field strength and therefore $(n-1)^{th}$ order in the bunch intensity. It is determined by the iteration condition [12]:

$$\frac{d^2}{ds^2}x_\nu^{(n)}(s) - k(s)\,x_\nu^{(n)}(s) = \frac{Ne^2}{E_0}\sum_\mu \lambda_\mu \overline{\overline{W}}^{\delta}_{\perp}(z_\mu - z_\nu)\,x_\mu^{(n-1)}(s)\,. \qquad \text{(B.16)}$$

The solution to Eq. (B.16) can be expressed in terms of a Green's function $G(s, s')$ as:

$$x_\nu^{(n)}(s) = \frac{Ne^2}{E_0}\sum_\mu \lambda_\mu \overline{\overline{W}}^{\delta}_{\perp}(z_\mu - z_\nu)\int_0^\infty G(s, s')\,x_\mu^{(n-1)}(s')\,. \qquad \text{(B.17)}$$

*Only the transverse dipole wake function has been taken into account.

†The wake function is defined per unit length.

Equations (B.13), (B.15), and (B.17) determine the complete solution of the so-called beam breakup [12].

For offsets comparable to the beam pipe radius higher multipole modes of the transverse wake function have to be taken into account. Then the motion of the ν^{th} macro particle depends additionally on the transverse position on the macro particle itself.

Note that the differential Eq. (B.14) is local. The strength of the wake forces seen by a macro particle at s depends only on the transverse displacement of the ensemble of macro particles at the same position s in the undulator. If the beam-wake interaction distance D becomes important, hence when the average betatron wave length $\overline{\lambda} = 2\pi\overline{\beta}$ is in the order of D, the wake forces at s are functions of the macro particles at $s - \triangle s$, an earlier position in the undulator. The system of equations becomes then non-local and has to be described for instance by a integro-differential equation.

However, as derived in section 1.6 the typical distances D for the TTF-FEL beam in the undulator is approximately 25 cm, while the betatron wave length $\overline{\lambda}$ is 18.8 m. Therefore the approximation by using a local differential equation seem to be justified.

B.1.3 Construction of the Green's function for the Hill Equation

A Green's function, which is a solution of the inhomogeneous Hill equation:

$$\left[\partial_s^2 - k(s)\right] G(s,s') = \delta(s-s') . \tag{B.18}$$

and vanishes for $s' > s$ (due to causality) can be written as:

$$G(s,s') = \frac{\hat{x}_1(s)\,\hat{x}_2(s') - \hat{x}_1(s')\,\hat{x}_2(s)}{[\hat{x}_1,\hat{x}_2]_W} \cdot \theta(s-s') , \tag{B.19}$$

where $\hat{x}_1$ and $\hat{x}_2$ are two arbitrary homogeneous solutions of the Hill equation with a non-vanishing Wronski-determinant*($[\hat{x}_1,\hat{x}_2]_W \neq 0$). Obviously, the Green's function is a homogeneous solution of the Hill equation for $s \neq s'$ and fulfills Eq. (B.18) as one can see by integrating Eq. (B.18) respect to s over the interval $[s'-\epsilon, s'+\epsilon]$.

The Wronski-determinant is a constant quantity and vanishes if and only if the solutions $\hat{x}_1$ and $\hat{x}_2$ of the Hill equations are linear dependent. Therefore the Green's function given in Eq. (B.19) is well defined. The simplest choice for $\hat{x}_1$ and $\hat{x}_2$ is

$$\hat{x}_1 = \sqrt{\beta_x(s)}\sin(\Psi(s)) , \quad \text{and} \quad \hat{x}_2 = \sqrt{\beta_x(s)}\cos(\Psi(s)) \tag{B.20}$$

with

$$[\hat{x}_1,\hat{x}_2]_W = 1 . \tag{B.21}$$

Hence, inserting the solutions Eq. (B.20) in Eq. (B.19) one obtains:

$$G(s,s') = \sqrt{\beta_x(s)\beta_x(s')}\,\sin(\Psi(s)-\Psi(s'))\,\theta(s-s') . \tag{B.22}$$

*The Wronski-determinant in two dimension is defined as: $[\hat{x}_1,\hat{x}_2]_W(s) = \hat{x}_1'(s)\hat{x}_2(s) - \hat{x}_1(s)\hat{x}_2'(s)$.

B.1.4 Emittance Growth in First Order Perturbation Theory

Using first order perturbation theory one can derive a simple formula for the emittance growth $\delta\epsilon(s)$. According to Eq. (B.17) the solution for $n = 1$ reads:

$$\begin{aligned} x_\nu(s) &= x_\nu^{(0)}(s) + x_\nu^{(1)}(s) \\ &= x^{(0)}(s) + \frac{Ne^2}{E_0} \sum_\mu \lambda_\mu \overline{\overline{W}}_\perp^\delta(z_\mu - z_\nu) \int_0^\infty G(s,s')\, x^{(0)}(s) \\ &= x^{(0)}(s) + \frac{Ne^2}{E_0} \overline{\overline{W}}_\perp^\lambda(z_\nu) \int_0^\infty G(s,s')\, x^{(0)}(s) \end{aligned} \tag{B.23}$$

with

$$x_\nu^{(0)}(s) = x^{(0)}(s) = \tilde{x} \sqrt{\frac{\beta_x(s')}{\beta_x(0)}} \cos\left(\Psi(s)\right). \tag{B.24}$$

Obviously, the strength of the perturbation of the transverse motion is proportional to the amplitude of the transverse wake potential at the position of the macro particle. The dynamics are described by the integral over the Green's function multiplied with the unperturbed motion, the latter being independent of the macro particle considered. Therefore, the position and the slope of the macro particles are correlated:

$$\frac{x'_\nu(s)}{x_\nu(s)} = f(s), \tag{B.25}$$

where the function f is equal for all ν. Consequently, the centroid emittance ϵ_{xC} vanishes for all s in first order perturbation theory.

For the variances one can write:

$$\sigma_{xxC}(s) = \Upsilon^2 \cdot \left(\int_0^\infty G(s,s')\, x^{(0)}(s') \right)^2 \tag{B.26}$$

$$\sigma_{xx'C}(s) = \Upsilon^2 \cdot \left(\int_0^\infty \partial_s G(s,s')\, x^{(0)}(s') \right) \left(\int_0^\infty G(s,s')\, x^{(0)}(s') \right) \tag{B.27}$$

$$\sigma_{xxC}(s) = \Upsilon^2 \cdot \left(\int_0^\infty \partial_s G(s,s')\, x^{(0)}(s') \right)^2, \tag{B.28}$$

where Υ is given by

$$\Upsilon^2 = \left(\frac{Ne^2}{E_0} \right)^2 \cdot \left(< \overline{\overline{W}}_\perp^{\lambda\,2} >_\lambda - k_\perp^2 \right) \tag{B.29}$$

with

$$< \overline{\overline{W}}_\perp^{\lambda\,2} >_\lambda = \sum_\nu \lambda_\nu \overline{\overline{W}}_\perp^{\lambda\,2}(z_\nu), \qquad k_\perp = < \overline{\overline{W}}_\perp^\lambda >_\lambda . \tag{B.30}$$

Next, one uses the particular Green's function Eq. (B.22). The derivative with respect to s yields:

$$\partial_s G(s,s') = \left(\frac{\beta_x'(s)}{2\sqrt{\beta_x(s)}}\theta(s-s') + \sqrt{\beta_x(s)}\delta(s-s')\right)\sqrt{\beta_x(s')}\sin\left(\Psi(s)-\Psi(s')\right) + \sqrt{\frac{\beta_x(s')}{\beta_x(s)}}\cos\left(\Psi(s)-\Psi(s')\right). \quad \text{(B.31)}$$

As $\sin(\Psi(s)-\Psi(s'))=0$ for $s=s'$ the term including the delta-function can be dropped. Using $\alpha_x = -\beta_x'/2$ the derivative of the Green's function can be rewritten as:

$$\partial_s G(s,s') = -\frac{\alpha_x(s)}{\sqrt{\beta_x(s)}}g_s(s,s') + \frac{1}{\sqrt{\beta_x(s)}}g_c(s,s'), \quad \text{(B.32)}$$

where the functions g_s and g_c are defined by:

$$g_s(s,s') \equiv \sqrt{\beta_x(s')}\sin\left(\Psi(s)-\Psi(s')\right)\theta(s-s'), \quad \text{(B.33)}$$

$$g_c(s,s') \equiv \sqrt{\beta_x(s')}\cos\left(\Psi(s)-\Psi(s')\right)\theta(s-s'). \quad \text{(B.34)}$$

The Green's function itself expressed by g_s is written:

$$G(s,s') = \sqrt{\beta_x(s)}g_s(s,s'). \quad \text{(B.35)}$$

Finally, according to the expressions for the centroid variances Eqs. (B.26-B.29) the relative emittance growth Eq. (B.12) yields:

$$\frac{\delta\epsilon_x(s)}{\epsilon_x(0)} = \frac{1}{2\epsilon_x(0)}\left[\beta_x\sigma_{x'x'C} + 2\,\alpha_x\sigma_{xx'C} + \gamma_x\sigma_{xxC}\right] \quad \text{(B.36)}$$

$$= \frac{1}{2\epsilon_x(0)}\cdot\Upsilon^2\cdot\left[\left(\int_0^\infty ds'\,g_s(s,s')\,x^{(0)}(s')\right)^2 + \left(\int_0^\infty ds'\,g_c(s,s')\,x^{(0)}(s')\right)^2\right].$$

Therefore, the emittance growth is known when the two integrals with the integral kernels g_s and g_c as functions of s are evaluated:

$$\int_0^\infty ds'\,g_s(s,s')\,x^{(0)}(s') = \frac{\tilde{x}}{\sqrt{\beta_x(0)}}\int_0^s ds'\,\beta_x(s')\,\sin\left(\Psi(s)-\Psi(s')\right)\cos\left(\Psi(s')\right), \quad \text{(B.37)}$$

$$\int_0^\infty ds'\,g_c(s,s')\,x^{(0)}(s') = \frac{\tilde{x}}{\sqrt{\beta_x(0)}}\int_0^s ds'\,\beta_x(s')\,\cos\left(\Psi(s)-\Psi(s')\right)\cos\left(\Psi(s')\right). \quad \text{(B.38)}$$

Displacement of the Beam Pipe Center

Additional wake fields occur, if the geometrical axis given by the center of the undulator vacuum chamber is displaced by x_{geo} from the optical axis defined by the quadrupoles of the undulator. These wake fields can be taken into account by replacing $x^{(0)}$ in Eq. (B.36)

by $x^{(0)} - x_{geo}$. The integrals, which have to be added to the integrals in Eqs. (B.37-B.38) read:

$$-\int_0^\infty ds'\, g_s(s,s')\, x_{geo} \;=\; -x_{geo} \int_0^s ds' \sqrt{\beta_x(s')}\, \sin\left(\Psi(s) - \Psi(s')\right) \tag{B.39}$$

$$-\int_0^\infty ds'\, g_c(s,s')\, x_{geo} \;=\; -x_{geo} \int_0^s ds' \sqrt{\beta_x(s')}\, \cos\left(\Psi(s) - \Psi(s')\right). \tag{B.40}$$

B.1.5 Approximation by using the Average Beta Function

The integrals Eqs. (B.37-B.40) can be solved analytically when the beta function $\beta_x(s)$ is substituted by the average beta function $\overline{\beta}$. The phase Ψ can be written as $\Psi(s) = k_{\overline{\beta}}\, s$ with the average wave number $k_{\overline{\beta}} = 1/\overline{\beta}$. The initial offset of the bunch $\overline{x}$ is related to the initial offset $\tilde{x}$ defined at the center of the first quadrupole as:

$$\overline{x} \;=\; \frac{\overline{\sqrt{\beta_x}}}{\sqrt{\beta_x(0)}}\, \tilde{x}\,. \tag{B.41}$$

According to Eq. (B.23) and Eq. (B.35) the integrals with the integral kernel g_s are related to the perturbation of the transverse macro particles motion of the macro. The strength of the perturbation is proportional to the amplitude of the transverse wake potential, and hence, depends on the longitudinal position z_ν of the macro particle. Since the beta function is considered to be constant ($\alpha \equiv 0$) the integrals including g_c are related to the macro particles slope (see Eq. (B.32)).

For the integrals Eq. (B.37) and Eq. (B.38) one finds:

$$\begin{aligned}
\int_0^\infty ds'\, g_s(s,s')\, x^{(0)}(s') \;&=\; \overline{x}\sqrt{\overline{\beta}} \int_0^s ds'\, \sin\left(k_{\overline{\beta}}(s-s')\right) \cos\left(k_{\overline{\beta}}\, s'\right) \\
&=\; \frac{\overline{x}\sqrt{\overline{\beta}}}{2}\, s\, \sin\left(k_{\overline{\beta}}\, s\right) \qquad \text{(B.42)} \\
\int_0^\infty ds'\, g_c(s,s')\, x^{(0)}(s') \;&=\; \overline{x}\sqrt{\overline{\beta}} \int_0^s ds'\, \cos\left(k_{\overline{\beta}}(s-s')\right) \cos\left(k_{\overline{\beta}}\, s'\right) \\
&=\; \frac{\overline{x}\sqrt{\overline{\beta}}}{2} \left(s\, \cos\left(k_{\overline{\beta}}\, s\right) + \overline{\beta} \sin\left(k_{\overline{\beta}}\, s\right)\right). \qquad \text{(B.43)}
\end{aligned}$$

The solutions of both integrals contain terms which grow linear with the distance s already covered by the bunch in the undulator. In contrast to that, one finds for the integrals Eq. (B.39) and Eq. (B.40):

$$\begin{aligned}
-\int_0^\infty ds'\, g_s(s,s')\, x_{geo} \;&=\; -x_{geo}\sqrt{\overline{\beta}} \int_0^s ds'\, \sin\left(k_{\overline{\beta}}(s-s')\right) \\
&=\; -x_{geo}\, \overline{\beta}^{3/2} \left[1 - \cos\left(k_{\overline{\beta}}\, s\right)\right] \qquad \text{(B.44)} \\
-\int_0^\infty ds'\, g_c(s,s')\, x_{geo} \;&=\; -x_{geo}\sqrt{\overline{\beta}} \int_0^s ds'\, \cos\left(k_{\overline{\beta}}(s-s')\right) \\
&=\; -x_{geo}\, \overline{\beta}^{3/2} \sin\left(k_{\overline{\beta}}\, s\right) \qquad \text{(B.45)}
\end{aligned}$$

only contributions that are bounded in their amplitudes. Using the above results (Eqs. (B.42-B.45)) the motion of the ν^{th} macro particle (or slice) in the $\{x, x'\}$-space reads:

$$x_\nu(s) = \overline{x}\cos\left(k_{\overline{\beta}}\, s\right) + \frac{Ne^2}{E_0}\overline{\overline{W}}_\perp^{\lambda}(z_\nu)\left\{\frac{\overline{x}\overline{\beta}}{2}\, s\, \sin\left(k_{\overline{\beta}}\, s\right) - x_{geo}\,\overline{\beta}^2\left[1 - \cos\left(k_{\overline{\beta}}\, s\right)\right]\right\} \tag{B.46}$$

$$x'_\nu(s) = -\frac{\overline{x}}{\overline{\beta}}\sin\left(k_{\overline{\beta}}\, s\right) + \frac{Ne^2}{E_0}\overline{\overline{W}}_\perp^{\lambda}(z_\nu)\left\{\frac{\overline{x}}{2}\left(s\, \cos\left(k_{\overline{\beta}}\, s\right) + \overline{\beta}\sin\left(k_{\overline{\beta}}\, s\right)\right) - x_{geo}\,\overline{\beta}\sin\left(k_{\overline{\beta}}\, s\right)\right\}. \tag{B.47}$$

The behavior of the perturbation of motion $x_\nu^{(1)}$ and the slope $x_\nu^{(1)'}$ of the macro particles at the positions $z = 2\sigma_z$, σ_z, 0, $-\sigma_z$, $-2\,\sigma_z$ inside the bunch along the undulator are shown in Figs. B.1-B.3.

Finally, one finds for the emittance growth the following formula:

$$\frac{\delta\epsilon_x(s)}{\epsilon_x(0)} = \frac{1}{2\epsilon_x(0)}\cdot\left(\frac{Ne^2}{E_0}\right)^2\cdot\left(<\overline{\overline{W}}_\perp^{\lambda\,2}>_\lambda - k_\perp^2\right) \times \left\{\left(\frac{\overline{x}\sqrt{\overline{\beta}}}{2}\, s\, \sin\left(k_{\overline{\beta}}\, s\right) - x_{geo}\,\overline{\beta}^{3/2}\left[1 - \cos\left(k_{\overline{\beta}}\, s\right)\right]\right)^2 + \left(\frac{\overline{x}\sqrt{\overline{\beta}}}{2}\left[s\, \cos\left(k_{\overline{\beta}}\, s\right) + \overline{\beta}\sin\left(k_{\overline{\beta}}\, s\right)\right] - x_{geo}\,\overline{\beta}^{3/2}\sin\left(k_{\overline{\beta}}\, s\right)\right)^2\right\} \tag{B.48}$$

B.1.6 Comparison of Analytical Solutions with Numerical Simulations

The optics of the undulator consist of a series of equidistant alternating focusing and defocusing quadrupoles (FODO-cell structure). The length a FODO-cell is $L_{FODO} = 0.96\,\mathrm{m}$ (see Tab. 3.1). The undulator has a length of about 28.7 m and is subdivided into 6 modules. Each of the module contains 5 FODO-cells. The twist parameters β_x, α_x, γ_x and the phase Ψ in the x-plane of the first module are sketched in Fig. B.4.

The transverse motion Eq. (B.24) and the slope of the bunch with an average offset of $\overline{x} = 100\,\mu\mathrm{m}$ are plotted in Fig. B.5, together with the approximation Eq. (B.41) for a constant beta function $\overline{\beta}$.

The correction in the transverse motion $x^{(1)}$ and the slope $x^{(1)'}$ of the center of the bunch in first order perturbation theory (see Eqs. (B.23,B.46, B.47)) for the numerical simulation and the analytical solution are shown in Figs. B.6-B.7.

Finally, the emittance growth calculated by using the complete beta function Eq. (B.36) has been compared with the analytical result in Eq. (B.48). Both solutions are in very good agreement (see Fig. 3.4 and Fig. 3.5). Therefore, the emittance growth due to the resistive wall wake fields is determined by the average beta function and approximately independent of the particular FODO-cell structure of the undulator.

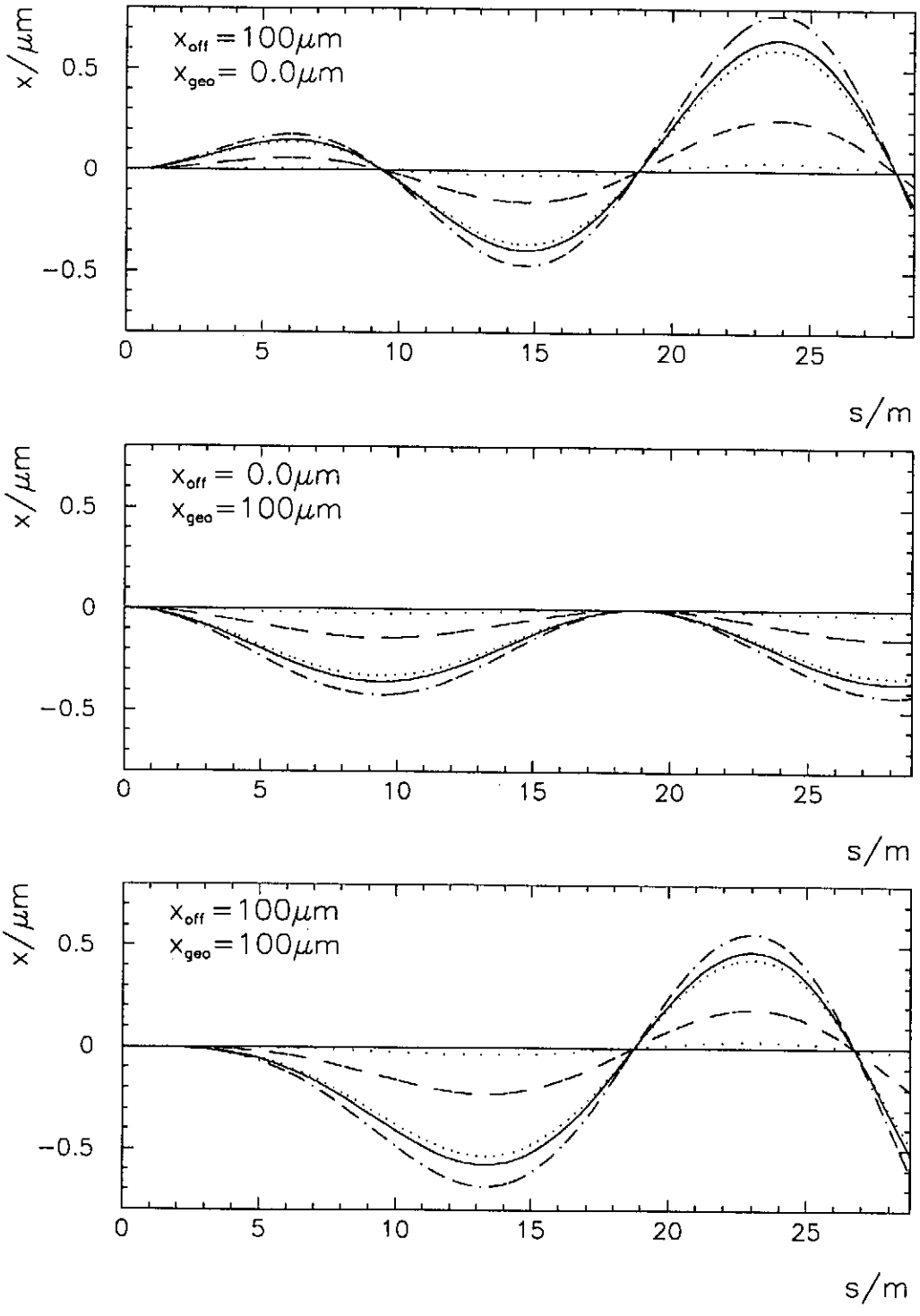

Figure B.1: Development of the macro particles offsets from the free betatron oscillation along the undulator obtained by first order perturbation theory. The longitudinal macro particles positions in the bunch are $z = 2\sigma_z$, σ_z, 0, $-\sigma_z$, $-2\,\sigma_z$ (dotted, dashed, solid, dashed-dotted and short-dotted line). The undulator vacuum chamber made of aluminum has a beam tube radius of 4.75 mm.

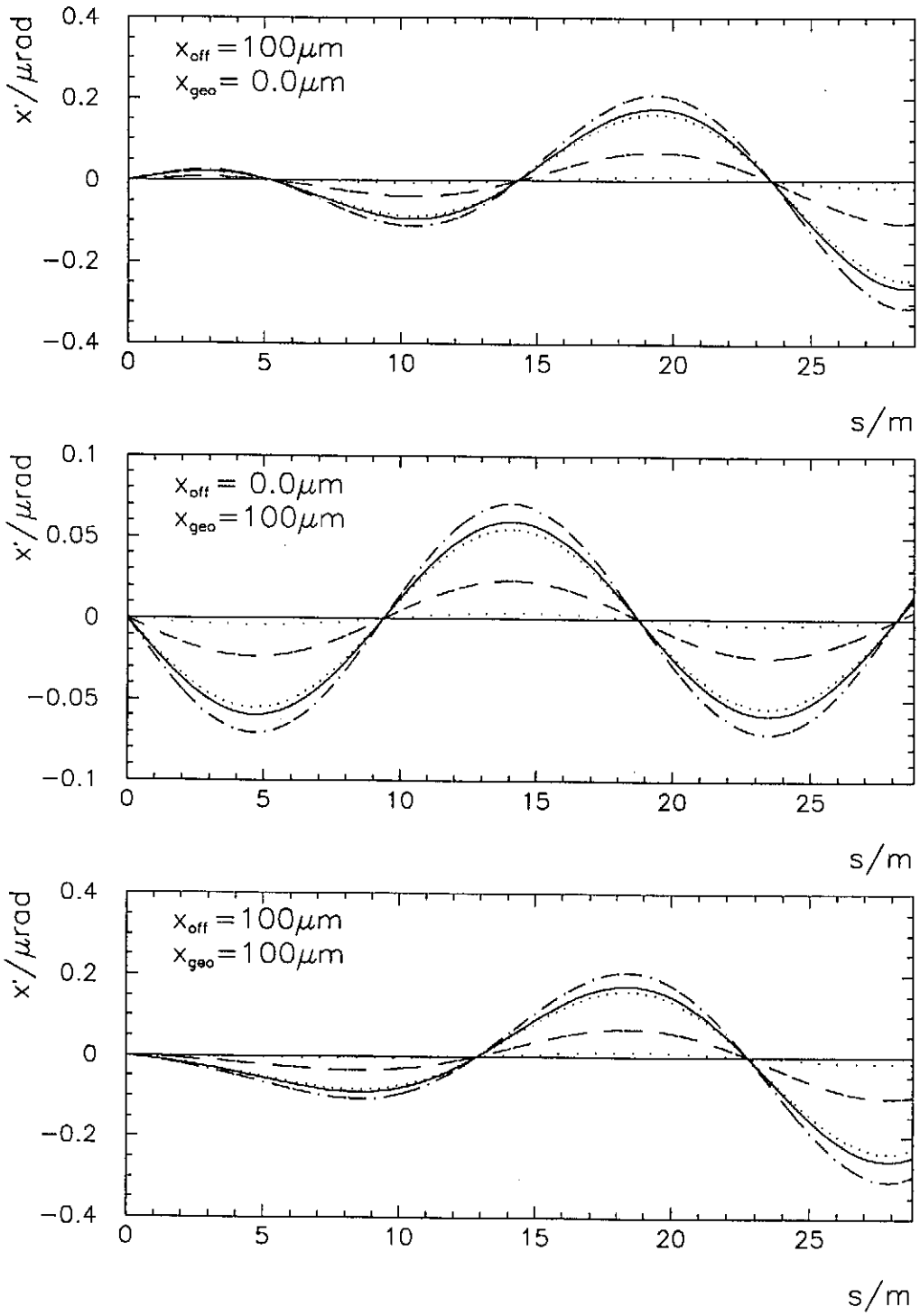

Figure B.2: Development of the macro particles slope from the free betatron oscillation along the undulator obtained by first order perturbation theory. The longitudinal macro particles positions in the bunch are $z = 2\sigma_z, \sigma_z, 0, -\sigma_z, -2\sigma_z$ (dotted, dashed, solid, dashed-dotted and short-dotted line). The undulator vacuum chamber made of aluminum has a beam tube radius of 4.75 mm.

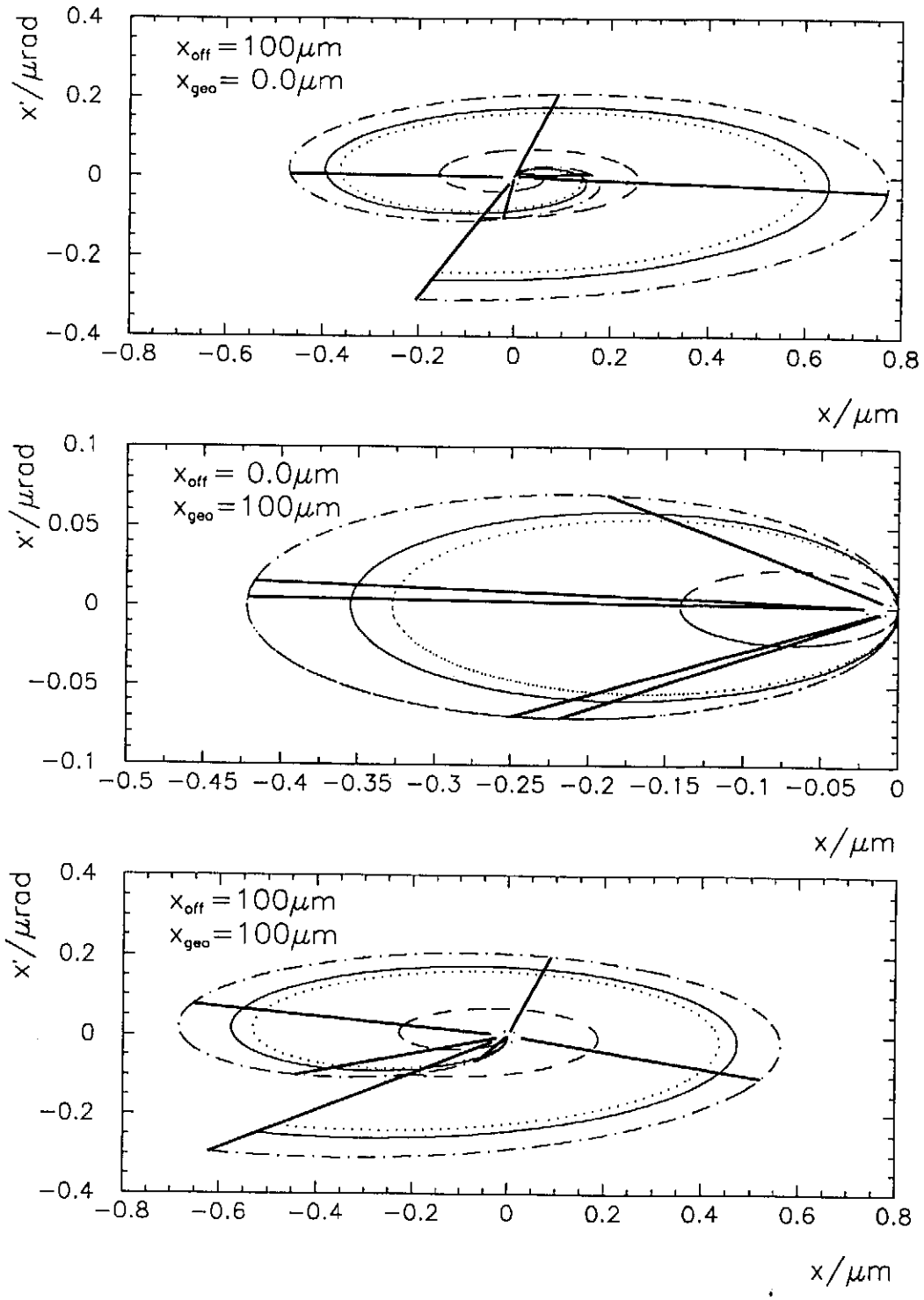

Figure B.3: Development of the macro particles in the $\{x, x'\}$-space along the undulator ($z = 2\sigma_z, \sigma_z, 0, -\sigma_z, -2\sigma_z$ is plotted by the dotted, dashed, solid, dashed-dotted and short-dotted line). Each of the connection between the curves for the various z (thick solid line) corresponds to the end of one undulator module (module length $L_{mod} = 4.8\,m$).

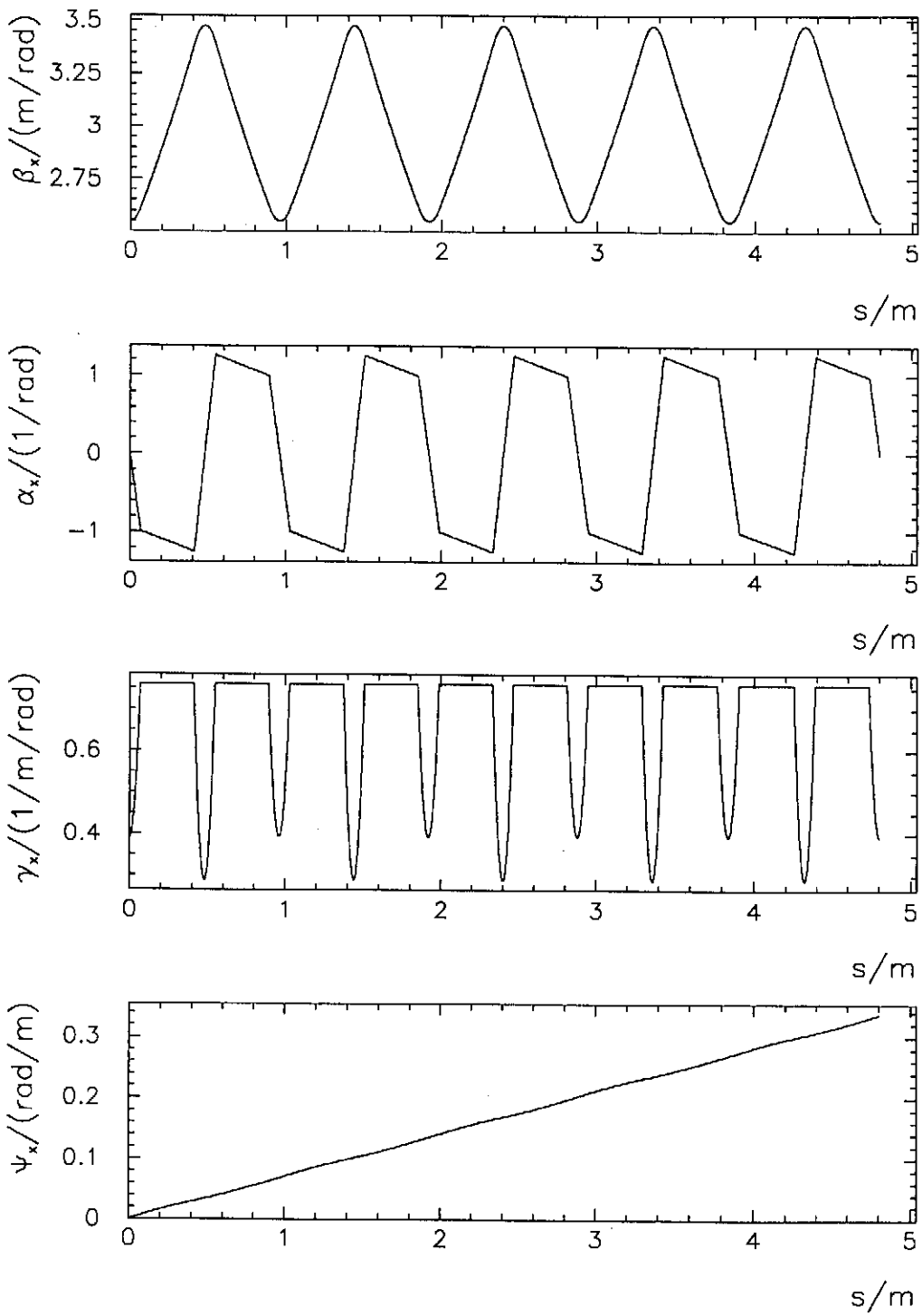

Figure B.4: Twist parameter β_x, α_x, γ_x and the phase Ψ_x of the first undulator module (beginning from the center of the first defocusing quadrupole).

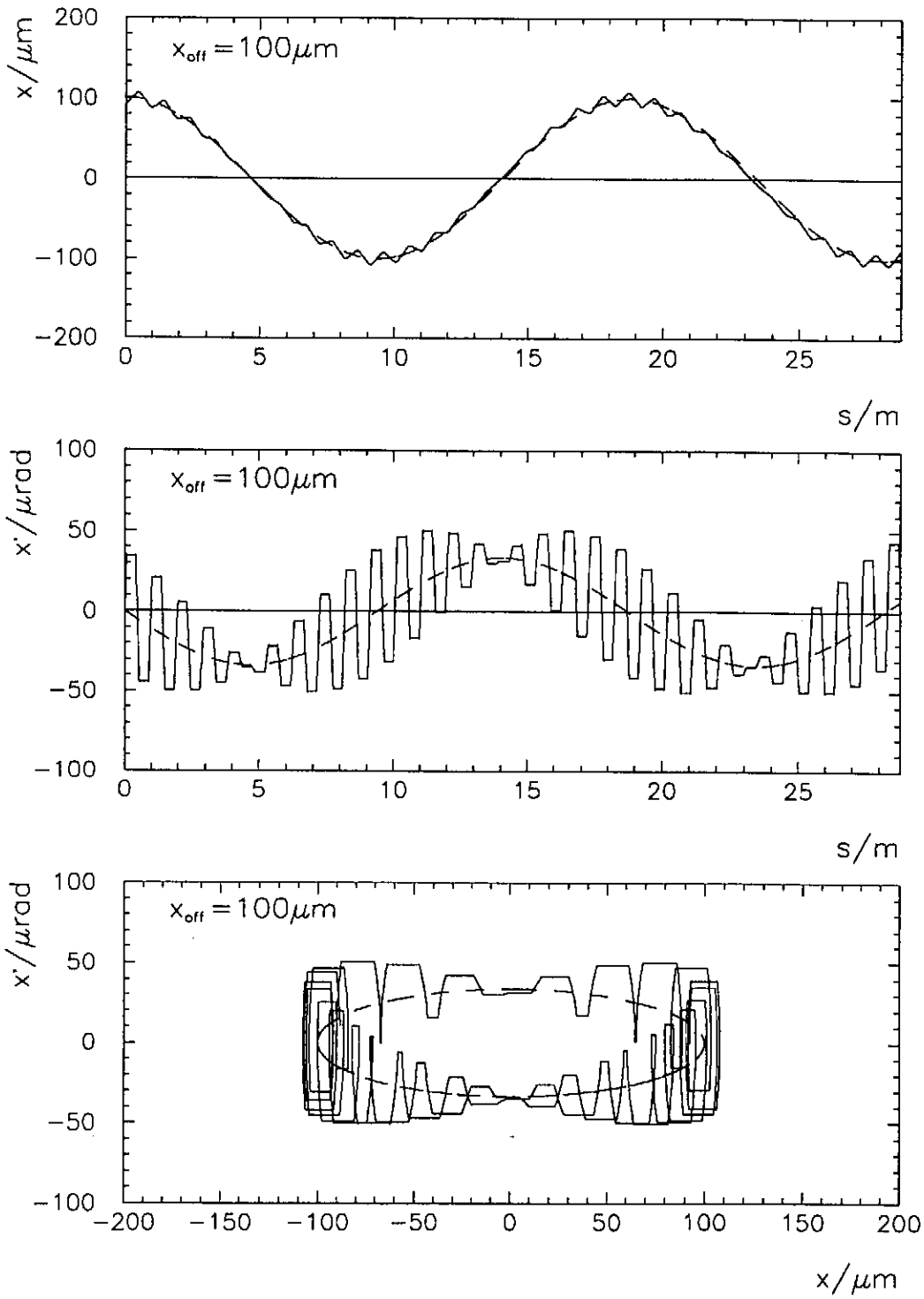

Figure B.5: Free betatron oscillation and the slope of a bunch with an initial offset of $\overline{x} = 100\,\mu$m (with respect to the average beta function). The numerical result is represented by the solid line and the analytical solution by the dashed line.

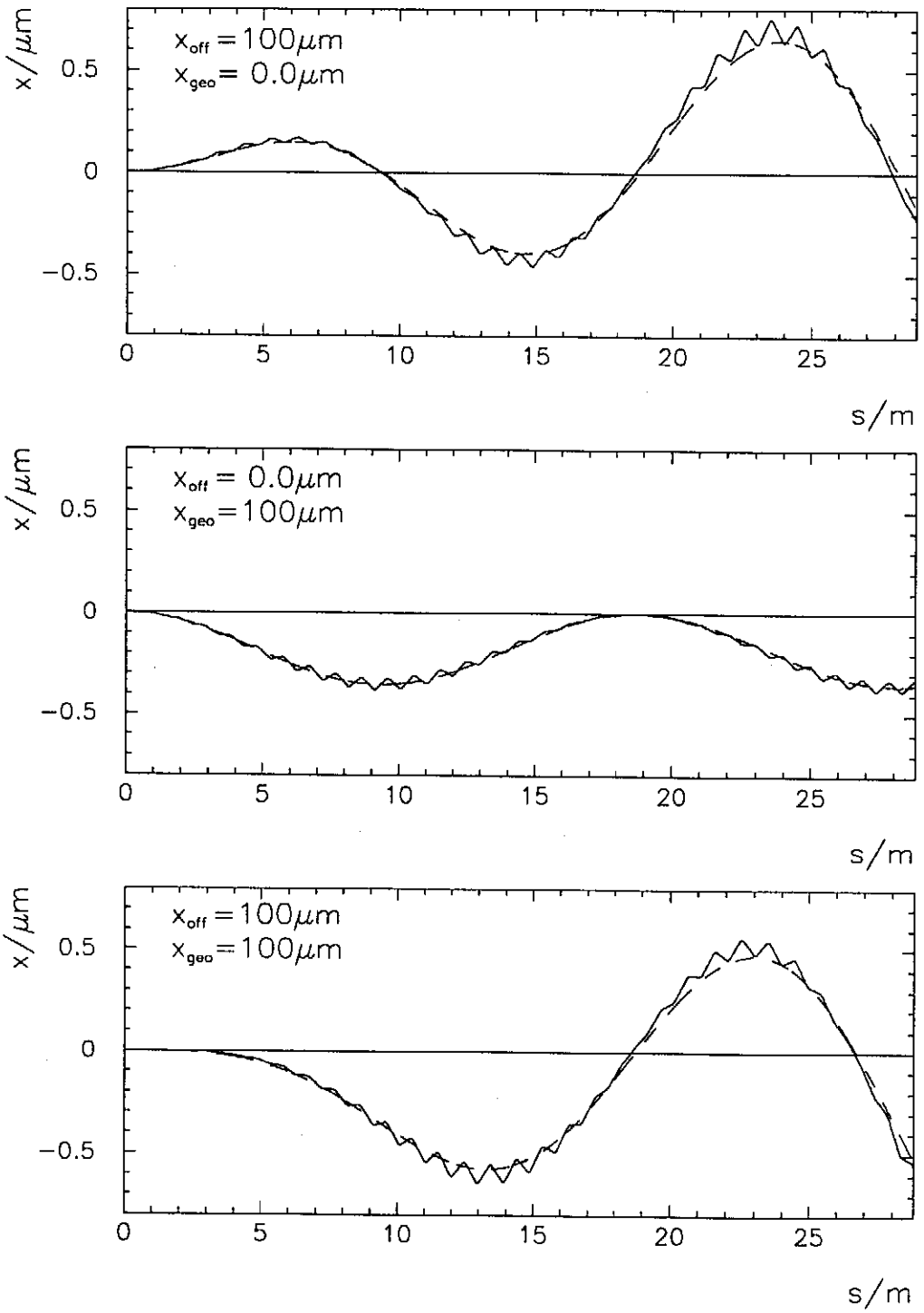

Figure B.6: Correction of the transverse motion of the center of the bunch due to resistive wall wake fields. The numerical simulation is given by the solid line, the analytical result by the dashed line; (aluminum vacuum chamber, radius 4.75 mm).

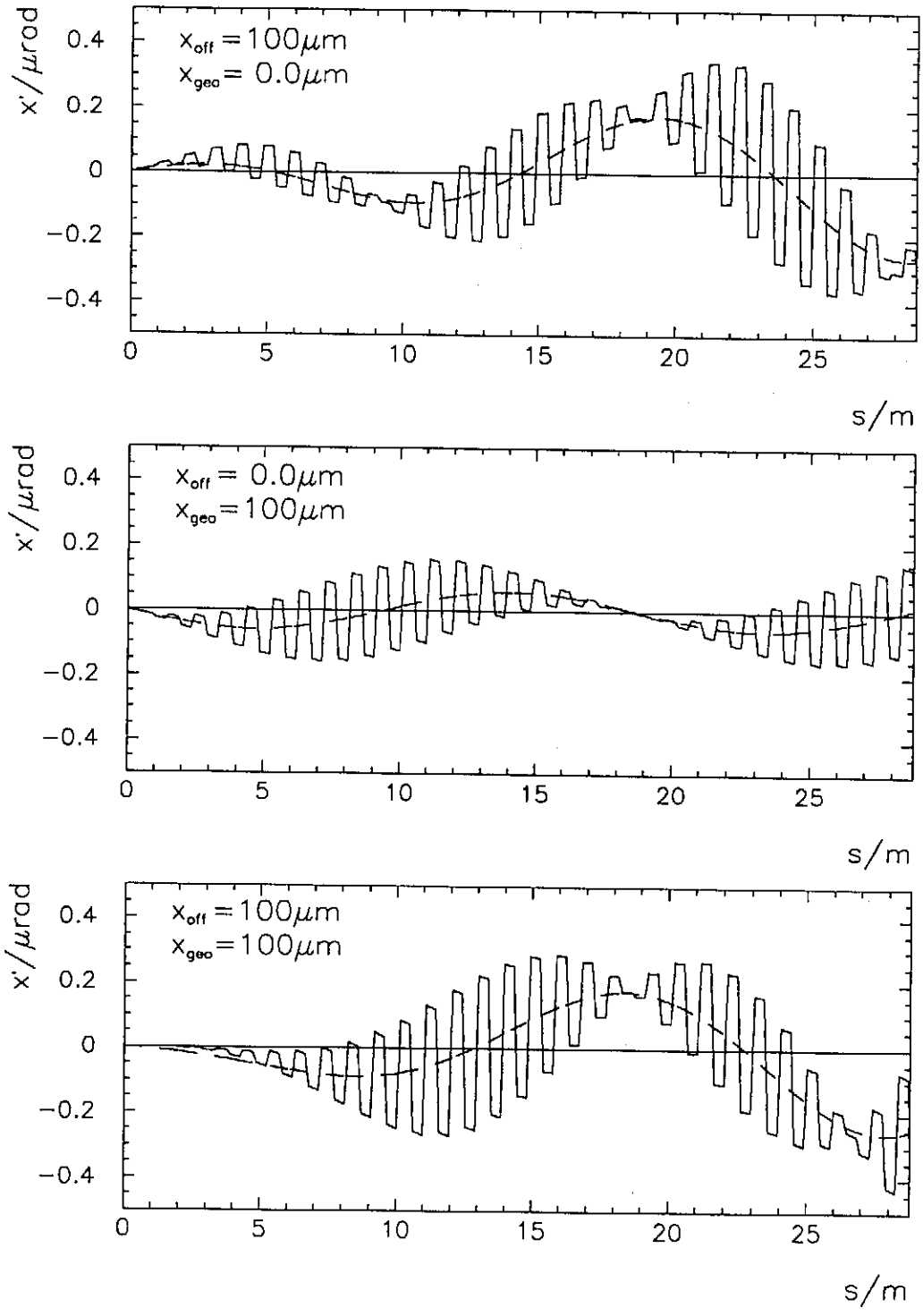

Figure B.7: Correction of the slope of the center of the bunch due to resistive wall wake fields. The numerical simulation is given by the solid line, the analytical result by the dashed line; (aluminum vacuum chamber, radius 4.75 mm).